福　井　大　学　工　学　審　査

学位論文 [博士]

A Dissertation Submitted to the University of Fukui
for the Degree of Doctor of Engineering

Research on Channel Capacity Characteristics of Near-Field MIMO Systems

「近距離 MIMO システムの通信容量に関する研究」

September 2013

Dalin ZHANG
張　大霖

A Dissertation for the Degree of Doctor of Engineering 2011

Graduate School of Engineering, University of Fukui

Research on Channel Capacity Characteristics of Near-Field MIMO Systems

近距離MIMOシステムの通信容量に関する研究

System Design Engineering – Dalin Zhang

Abstract

Recently, the near field communication, abbreviated NFC, which is a form of contactless communication between devices like smartphones or tablets, is emerging quickly. Contactless communication allows a user to wave the smartphone over a NFC compatible device to send information without needing to touch the devices together or go through multiple steps setting up a connection. Fast and convenient, NFC technology is popular in parts of Europe and Asia, and is quickly spreading throughout the whole world. Over the past decade, we have witnessed the rapid evolution of Multiple-Input Multiple-Output (MIMO) systems which promise to break the frontiers of conventional architectures and deliver high throughput by employing more than one element at the transmitter (Tx) and receiver (Rx) in order to exploit the spatial domain. This is achieved by transmitting simultaneous data streams from different elements which impinge on the Rx with ideally unique spatial signatures as a result of the propagation paths' interactions with the surrounding environment.

For exchanging massive information, for instance the videos or photos, between two devices, the future NFC systems will require higher channel capacity than current systems. Therefore, the MIMO system, which has a wider bandwidth, multi-value modulation system, and spatial multiplexing scheme, is the appropriate candidate to be employed in the high-speed NFC systems. Contrary to conventional MIMO systems, near-field MIMO communication systems transfer data in a very

short range, the transmission lines are formed in parallel without multipath, and the LOS (line-of-sight) paths are the major components. The conventional MIMO works in a multipath-rich propagation environment, and is expected to achieve a high channel capacity by utilizing multipath components. The near-field MIMO, however, transfers data directly from the transmitter to the receiver, without any fading caused by multipath components.

In the near-field MIMO system, a higher channel capacity results from a higher SNR and lower spatial correlation characteristics. Considering the short distance, the LOS components from each of the Tx elements arrive at the Rx array with a spherical wavefront. Therefore the beamwidth of the antenna element radiation pattern affects not only the receiving gain but also the spatial correlation characteristics. Usually, the conventional dipole antennas are used to investigate the MIMO channel capacity. However, the conventional dipoles are omni-directional in the horizontal plane. In this paper, a bi-directional element named dual-dipole element is utilized to improve the channel capacity. In the dual-dipole array, two half wave-length dipole antennas are settled parallel as only one element. By changing the internal distance between the two dipoles in one Tx element, the HPBW (half power beam width) of the element can be adjusted. Therefore, the shape of the radiation pattern can be determined by the internal distance between the two dipoles in one element.

The effect of the HPBW on the channel capacity is investigated in detail. The narrower beam width of the Tx element can result for a higher SNR in the facing Rx element, however, at the meantime the power in the other sub channels will decrease. Hence, it is expected that there would be an optimum HPBW when the system could obtain the maximum channel capacity. And we find out the optimum HPBW for the near-field MIMO system with dual-dipole arrays. In addition, the improvement in the channel capacity from the conventional dipole array is considerable.

Basically two factors determine the capacity of a MIMO system—the path loss and the multipath richness. The dual-dipole arrays lead to much lower path loss than the conventional dipole arrays, hence, the channel capacity improves

significantly. However, the multipath richness rarely exists in the near-field MIMO. So far, all the researches on the near-field MIMO are in the free space without any obstacle. However, due to the short transfer distance of the near-field MIMO, a tiny variation of the channel will lead to a significant difference on the channel capacity. Therefore, we employ metal wire in the near-field MIMO system to increase the multipath richness and clarify the effect of obstacles in the system.

The characteristics of the single metal wire are detailed investigated. And the most significant aspect is the location of the metal wire placed in the system. Generally, an object placed between two transmission antennas will decrease the channel capacity of the system. Here, we try to determine the optimal location of the object between the opposing antennas. We expect that the optimal location will alleviate the deterioration in the capacity caused by the object. However, the simulation results indicate that if the metal wire is placed in an appropriate location, a higher channel capacity can be obtained. In addition, we can set multiple metal wires in the optimum locations to achieve higher channel capacity. The different types of objects in the different types of arrays are also researched.

Finally, this paper clarifies the frequency dependency of channel capacity in near-field MIMO system with metal wire. As the frequency increases, the absolute value of the channel capacity decreases. The improvement on channel capacity of using a metal wire also changes with frequency. In addition, when the frequency is very large, the effect of the metal wire is negligible. The proper location for the metal wire is found related with the corresponding wavelength of each specific frequency.

Confidently, the research of the effect of the element HPBW and the objects between Tx and Rx introduced in this study can be beneficially applied in actual network preparation of future near-field MIMO wireless communications in which the improvement in the channel capacity are required.

List of Publications

The work in this dissertation is based on the following publications.

Transactions

1. **Dalin Zhang**, Toshikazu Hori, and Mitoshi Fujimoto, "Channel Capacity Improvement in Near-Field MIMO System Using Metal Wires," IEICE Trans. Commun., vol. E96-B, no.5, pp. 1141-1148, May 2013.

Letters

2. **Dalin Zhang**, Toshikazu Hori, and Mitoshi Fujimoto, "Effect of HPBW on channel capacity in near-field MIMO system," IEICE Communications Express, Vol.1, No.5, pp. 177-183, Oct. 2012.

3. **Dalin Zhang**, Toshikazu Hori, and Mitoshi Fujimoto, "Frequency dependency of channel capacity improvement in near-field MIMO system with metal wire," IEICE Communications Express, Vol.2, No.6, pp. 257-262, June 2013.

International Conferences

4. **Dalin Zhang**, Toshikazu Hori, and Mitoshi Fujimoto, "Effect of spacing and radiation pattern of antenna elements on capacity in near-field MIMO system," Proc. of ISAP2010, Macao, China, pp. 179-182, Nov. 2010.

5. **Dalin Zhang**, Toshikazu Hori, and Mitoshi Fujimoto, "Study on channel capacity in near-field MIMO system when using dual-dipole array," Proc. of ISAP2011, Jeju, Korea, FrP2-23, Oct. 2011.

6. **Dalin Zhang**, Toshikazu Hori, and Mitoshi Fujimoto, "Effect of Metal Wire on Channel Capacity in Near-Field MIMO System," IEEE Antennas and

Propagation Society International Symposium (APSURSI) 2012, Chicago, IL, USA, IF51.6, July 2012.

Domestic Conferences

7. **Dalin Zhang**, Toshikazu Hori, and Mitoshi Fujimoto, "Effect of Obstacle Metal Wire in Near-field MIMO System," 2011 IEICE Society Conference, B-1-188, Sept. 2011.

Relative Publications

Transactions

8. **Dalin Zhang**, Mitoshi Fujimoto, and Toshikazu Hori, "Novel Scheme for Blind Multiuser Detection Using CMA Adaptive Array," IEICE Trans. Commun., vol. E94-B, no.5, pp. 1225-1233, May 2011.

Technical Reports

9. **Dalin Zhang**, Mitoshi Fujimoto, and Toshikazu Hori, A Novel Multiuser Detection Scheme Using CMA Adaptive Array," IEICE Technical Report, A•P2008-61, pp.139-142, July 2008.

Domestic Conferences

10. **Dalin Zhang**, Mitoshi Fujimoto, and Toshikazu Hori, "Novel Scheme for Multiuser Detection Using CMA," 2008 IEICE Society Conference, B-1-181, Sept. 2008.

As a general guideline, the author of this dissertation has had the main responsibility of each publication. This dissertation work is supervised by Prof. Dr. Toshikazu Hori and Asst. Prof. Dr. Mitoshi Fujimoto.

Contents

Chapter 1 Introduction

1.1 Motivation and Scope of Dissertation

The past couple decades has been signified by two parallel trends that radically changed the way people work and live—the advent of the Internet and the widespread introduction of personal mobile communications. As it was widely anticipated, these two digital industries have converged in the last years by the smart phones. Seamless interoperation of the available communication infrastructure—wireless as well as cable based—will provide users with the desired information anywhere at any time. As the development of bandwidth of Internet, the applications are not limited to the access to email, website or flash game, but also including the video games, HD videos and the distribution of other multimedia contents. Such applications require an air interface which offers high peak data rates, makes the best possible use of the available spectrum, and still enables low cost terminals. Therefore, we are motivated to improve the information exchanging capability between two mobile devices or two networks. This dissertation will combine the MIMO (multiple-input multiple-output) antenna to the NFC (near field communication) system to enhance the speed of data transmitting rate.

Recently, the near field communication [1-8], abbreviated NFC, which is a form of contactless communication between devices like smart phones or tablets, is emerging quickly. Contactless communication allows a user to wave the smart phone over a NFC compatible device to send information without needing to touch the devices together or go through multiple steps setting up a connection. Fast and convenient, NFC technology is popular in parts of Europe and Asia, and is quickly spreading throughout the whole world.

Over the past decade, we have witnessed the rapid evolution of Multiple-Input Multiple-Output systems [9-16] which promise to break the frontiers of conventional

architectures and deliver high throughput by employing more than one element at the transmitter (Tx) and receiver (Rx) in order to exploit the spatial domain. This is achieved by transmitting simultaneous data streams from different elements which impinge on the Rx with ideally unique spatial signatures as a result of the propagation paths' interactions with the surrounding environment.

For exchanging massive information, for instance the videos or photos, between two devices, the future NFC systems will require higher channel capacity than current systems [17, 18]. Therefore, the MIMO system [19, 20], which has a wider bandwidth, multi-value modulation system, and spatial multiplexing scheme, is the appropriate candidate to be employed in the high-speed NFC systems [21]. Contrary to conventional MIMO systems, near-field MIMO communication systems transfer data in a very short range [22], the transmission lines are formed in parallel without multipath, and the LOS (line-of-sight) paths are the major components [23, 24]. The conventional MIMO works in a multipath-rich propagation environment, and is expected to achieve a high channel capacity by utilizing multipath components. The near-field MIMO, however, transfers data directly from the transmitter to the receiver, without any fading caused by multipath components.

In the near-field MIMO system, a higher channel capacity results from a higher SNR and lower spatial correlation characteristics [21]. Considering the short distance, the LOS components from each of the Tx elements arrive at the Rx array with a spherical wavefront [24]. Therefore the beamwidth of the antenna element radiation pattern affects not only the receiving gain but also the spatial correlation characteristics. Usually, the conventional dipole antennas are used to investigate the MIMO channel capacity. However, the conventional dipoles are omni-directional in the horizontal plane. In this paper, a bi-directional element named dual-dipole element is utilized to improve the channel capacity. In the dual-dipole array, two half wave-length dipole antennas are settled parallel as only one element. By changing the internal distance between the two dipoles in one Tx element, the HPBW (half power beam width) of the element can be adjusted. Therefore, the shape of the radiation

pattern can be determined by the internal distance between the two dipoles in one element.

The effect of the HPBW on the channel capacity is investigated in detail. The narrower beam width of the Tx element can result for a higher SNR in the facing Rx element, however, at the meantime the power in the other sub channels will decrease. Hence, it is expected that there would be an optimum HPBW when the system could obtain the maximum channel capacity. And we find out the optimum HPBW for the near-field MIMO system with dual-dipole arrays. In addition, the improvement in the channel capacity from the conventional dipole array is considerable.

Basically two factors determine the capacity of a MIMO system—the path loss and the multipath richness [25]. The dual-dipole arrays lead to much lower path loss than the conventional dipole arrays, hence, the channel capacity improves significantly. However, the multipath richness rarely exists in the near-field MIMO. So far, all the researches on the near-field MIMO are in the free space without any obstacle. However, due to the short transfer distance of the near-field MIMO, a tiny variation of the channel will lead to a significant difference on the channel capacity. Therefore, we employ metal wire in the near-field MIMO system to increase the multipath richness and clarify the effect of obstacles in the system.

The characteristics of the single metal wire are detailed investigated. And the most significant aspect is the location of the metal wire placed in the system. Generally, an object placed between two transmission antennas will decrease the channel capacity of the system. Here, we try to determine the optimal location of the object between the opposing antennas. We expect that the optimal location will alleviate the deterioration in the capacity caused by the object. However, the simulation results indicate that if the metal wire is placed in an appropriate location, a higher channel capacity can be obtained. In addition, we can set multiple metal wires in the optimum locations to achieve higher channel capacity. The different types of objects in the different types of arrays are also researched.

Confidently, the research of the effect of the element HPBW and the objects between Tx and Rx introduced in this study can be beneficially applied in actual network preparation of future near-field MIMO wireless communications in which the improvement in the channel capacity are required.

1.2 Contributions and Outline of Dissertation

Figure 1.1 shows the structure of this dissertation. The rest of this dissertation which represent the contribution and outline of this study is constructed as follows.

In Chapter 2, the overview of near field wireless communications and MIMO antenna systems will be introduced. The existing theories, applications and problems in the near-field MIMO system will be mentioned in this chapter. The background of near field communication technology and application scenario will be explained as well as the future expending application image is also described. Basic knowledge of MIMO wireless communications including the benefits of MIMO system will be introduced. The theory about the capacity of MIMO systems will be represented along with those of various kinds of static and fading channels.

In Chapter 3, all the analysis models, including the dual-dipole array model and the near-field MIMO with metal wires will be introduced. The variation of the HPBW in the dual-dipole element will be state. Besides the analysis models, the evaluation methods concerning all parameters which are considered throughout this study will be introduced in this chapter. Such as the definition of the eigen value and the effect of spatial correlation in the system are explained in detail. In addition, the main evaluation index—channel capacity is also explicated at great length.

In Chapter 4, the performance of the channel capacity in the near-field MIMO system with dual-dipole arrays will be investigated. The dual-dipole arrays are utilized to investigate the effect of HPBW on channel capacity. The HPBW can be changed by varying the internal distance between two dipoles in one element. With a proper HPBW of the antenna element, the channel capacity of a dual-dipole array is improved obviously from a conventional dipole array. The generality of the channel capacity improvement by the optimum HPBW is also clarified. In addition,

considering the usage error in the practical application, we also address the deterioration in the channel capacity caused by antenna location errors in this chapter. The offset errors and rotational errors are discussed respectively.

In Chapter 5, the performance of the objects in near-field MIMO systems will be evaluated. The metal wires are chosen as the objects between the transmitting antennas and the receiving antennas for the fundamental research. First of all, one single metal wire is investigated to confirm the effects of metal wire's length, radius and polarization. Especially, the effect of the metal wire's location is verified clearly, the proper locations in the system for the metal wire are pointed out. In addition, the effect of multiple metal wires placed at the proper locations in the system is also described in detail.

In Chapter6, it clarifies the frequency dependency of channel capacity in near-field MIMO system with metal wire. As the frequency increases, the absolute value of the channel capacity decreases. The improvement on channel capacity of using a metal wire also changes with frequency. In addition, when the frequency is very large, the effect of the metal wire is negligible. The proper location for the metal wire is found related with the corresponding wavelength of each specific frequency.

Finally, the contributions of this dissertation will be concluded in Chapter 7. It will be summarized how the HPBW affect channel capacity in the near-field MIMO systems, and how the metal wire improve the channel capacity. The metal wire that was supposed as the obstacle in the system but with the proper location will improve the channel capacity.

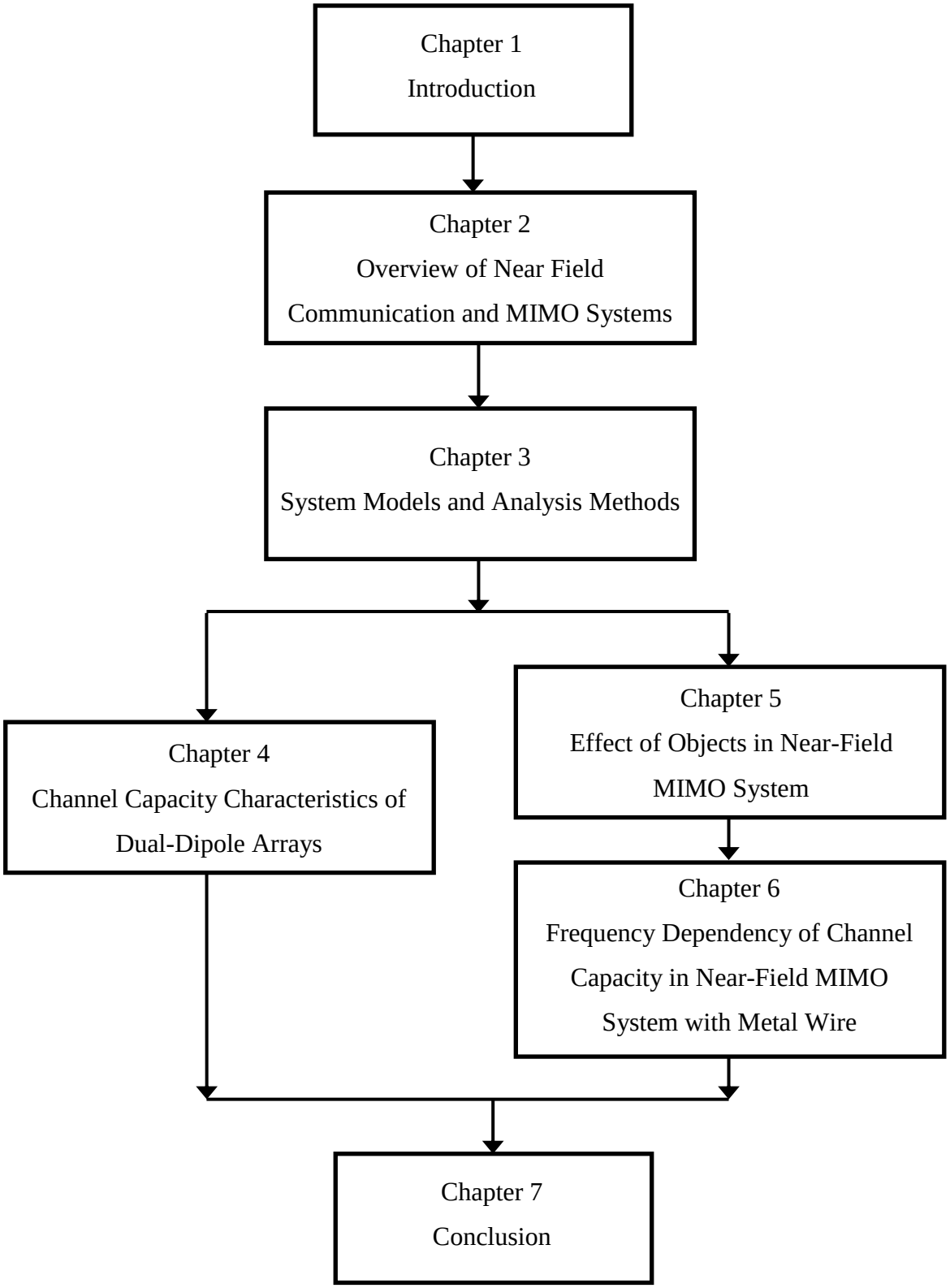

Fig. 1.1 Structure of dissertation.

Chapter 2 Overview of Near Field Communication and MIMO Systems

In this chapter, the intention is to give basic overview of NFC technology and MIMO wireless communications. This part describes NFC functional operating modes, application scenario and expending future application image. The theory about the capacity of MIMO systems is represented along with those of various kinds of static and fading channels. It is clarifies to understand the function of the MIMO system utilized in the near field communication.

2.1 Brief Introduction of Near Field Communication

Within the last couple of years an expansive process has begun to emerge integrating computational logic into various kinds of objects of our everyday life and allowing us to persistently interact with those objects. The idea is to thoroughly connect virtual information to objects of the physical world and thus providing ubiquitous computing. Related to the concept of network ubiquity is the term ’Internet of Things’ referring to objects of daily use being identifiable, trackable, and even virtually connected via an internet-like structure [26].An essential enabler for this vision is the technology of Near Field Communication (NFC) that provides the possibility of linking virtual information between physical devices through proximity.

2.1.1 NFC Technology Background

In March 2004, a new interconnection technology, Near Field Communication, was launched by Sony, Philips and Nokia with the establishment of the NFC Forum [27-31]. The NFC Forum is a non-profit industry association for advancing the use of NFC short-range wireless interaction in consumer electronics, mobile devices and

PCs. NFC is a short range (max. 20 cm), standards based wireless connectivity solution, based on RFID sensor technology that enables active and/or passive communication between electronic devices in close proximity. NFC allows people to use the simple act of touching or placing their device close to something, another device or an RFID tag to initiate the desired service. This is making to use any form of electronic "service" and other interactions easier accessible to people, whatever their age or ability. NFC secures, while the initiation of "service" handshake is always under user controlled. It removing the user need to perform complex manual operations. Once the connection is established – within milliseconds – information can be exchanged between the two devices using either NFC directly or via another wireless technology.

2.1.2 Operating Modes

The technology has three operating modes, namely 1) Reader – when the NFC enabled device reads a passive RFID tag, 2) Card emulation – when an external reader reads the content of the NFC chip and 3) P2P which means that both communicating devices are in active mode, sending and receiving messages to each other. In this mode, NFC is comparable to other short-range communication technologies such as Bluetooth, Wibree and IrDA, although the physical data transfer mechanism is different. (VTT 2007, 13.) In this respect, NFC can be seen as a rival of these technologies, even though it can also complement them. NFC can open a connection between two devices that are brought close to each other, and the actual communication will then occur by Bluetooth or WLAN [27].

The legacy of earlier standards gives NFC compatibility benefits with existing RFID applications, such as access control or public transport ticketing. It is often possible to operate with old infrastructure, even if the RFID card or reader is replaced with an NFC-enabled mobile phone, for example. This is possible because of NFC.s capability to emulate both RFID readers (reader/writer mode) and RFID tags (card emulation mode). NFC hardware can include a secure element for improved security in critical applications such as payments. For example, a credit card could be

integrated into a mobile phone and used by contactless credit card readers over NFC. (VTT 2007, 13.)

NFC has even greater potential when it is combined with mobile communication. Integrating NFC chip into a mobile handset the combination of proximity and remote communication is achieved opening further new perspectives. NFC is a standard technology that has recently achieved commercial availability via NFC chips, modules, mobile phones and PDAs. NFC is also backed by the leading mobile phone manufacturers and its deployment and chip development will be strongly driven via its integration into cellular handsets [32-35]. For example, standardised interfaces to SIM cards and to dedicated security chips, as well as chip level integration of NFC with Bluetooth can be expected in the near future.

2.1.3 Application Scenario

Almost every object or place can be equipped with a NFC tag and thus provide proximate identification and useful related information to a nearby user of a smart device, like a tablet computer or a smartphone. A poster advertising a music concert, as shown in Fig. 2.1, could for example not only offer information about the event itself to a user who taps the poster with his device, but also allow him to buy a concert ticket dispensed directly to his phone. The interaction technology behind remains invisible to the user, being unobtrusively stuck to the object, i.e. the concert poster, whilst being available anytime [36-39]. When entering the concert hall, the validity of the ticket can be approved by simply waving the smartphone across a NFC reader device at the entrance control. After having enjoyed the performance, the visitor could share photos he’s taken during the concert with another visitor by simply holding their tow phones together. And - just to follow this scenario - when taking the bus home afterwards, the user is not required to tediously gather coins the get a bus ticket at the vendor machine. Instead, when entering and leaving the bus, he touches his phone to a reader device and the cheapest ticket price is automatically debited from his account.

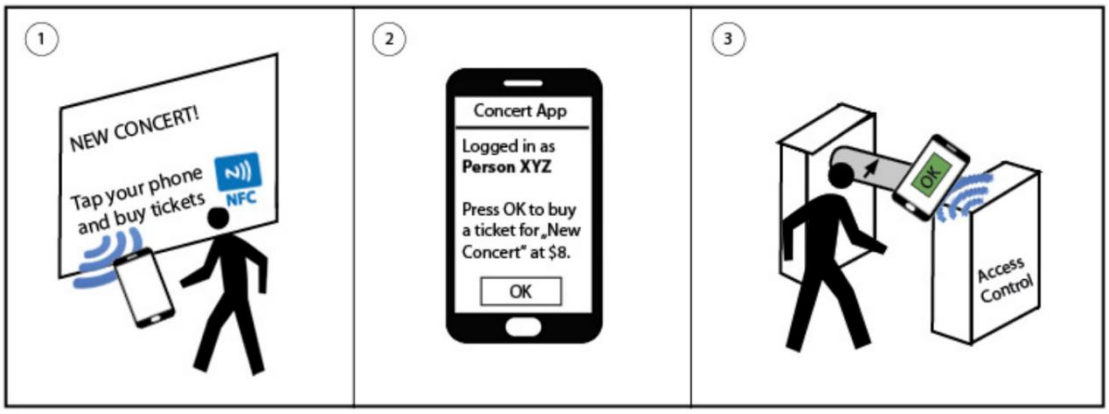

Fig. 2.1. A typical NFC application scenario: A user spots a smart poster advertising an upcoming concert and taps the poster with his NFC phone (1). A dedicated pre-installed application opens on his phone displaying details of the concert. As the user has already registered an account and is signed in, he is able to directly buy a ticket (2). The ticket is securely stored on his phone. Later, on site of the concert, the access control gates are equipped with a NFC reader and provide immediate access to the user (3).

2.1.4 Future NFC Expending Application Image

As mentioned above, the secure and convenient short range wireless communication technology, NFC, is emerging very quickly. However, the NFC is used by transfer very simple information, so where else can NFC be used, outside of simple data transfers and mobile payments? We can expect that in the future, we can exchange our videos or photos in our cell phone with our friends by approaching each other without the process of pair them as a Bluetooth. Or we can share the videos to a big screen TV, just take the tablet or phone, tap it to the TV and the video will begin to stream. Even when we want to connect the networks of two rooms, we can just set the antennas on the both sides of the wall, and we don't need to dig a hole through the wall with a cable, as shown in Fig. 2.2.

(a) Exchange massive data between phones.

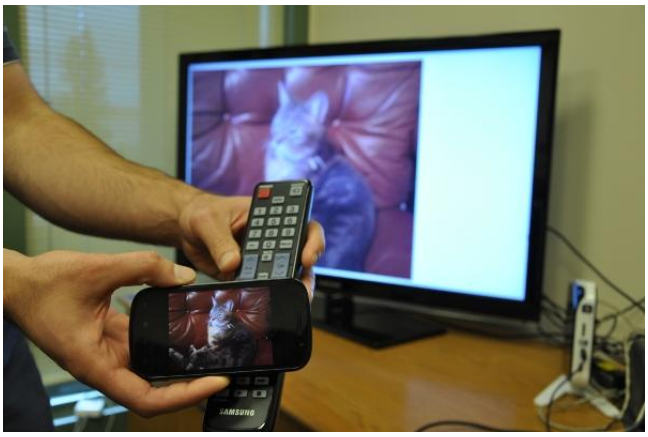

(b) Transfer massive data to a TV.

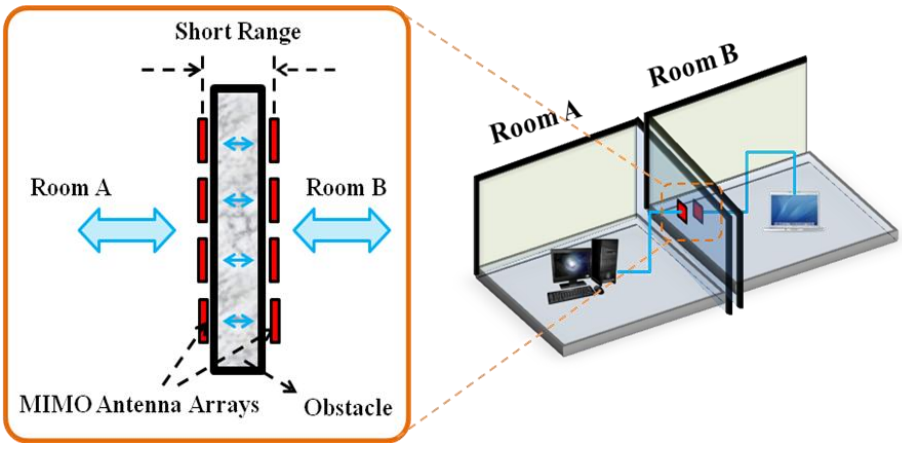

(c) Connect networks through a wall.

Fig. 2.2. Future NFC Expending Application Image.

The future image of the NFC is so attracting to us. However, the massive data transmission requires a higher speed or a higher channel capacity than current systems. Therefore, the MIMO system [19, 20], which has a wider bandwidth, multi-value modulation system, and spatial multiplexing scheme, is the appropriate candidate to be employed in the high-speed NFC systems [21].

2.2 Fundamentals of MIMO Technology

MIMO technology is well-known as the use of multiple antennas at the transmitter and receiver in wireless communication systems. It has rapidly gained in popularity over the past decade due to its powerful performance-enhancing capabilities. Communication in wireless channels is mainly deteriorated by the multipath fading. Multipath is the arrival of the transmitted signal at an intended receiver through differing angles, differing time delays, and differing frequency shifts due to the scattering of electromagnetic waves in the propagation environment. In consequence, the received signal power fluctuates in space, frequency, and time divisions through the random multi-path components. This random fluctuation in signal level is known as fading. It can severely affect the quality and reliability of wireless communication [41].

2.2.1 Background of MIMO systems

Presently in the natural world radio waves are radiated onto the surface of the earth from the sun and the other stars, and electromagnetic waves (radio waves) also arise from movement of the earth's crust and from lightening and so on.

The potential of employing multiple antennas at both ends of a radio link in order to improve the channel throughput was sparked by the pioneering work of Winters in 1987 [41]. Surprisingly, it was not until mid-90s that two breakthrough papers by Foschini [42] and Telatar [43] separately investigated this promising technology in detail. Both authors showed that MIMO systems have the unique ability to turn multipath propagation, usually regarded as a serious hindrance in wireless communications, into an advantage for increasing the spectral efficiency. Under independent Rayleigh fading conditions, MIMO systems offer a linear capacity

increase that is proportional to the minimum number of receive M and transmit N antenna elements, i.e. min {M,N}.

The boost in spectral efficiency offered by an ideal MIMO system was firstly demonstrated in [41], where an architecture called BLAST (Bell Labs Layered Space Time) along with a reconstruction algorithm and a coding/decoding scheme were devised. The most attractive feature of MIMO systems is their ability to simultaneously transmit individual (orthogonal) data streams from each antenna element; in the literature, this feature is widely known as spatial multiplexing (SM) [44]. The number of orthogonal multiplexed streams depends on the spatial properties of the surrounding environment and is upper limited by min {M,N}.

Another feature of MIMO systems is spatial diversity which is a means to combat fading by exploiting multiple uncorrelated replicas of the transmitted signal. Diversity occurs when the antenna spacing is high enough so that independent signal paths are created, resulting in a reduced variation of the received signal's power. Diversity reduces the probability that all branches are in a deep fade simultaneously and thus it enhances the error rate performance (channel hardening). MIMO techniques permit the spatial diversity to be exploited at both sides of the radio link with the maximal diversity gain being MN.

However, there is an inherent trade-off between SM and spatial diversity. This means that increasing the diversity advantage comes at the expense of decreasing the SM gain, and vice versa. In fact, the authors in [45] showed that the diversity-multiplexing trade-off achievable by a system is a more fundamental measure of its performance than just its maximal diversity gain or its maximal multiplexing gain alone. Generally, the optimal trade-off is determined by system requirements such as the desired data rate and reliability of transmission. High data rates can be achieved by employing multiplexing to full extent while high reliability benefits from diversity [46].

Smart antenna systems, which use an antenna array at a single end, make use of beamforming in order to increase the average SNR and suppress interference from

other users by steering energy into desired directions. Likewise, for MIMO systems beamforming may be applied at the Tx and/or the Rx side. The more directive a channel is the higher its beamforming gain. For pure LoS conditions with only one path present, the maximal beamforming gain MN is obtained, albeit at the expense of an increased spatial correlation that diminishes the beneficial effects of spatial diversity. Finally, it should be underlined that full beamforming excludes full diversity or multiplexing and the same is true for full diversity and beamforming/multiplexing; however, full multiplexing excludes beamforming whereas it only reduces diversity.

MIMO technology promises a breakthrough in wireless communication system by offering a number of benefits that help meet the challenges posed by both the deteriorations in the wireless channel as well as limited bandwidth. In addition to the time and frequency dimensions that are utilized in conventional single-antenna wireless systems (Single-Input Single-Output, SISO), MIMO is considered by utilizing the spatial dimension which is provided by the multiple antennas at the transmitter and the receiver. The performance gains that are expected from the use of MIMO technology is shown in Fig. 2.3 [50] . The relationship between data rate and receive Signal-to-Noise Ratio (SNR) for an $M \times M$ (i.e., M receiving and M transmitting antennas) fading link with $M = 1, 2, 4$. Assuming a target receive SNR of 25 decibels (dB), a conventional SISO (i.e., $M = 1$) system can deliver a data rate of 0.7 Mbps, as with $M = 2$ and 4 we can realize data rates of 1.4 Mbps and 2.8 Mbps, respectively. This increase in data rate is realized for no additional power or bandwidth expenditure compared to the SISO system.

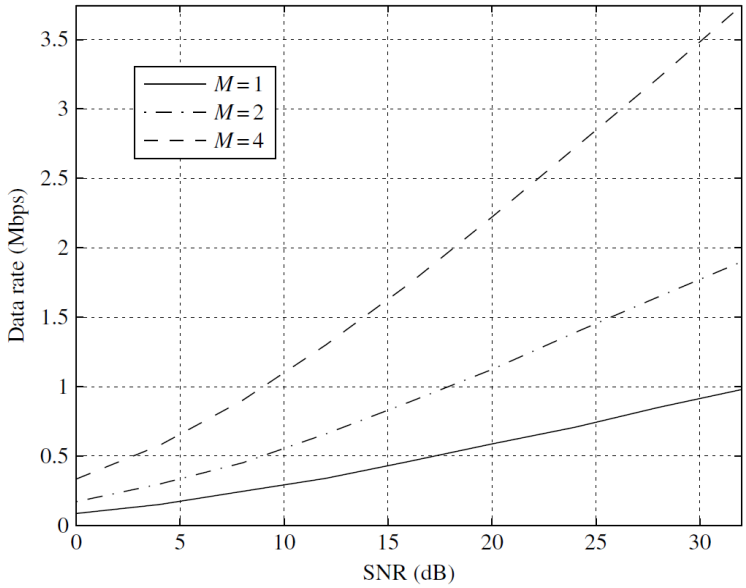

Fig. 2.3. Average data rate versus SNR for different antenna configurations.

Figure 2.4 [50] shows the basic block diagram that comprises a MIMO system, where **x** and **y** stand for the transmitted and received signal vectors respectively. The information bits to be transmitted are encoded and interleaved. The interleaved codeword is mapped to data symbols by the symbol mapper. These data symbols are input to a space-time encoder that outputs one or more spatial data streams. The spatial data streams are mapped to the transmit antennas by the space-time pre-coding block. The signals launched from the transmit antennas propagate through the channel and arrive at the receive antenna array. The receiver collects the signals at the output of each receive antenna element and reverses the transmitter operations in order to decode the data: receive space-time processing, followed by space-time decoding, symbol de-mapping, de-interleaving and decoding. Each of the blocks offers the opportunity for significant design challenges and complexity-performance trade-offs.

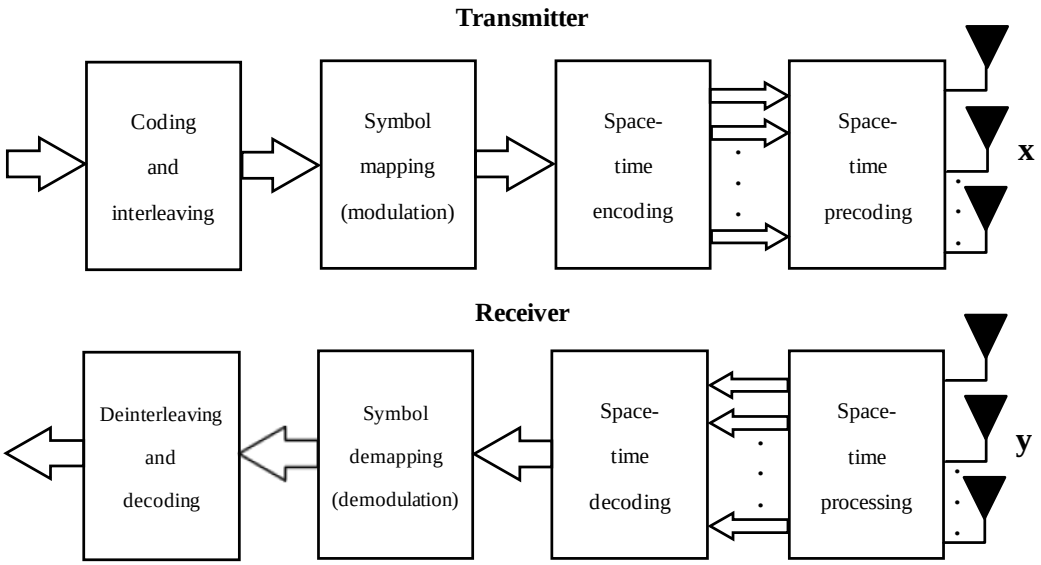

Fig. 2.4. Block diagram of a MIMO communication system.

2.2.2 Benefits of MIMO systems

The benefits of MIMO technology that help achieve such significant performance gains are described in brief below.

A. Array Gain

Array gain is the increase in receive SNR that results from a coherent combining effect of the wireless signals at a receiver, which is realized through spatial processing at the receiver array and spatial pre-processing at the transmitter array. Array gain improves resistance to noise, thereby improving the coverage and the range of a wireless network [16, 51].

B. Spatial Diversity Gain

Spatial diversity gain reduces fading and is realized by providing the receiver with multiple copies of the transmitted signal in space, frequency or time. With an increasing number of independent copies, the probability in which at least one of the

copies is not going into a deep fade increases, thereby improving the quality and reliability of reception [52].

C. Spatial Multiplexing Gain

MIMO systems offer a linear increase in data rate through spatial multiplexing [53-55], i.e., transmitting multiple, independent data streams within the operating bandwidth. Under suitable channel conditions, such as rich scattering in the environment, the receiver can separate the data streams. Furthermore, each data stream experiences at least the same channel quality that would be experienced by a SISO system, effectively enhancing the capacity. It can be said that the spatial multiplexing gain increases the capacity of a wireless network [56, 57].

D. Interference Reduction

Interference in wireless networks occurs from multiple users sharing time and frequency resources. Interference may be reduced in MIMO systems by utilizing the spatial dimension to increase the separation between users. For instance, in the presence of interference, array gain increases the tolerance to noise as well as the interference power, hence improving the Signal-to-Interference-plus-Noise Ratio (SINR). Additionally, the spatial dimension may avoid the interference by directing signal energy towards the intended user and minimizing interference to other users. Interference reduction and avoidance improve the coverage and range of a wireless network [19].

Generally, it may not be possible to utilize all above benefits at the same. However, using some combination of the benefits across a wireless network will result in improved capacity, coverage and reliability.

2.3 Channel Capacity of MIMO Systems

In Section 2.2, it is clearly described that MIMO systems provide tremendous capacity gains, which has lead significant activity to develop transmitter and receiver techniques that realize these capacity benefits and utilize diversity-multiplexing trade-offs. In this section, more detail about the Shannon capacity limits of SU and

MU-MIMO systems will be explored. These fundamental limits indicate the maximum data rates that can be transmitted over the MIMO channel to one or more users, assuming no constraints on the delay or the complexity of the encoder and decoder. Many studies by Foschini [54] and Telatar [55] predict remarkable capacity growth for wireless systems with multiple antennas when the channel represents rich. However, these predictions are based on somewhat unrealistic assumptions about the underlying time-varying channel model and how well it can be tracked at the receiver as well as at the transmitter. More realistic assumptions can dramatically impact the potential capacity gains of MIMO techniques.

2.3.1 Mutual information and Shannon capacity

In the late 1940s, Claude Shannon has introduced the channel capacity using a mathematical theory of communication [58-60]. The channel capacity (C) is denoted as the maximum rate at which reliable communication can be performed, without any constraints on transmitter and receiver complexity. He showed that for any rate $R < C$, there exist rate R channel codes with arbitrarily small block error probabilities. However, such a code may have a very long block length, and the encoding and decoding complexity may also be extremely large. In fact, the required block length may increase as the desired probability of error (P_e) is decreased and the rate R is increased towards C. In addition, Shannon showed that codes operating at rates $R > C$ cannot achieve an arbitrarily small error rate. Therefore, the channel capacity is truly the fundamental limit to communication.

Theoretically, even if it is possible to communicate at any rate below capacity, it is actually a very difficult problem to design practical channel codes with reasonable block length and encoding/decoding complexity at rates close to capacity. Tremendous progress has been made in code design over the past few decades, and practical codes at rates very close to capacity do exist for certain channels, such as single antenna Gaussian channels. However, these codes generally cannot be directly used for MIMO channels, as codes for MIMO channels must also utilize the spatial dimension. Practical space-time coding and decoding techniques for MIMO channels have been shown to achieve near-capacity limits in some scenarios [50]. The capacity

limits of MIMO channels provide a benchmark against which performance of space-time codes and general MIMO transmission and reception strategies can be compared.

It has been shown in Shannon's study that the channel capacity, defined as the maximum rate at which reliable communication is possible, can be simply characterized in terms of the mutual information between the input and the output of the channel. The basic channel model consists of a random input X, a random output Y, and a probabilistic relationship between X and Y which is generally characterized by the conditional distribution of Y given X, or $f(y|x)$. The mutual information of a SU channel is then defined as [50]

$$I(X;Y) = \int_{S_x,S_y} f(x,y)\log_2\left(\frac{f(x,y)}{f(x)f(y)}\right)dxdy, \qquad (2.1)$$

where the integral is taken over the supports S_x, S_y of the random variables X and Y, respectively, and $f(x)$, $f(y)$, and $f(x,y)$ denote the probability distribution functions of the random variables. The units of mutual information are bits per channel use.

Furthermore, he proved that the channel capacity of most channels is equal to the mutual information of the channel maximized over all possible input distributions [50]:

$$C = \max_{f(x)} I(X;Y) = \max_{f(x)} \int_{S_x,S_y} f(x,y)\log_2\left(\frac{f(x,y)}{f(x)f(y)}\right)dxdy\,. \qquad (2.2)$$

For a time-invariant additive temporally white complex Gaussian noise (AWGN) channel with bandwidth B and received SNR γ, the maximizing input distribution is Gaussian, which results in the channel capacity in the units of bit per second (bps) [50]

$$C = B\log_2(1+\gamma)\,. \qquad (2.3)$$

Referring back to Fig. 2.4, the channel input is the vector **x** sent from the transmit antennas and the channel output is the vector **y** obtained at the receive antennas. Thus, the Shannon capacity of the MIMO AWGN channel is based on the maximum mutual information between its input and output vectors.

The capacity of a channel has multiple definitions when the channel is time-varying, depending on what is known about the channel state or its distribution at the transmitter or receiver. These definitions have different operational meanings. Specifically, when the instantaneous channel gains, also called the channel state information (CSI), are known perfectly at both the transmitter and the receiver, the transmitter can adapt its transmission rate and power relative to the instantaneous channel state. In this case the Shannon (ergodic) capacity is the maximum mutual information averaged over all channel states. Essentially, ergodic means that a reasonably long time fading realizations has a distribution similar to the statistical distribution of the channel. Hence, ergodic capacity is an appropriate capacity metric for channels that vary quickly.

An alternate capacity definition for time-varying channels with perfect transmitter and receiver CSI is outage capacity. Outage capacity requires a fixed data rate in all non-outage channel states, which is needed for applications with delay-constrained data where the data rate cannot depend on channel variations. The average rate associated with outage capacity is typically smaller than the ergodic capacity due to the additional constraint associated with this definition. Outage capacity is the appropriate capacity metric in slowly varying channels, where the channel coherence time exceeds the duration of a codeword. In this case each codeword experiences only one channel state: if the channel state is not good enough to support the desired rate then an outage is declared and no data are transmitted, since the transmitter knows that the channel is in outage. Outage capacity under perfect CSI at the transmitter and the receiver (CSIR) has been studied for single-antenna channels [61-63], but this work has yet to be extended to MIMO channels. A more common assumption for studying capacity of time-varying MIMO

channels is perfect CSIR but no CSIT. In such a case, the transmission (reception) strategy is based on the channel distribution instead of the instantaneous channel state.

2.3.2 MIMO Channel Model

In order to understand the performance limits in MIMO systems and to design efficient communication algorithms, it is important to understand the nature of the MIMO channel. For a system with M transmit antennas and N receive antennas in Fig. 2.5 [41], the MIMO channel at a given time instant may be represented as an $M \times N$ matrix [41]

$$\mathbf{H} = \begin{bmatrix} h_{11} & h_{12} & \cdots & h_{1M} \\ h_{21} & h_{22} & \cdots & h_{2M} \\ \vdots & \vdots & \ddots & \vdots \\ h_{N1} & h_{N2} & \cdots & h_{NM} \end{bmatrix}, \tag{2.4}$$

where h_{mn} is the channel gain between the m-th receive and n-th transmit antenna pair. The n-th column of $\mathbf{H}$ is often referred to as the spatial signature of the n-th transmit antenna across the receive antenna array. This is particularly important when independent data streams are launched from the transmit antennas, as is done in the case of spatial multiplexing. As for the case of SISO channels, the individual channel gains comprising the MIMO channel are commonly modeled as zero-mean circularly symmetric complex Gaussian random variables. Consequently, the amplitudes $|h_{mn}|$ are Rayleigh-distributed random variables and the corresponding powers $|h_{mn}|^2$ are exponentially distributed.

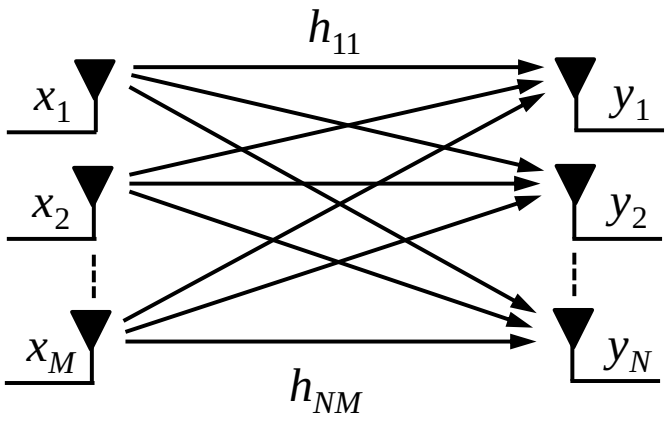

Fig. 2.5. M ×N MIMO system.

The degree of correlation between the individual *MN* channel gains comprising the MIMO channel is a complicated function of the scattering in the environment and antenna spacing at the transmitter and the receiver. Consider an extreme condition where all antenna elements at the transmitter and are co-located and likewise at the receiver. In this case, all the elements of **H** will be fully correlated and the spatial diversity order of the channel is one. De-correlation between the channel elements will increase with antenna spacing. However, antenna spacing alone is not sufficient to ensure de-correlation. Rich scattering in the environment in combination with adequate antenna spacing ensures de-correlation of the MIMO channel elements. With rich scattering, the typical antenna spacing required for de-correlation is approximately a half-wavelength ($\lambda/2$). Under ideal conditions, when the channel elements are perfectly de-correlated, the channel becomes the classical independent, identically distributed (iid) Rayleigh fading MIMO channel with the spatial diversity order of *MN*.

In practice, the behavior of **H** can significantly deviate from the de-correlated matrix due to a combination of inadequate antenna spacing and inadequate scattering leading to spatial fading correlation. Furthermore, the presence of a fixed (possibly Line-of-Sight, LOS) component in the channel will result in Ricean fading. In the presence of an LOS component between the transmitter and the receiver, the MIMO

channel may be modeled as the sum of a fixed (LOS) component and a fading component, assuming uncorrelated fading, as [41]

$$\mathbf{H} = \sqrt{\frac{K}{1+K}}\overline{\mathbf{H}} + \sqrt{\frac{1}{1+K}}\mathbf{H}_w. \tag{2.5}$$

$K \geq 0$ is the Ricean K-factor of the channel and is defined as the ratio of the power in the LOS component of the channel to the power in the fading component. Ricean K-factor which provides an indication of link quality is generally used as the propagation parameter in mobile communication. When $K = 0$, the channel becomes pure Rayleigh fading, as at $K = \infty$ corresponds to a non-fading channel.

In general, real-world MIMO channels will represent some combination of Ricean fading and spatial fading correlation. Furthermore, the use of polarized antennas will necessitate additional modifications to the channel model. These factors will affect the performance of a given MIMO signaling scheme. With appropriate knowledge of the MIMO channel at the transmitter, the signaling strategy can be appropriately adapted to meet performance requirements. The CSI which provides the precise channel realization could be completely or partially known.

Referring back to Figure 2-8, a narrowband point-to-point communication system of M transmit and N receive antennas can be represented by the discrete time model [41]

$$\begin{bmatrix} y_1 \\ y_2 \\ \vdots \\ y_N \end{bmatrix} = \begin{bmatrix} h_{11} & h_{12} & \cdots & h_{1M} \\ h_{21} & h_{22} & \cdots & h_{2M} \\ \vdots & \vdots & \ddots & \vdots \\ h_{N1} & h_{N2} & \cdots & h_{NM} \end{bmatrix} \begin{bmatrix} x_1 \\ x_2 \\ \vdots \\ x_M \end{bmatrix} + \begin{bmatrix} n_1 \\ n_2 \\ \vdots \\ n_N \end{bmatrix}, \tag{2.6}$$

or simply as

$$\mathbf{y} = \mathbf{H}\mathbf{x} + \mathbf{n}, \tag{2.7}$$

where **x** represents the *M*-dimensional transmitted symbol, **n** is the *N*-dimensional AWGN vector with $E[\mathbf{nn}^H] = \sigma^2 \mathrm{I}_N$. We assume a channel bandwidth of *B*, where typically $\sigma^2 = N_0 B$. For simplicity, given a transmit power constraint *P*, we will assume an equivalent model with a noise power of unity and transmit power $P/\sigma^2 = \rho$, where ρ can be interpreted as the average SNR per receive antenna and is simply referred to as SNR henceforth. This power constraint implies that the input symbols satisfy [41]

$$\sum_{m=1}^{M} \mathrm{E}\left[x_m x_m^* \right] = \rho . \tag{2.8}$$

Different assumptions can be made about the knowledge of the channel gain matrix **H** at the transmitter and receiver, referred to as CSIT and CSIR, respectively. For a static channel CSIR is typically assumed, since the channel gains can be obtained by sending a pilot sequence for channel estimation. More details on estimation techniques for MIMO channels can be found in [44]. If a feedback path is available, then CSIR from the receiver can be sent back to the transmitter to provide CSIT. CSIT may also be available in time-division duplexing systems without a feedback path by utilizing reciprocal properties of propagation. When the channel is not known at either the transmitter or receiver then some distribution on the channel gain matrix must be assumed. The most common model for this distribution is a zero-mean spatially white (ZMSW) model, where the entries of **H** are assumed to be iid zero mean, unit variance, complex circularly symmetric Gaussian random variables. In general, different assumptions about CSI and about the distribution of the **H** entries lead to different channel capacities and different approaches to space-time signaling.

2.3.3 MIMO Channel Capacity

The Shannon capacity of a MIMO channel, which equals the maximum data rate that can be transmitted over the channel with arbitrarily small error probability, is focused in this section. The maximum rate that can be transmitted over the channel with some nonzero outage probability is defined by the capacity versus outage.

Channel capacity depends on what is known about the channel gain matrix or its distribution at the transmitter and/or receiver. It is assumed throughout this section that the receiver has knowledge of the channel matrix **H**, since for static channels a good estimate of H can be obtained easily.

A. Static Channels

The static channel capacity forms the basis for the capacity of fading channels. The capacity of a MIMO channel is an extension of the mutual information formula (Shannon) for a SISO channel given by (2.2) to a matrix channel. Specifically, the capacity is given in terms of the mutual information between the channel input vector **x** and output vector **y** as [41, 65]

$$C = \max_{f(x)} I(\mathbf{X};\mathbf{Y}) = \max_{f(x)} \left[H(\mathbf{Y}) - H(\mathbf{Y} \mid \mathbf{X}) \right], \tag{2.9}$$

where $H(\mathbf{Y})$ and $H(\mathbf{Y}|\mathbf{X})$ are the entropy in **y** and **y**|**x**, respectively. The definition of entropy yields that $H(\mathbf{Y}|\mathbf{X}) = H(\mathbf{N})$, which is the entropy in the noise. Since this noise **n** has fixed entropy independent of the channel input, maximizing mutual information is equivalent to maximizing the entropy in **y**.

The mutual information of **y** depends on its covariance matrix, which for the narrowband MIMO model is given by [41]

$$\mathbf{R}_{\mathbf{y}} = E[\mathbf{y}\mathbf{y}^H] = \mathbf{H}\mathbf{R}_{\mathbf{x}}\mathbf{H}^H + \mathbf{I}_N, \tag{2.10}$$

where $\mathbf{R}_{\mathbf{x}}$ is the covariance of the MIMO channel input. It turns out that for all random vectors with a given covariance matrix $\mathbf{R}_{\mathbf{y}}$, the entropy of **y** is maximized when **y** is a zero-mean circularly-symmetric complex Gaussian (ZMCSCG) random vector [54]. But **y** is ZMCSCG if only the input **x** is ZMCSCG, and therefore this is the optimal distribution on **x**. This results in the mutual information [41]

$$I(\mathbf{X};\mathbf{Y}) = B \log_2 \det\left[\mathbf{I}_N + \mathbf{H}\mathbf{R}_{\mathbf{x}}\mathbf{H}^H \right], \tag{2.11}$$

where det[**A**] and $\mathbf{A}^H$ denotes the determinant and the Hermitian of a matrix **A**, respectively. This formula was derived in [49, 55] for the mutual information of a multi antenna system, and also appeared in earlier works on MIMO systems [45, 46].

The MIMO capacity is achieved by maximizing the mutual information (2.11) over all input covariance matrices $\mathbf{R_x}$ satisfying the power constraint [41]

$$C = \max_{\mathbf{R_x}:\mathrm{Tr}(\mathbf{R_x})=\rho} B\log_2 \det\left[\mathbf{I}_N + \mathbf{H}\mathbf{R_x}\mathbf{H}^H\right]. \qquad (2.12)$$

The optimization relative to $\mathbf{R_x}$ will clearly depend on whether or not **H** is known at the transmitter. We now consider this maximizing under different assumptions about CSIT.

Channel Known at Transmitter: Water-Filling

The MIMO parallel decomposition in Fig. 2.6 [41] allows a simple characterization of the MIMO channel capacity for a fixed channel matrix **H** known at the transmitter and receiver. Specifically, the capacity equals the sum of capacities on each of the independent parallel channels with the transmit power optimally allocated between these channels [66, 67].

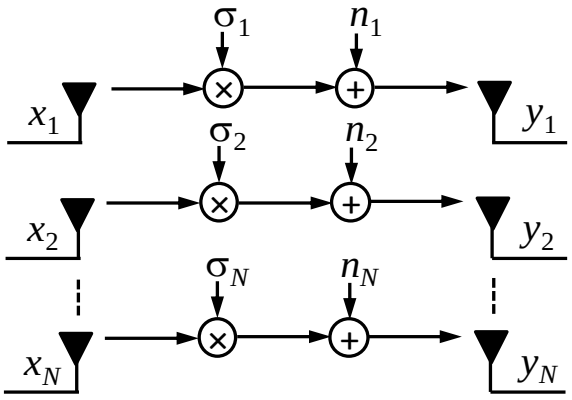

Fig. 2.6. Parallel Decomposition of the MIMO Channel.

This optimization of transmit power across the independent channels results from optimizing the input covariance matrix to maximize the capacity in (2.12). Using

properties of unitary matrices, we get the MIMO capacity with CSIT and CSIR as [41]

$$C = \max_{\rho_n : \sum_n \rho_n \le \rho} \sum_n B \log_2 \left(1 + \sigma_n^2 \rho_n\right). \tag{2.13}$$

Since $\rho = P/\sigma^2_N$, the capacity (2.13) can also be expressed in terms of the power allocation P_n to the n-th parallel channel as [40]

$$C = \max_{P_n : \sum_n P_n \le P} \sum_n B \log_2 \left(1 + \frac{P_n \gamma_n}{P}\right). \tag{2.14}$$

where $\rho_n = P_n/\sigma^2_N$ and $\gamma_n = \sigma^2_n P/\sigma^2_N$ is the SNR associated with the n-th channel at full power. This capacity formula can also be used in the case of flat fading or in frequency-selective fading. Solving the optimization leads to a water-filling power allocation for the MIMO channel [41]:

$$\frac{P_n}{P} = \begin{cases} \frac{1}{\gamma_0} - \frac{1}{\gamma_n} & \gamma_n \ge \gamma_0 \\ 0 & \gamma_n < \gamma_0 \end{cases} \tag{2.15}$$

for some cutoff value γ_0. The resulting capacity is then [40]

$$C = \sum_{n : \gamma_n \ge \gamma_0} B \log_2 \left(\frac{\gamma_n}{\gamma_0}\right). \tag{2.16}$$

The channel capacity under perfect CSIT and CSIR can also be defined on Single-Input Multiple-Output (SIMO) or Multiple-Input Single-Output (MISO) channels. These channels can only obtain diversity gain from the multiple antennas. When both transmitter and receiver know the channel the capacity equals that of a SISO channel with the signal transmitted or received over the multiple antennas coherently combined to maximize the channel SNR, as in MRC. This results in capacity $C = B \log_2(1+\rho \mathbf{hc})$, with the channel matrix $\mathbf{H}$ reduced to a vector $\mathbf{h}$ of channel gains, the optimal weight vector $\mathbf{c} = \mathrm{h}^*/\|\mathrm{h}\|$, and $\rho = P/\sigma^2_N$.

Channel Unknown at Transmitter: Uniform Power Allocation

In this part, assume that the receiver knows the channel but the transmitter does not. Without channel information, the transmitter cannot optimize its power allocation or input covariance structure across antennas. If the distribution of **H** follows the ZMSW channel gain model, there is no bias in terms of the mean or covariance of **H**. Thus, the best strategy should be to allocate equal power to each transmit antenna, resulting in an input covariance matrix equal to the scaled identity matrix: $\mathbf{R_x} = (\rho/M)\ \mathbf{I}_M$. It is shown in [55] that under these assumptions this input covariance matrix indeed maximizes the mutual information of the channel. For an *M*-transmit, *N*-receive antenna system, this yields mutual information given by using the SVD of **H**, we can express this as [41]

$$I = B\log_2 \det\left[\mathbf{I}_N + \frac{\rho}{M}\mathbf{H}\mathbf{H}^H\right] = \sum_{n=1}^{R_H} B\log_2\left(1+\frac{\gamma_n}{M}\right), \qquad (2.17)$$

where $\gamma_n = \sigma^2_n\,\rho = \sigma^2_n P/\sigma^2_N$ and R_H is the number of nonzero singular values of **H**.

The mutual information of the MIMO channel depends on the specific realization of the matrix **H**. The average mutual information of a random matrix **H**, averaged over the matrix distribution, depends on the probability distribution of the singular values of **H** [55, 64]. In fading channels, the transmitter can transmit at a rate equal to this average mutual information and insure correct reception of the data, as discussed in the next section. But for a static channel, if the transmitter does not know the channel realization or the average mutual information then it does not know at what rate to transmit such that the data will be received correctly. In this case, the appropriate capacity definition is capacity with outage. In capacity with outage, the transmitter fixes a transmission rate *C*, and the outage probability associated with *C* is the probability that the transmitted data will not be received correctly, i.e., the probability that the channel **H** has mutual information less than *C*. This probability is given by [41]

$$p_{out} = p\left(\mathbf{H} : B\log_2 \det\left[\mathbf{I}_N + \frac{\rho}{M}\mathbf{H}\mathbf{H}^H \right] < C \right). \qquad (2.18)$$

As the number of transmit and receive antennas grows large, random matrix theory provides a central limit theorem for the distribution of the singular values of **H** [68], resulting in a constant mutual information for all channel realizations. As an example of this limiting distribution, note that for fixed *N*, under the ZMSW model the law of large numbers implies that [40]

$$\lim_{M\to\infty} \frac{1}{M}\mathbf{H}\mathbf{H}^H = \mathbf{I}_N . \qquad (2.19)$$

Substituting this into (2.17) yields that the mutual information in the asymptotic limit of large *M* becomes a constant equal to $C = N\,B\,\log_2(1+\rho)$. Defining $L = \min(M, N)$, this implies that as *L* grows large, the MIMO channel capacity in the absence of CSIT approaches $C = L\,B\,\log_2(1+\rho)$, and hence grows linearly in *L*. Moreover, this linear growth of capacity with *L* in the asymptotic limit of large *L* is observed even for a small number of antennas [69]. Similarly, as SNR grows large, capacity also grows linearly with $L = \min(M, N)$, for any *M* and *N* [54].

Although the channel realization is not known at the transmitter, the capacity of MIMO channels still grows linearly with the minimum number of transmit and receive antennas, as long as the channel can be accurately estimated at the receiver. Thus, MIMO channels can provide very high data rates without requiring increased signal power or bandwidth. These results are the main reason for the widespread appeal of MIMO techniques. However, at very low SNR, the capacity only scales with the number of receive antennas. The reason is that the MIMO system is just trying to collect energy rather than utilize all available dimensions, so all energy is concentrated into one of the available transmit antenna to achieve capacity [55].

B. Fading Channels

In this section, assume that the channel gain matrix experiences flat-fading, so the gains h_{mn} vary with time. As in the case of the static channel, the capacity depends on what is known about the channel matrix at the transmitter and receiver. With perfect CSIR and CSIT the transmitter can adapt to the channel fading and its capacity equals the average over all channel matrix realizations with optimal power allocation. With CSIR and no CSIT, the outage capacity is used to characterize the outage probability associated with any given channel rate.

Channel Known at Transmitter: Water-Filling

With CSIT and CSIR, the transmitter optimizes its transmission strategy for each fading channel realization as in the case of a static channel. The capacity is then just the average of capacities associated with each channel realization, given by (2.12), with power optimally allocated. This average capacity is called the ergodic capacity of the channel, as mentioned in Section 2.4.1. There are two possibilities for allocating power under ergodic capacity. A short-term power constraint assumes that the power associated with each channel realization must equal the average power constraint P. In this case, the ergodic capacity becomes [41]

$$\begin{aligned} C &= \mathrm{E}_{\mathbf{H}}\left[\max_{\mathbf{R}_{\mathbf{x}}:\mathrm{Tr}(\mathbf{R}_{\mathbf{x}})=\rho} B\log_2\det\left[\mathbf{I}_N+\mathbf{H}\mathbf{R}_{\mathbf{x}}\mathbf{H}^H\right]\right] \\ &= \mathrm{E}_{\mathbf{H}}\left[\max_{P_n:\sum_n P_n\le P}\sum_n B\log_2\left(1+\frac{P_n\gamma_n}{P}\right)\right]. \end{aligned} \tag{2.20}$$

A less restrictive constraint is a long-term power constraint, where we can use different powers for different channel realizations subject to the average power constraint over all channel realizations. The ergodic capacity under this assumption is given by [41]

$$C=\max_{\rho_H:E[\rho_H]=\rho}\mathrm{E}_{\mathbf{H}}\left[\max_{\mathbf{R}_{\mathbf{x}}:\mathrm{Tr}(\mathbf{R}_{\mathbf{x}})=\rho} B\log_2\det\left[\mathbf{I}_N+\mathbf{H}\mathbf{R}_{\mathbf{x}}\mathbf{H}^H\right]\right]. \tag{2.21}$$

The short-term power constraint gives rise to a water-filling in space across the antennas, whereas the long-term power constraint allows for a two-dimensional water-filling across both space and time, similar to the frequency-time water-filling associated with the capacity of a time-varying frequency-selective fading channel.

Channel Unknown at Transmitter: Ergodic Capacity and Capacity with Outage

Consider a time-varying channel with random matrix **H** known at the receiver but not the transmitter. The transmitter assumes a ZMSW distribution for **H**. The two relevant capacity definitions in this case are ergodic capacity and capacity with outage. Ergodic capacity defines the maximum rate, averaged over all channel realizations that can be transmitted over the channel for a transmission strategy based only on the distribution of **H**. This leads to the transmitter optimization problem, i.e., finding the optimum input covariance matrix to maximize ergodic capacity subject to the transmit power constraint. The problem is to characterize the optimum $\mathbf{R_x}$ to maximize [41]

$$C = \max_{\mathbf{R_x}:\mathrm{Tr}(\mathbf{R_x})=\rho} \mathrm{E}_{\mathbf{H}}\left[B\log_2 \det\left[\mathbf{I}_N + \mathbf{H}\mathbf{R_x}\mathbf{H}^H \right]\right], \qquad (2.22)$$

where the expectation is with respect to the distribution on the channel matrix **H**, which for the ZMSW model is iid zero-mean circularly symmetric unit variance.

As in the case of scalar channels, the optimum input covariance matrix that maximizes ergodic capacity for the ZMSW model is the scaled identity matrix $\mathbf{R_x} = (\rho/M)\,\mathbf{I}_M$, i.e., the transmit power is divided equally among all the transmit antennas and independent symbols are sent over the different antennas. Thus, the ergodic capacity is given by [41]

$$C = \mathrm{E}_{\mathbf{H}}\left[B\log_2 \det\left[\mathbf{I}_N + \frac{\rho}{M}\mathbf{H}\mathbf{H}^H \right]\right]. \qquad (2.23)$$

Since the capacity of the static channel grows as $L = \min(M, N)$, for L large, this will also be true of the ergodic capacity since it just averages the static channel capacity. When the channel is not ZMSW, capacity depends on the distribution of the singular

values for the random channel matrix: these distributions and the resulting ergodic capacity in this more general setting are studied in [64]. Fig. 2.7 [41] shows the ergodic capacity of a 4×4 MIMO system with iid complex Gaussian channel gains. This figure shows capacity with both transmitter and receiver CSI and with receiver CSI only. There is little difference between the two, and this difference decreases with SNR.

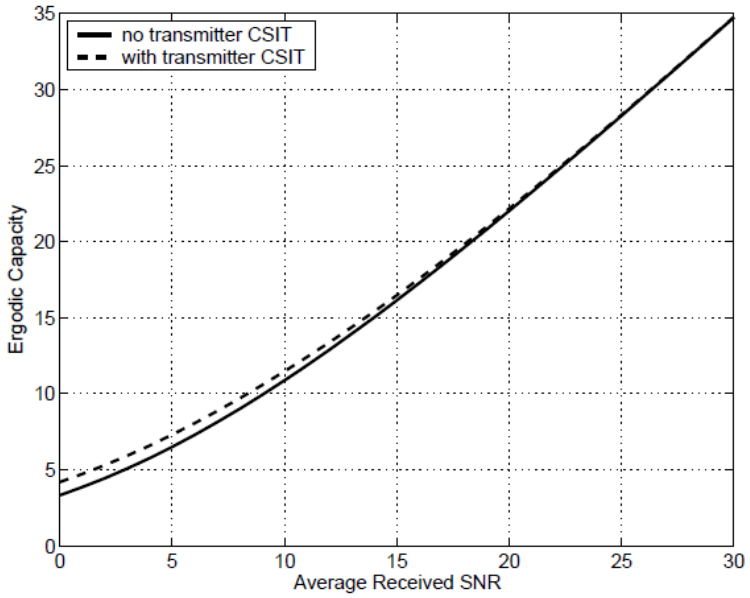

Fig. 2.7. Ergodic Capacity of 4×4 MIMO Channel.

When the channel gain matrix is unknown at the transmitter and the entries are complex Gaussian but not iid, then the channel mean or covariance matrix can be used at the transmitter to increase capacity. The basic idea is to allocate power according to the mean or covariance. This channel model is sometimes referred to as mean or covariance feedback. This model assumes perfect CSIR, and the impact of correlated fading depends on what is known at the transmitter. Although capacity with outage applies to a slowly-varying channel where the channel matrix **H** is constant over a relatively long transmission time, then changes to a new value, it is defined similar to the definition for static channels. As in the static channel case, the channel realization and corresponding channel capacity is not known at the transmitter, yet the transmitter must still fix a transmission rate to send data over the channel. For any

choice of this rate *C*, there will be an outage probability associated with *C*, which defines the probability that the transmitted data will not be received correctly. The outage capacity can sometimes be improved by not allocating power to one or more of the transmit antennas, especially when the outage probability is high [49]. This is because outage capacity depends on the tail of the probability distribution. With fewer antennas, less averaging takes place and the spread of the tail increases.

2.4 Equalization

Generally, delay spread causes intersymbol interference (ISI). ISI can cause an irreducible error floor when the modulation symbol time is on the same order as the channel delay spread. Signal processing provides a powerful mechanism to counteract ISI. In a broad sense, equalization defines any signal processing technique used at the receiver to mitigate the ISI problem caused by delay spread. Signal processing can also be used at the transmitter to make the signal less susceptible to delay spread. In the cases where the delay spread is small such as cordless phones typically operate indoors, since voice is also a relatively low date rate application, equalization is generally not needed. However, the IS-54 digital cellular standard is designed for outdoor use, where the delay spread is large, so equalization is part of this standard [41]. Higher data rate applications are more sensitive to delay spread, and generally require high-performance equalizers or other ISI mitigation techniques. In fact, mitigating the impact of delay spread is one of the most challenging hurdles for high-speed wireless data systems.

Equalizer design must typically balance ISI mitigation with noise enhancement, since both the signal and the noise pass through the equalizer, which can increase the noise power. Nonlinear equalizers suffer less from noise enhancement than linear equalizers, but typically entail higher complexity, as discussed in more detail below. Moreover, equalizers must typically have an estimate of the channel impulse or frequency response to mitigate the resulting ISI. In this section, the examples associated with linear and nonlinear equalizers are briefly described.

Equalization techniques fall into two broad categories: linear and nonlinear. The linear techniques are generally the simplest to implement and to understand conceptually. However, linear equalization techniques typically suffer from more noise enhancement than nonlinear equalizers, and are therefore not used in most wireless applications. Among nonlinear equalization techniques, the optimal equalization technique is maximum likelihood sequence estimation (MLSE). Unfortunately, the complexity of this technique grows exponentially with the length of the delay spread, and is therefore impractical on most channels of interest. However, the performance of the MLSE is often used as an upper bound on performance for other equalization techniques.

2.4.1 Minimum Mean Square Error (MMSE) Linear Equalizer

Generally, the performance metric in wireless systems is probability of error (or outage probability), so for a given channel, the optimal choice of equalizer coefficients would be the coefficients that minimize probability of error. Since desired performance metric is extremely difficult to be directly optimized, an indirect optimization that balances ISI mitigation with the prevention of noise enhancement must be used instead. Hence, linear equalizers, such as the Zero Forcing (ZF) equalizer [70, 71] and the Minimum Mean Square Error (MMSE) equalizer, are considered. The former equalizer cancels all ISI, but can lead to considerable noise enhancement. The latter technique minimizes the expected mean squared error between the transmitted symbol and the symbol detected at the equalizer output, thereby providing a better balance between ISI mitigation and noise enhancement. Because of this more favorable balance and MMSE equalizers tend to have better BER performance than equalizers using the ZF algorithm, MMSE is considered in this study as the example of linear equalizer.

In MMSE equalization as shown in Fig. 2.8 [41], the goal of the equalizer design is to minimize the average mean square error (MSE) between the transmitted symbol d_k and its estimate $\hat{d}_k$ at the output of the equalizer, In other words, the filter coefficients $\{w_i\}$ are chosen to minimize $\mathrm{E}[d_k - \hat{d}_k]^2$.

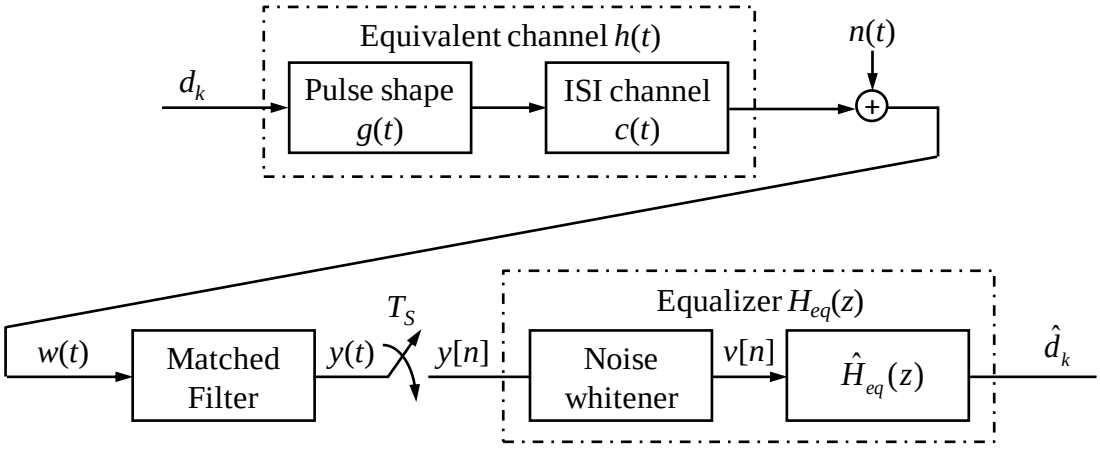

Fig. 2.8. MMSE equalizer with noise whitening filter.

The purpose of the noise whitening filter, as indicated by the name, is to whiten the noise such that the noise component output from this filter has a constant power spectrum. It might seem odd at first to introduce the matched filter at the receiver front end only to cancel its effect in the equalizer. However, that the matched filter is meant to maximize the SNR prior to sampling. By removing the effect of this matched filter through noise whitening after sampling, we merely simplify the design $\hat{H}_{eq}(z)$ to minimize MSE. Hence, the ideal infinite length MMSE equalizer cancels out the noise whitening filter and it is identical to the ZF filter in the absence of noise. This ideal equalizer can also show a balance between inverting the channel and noise enhancement.

2.4.2 Maximum Likelihood Sequence Estimation (MLSE) Nonlinear Equalizer

Maximum-likelihood sequence estimation (MLSE) avoids the problem of noise enhancement since it does not use an equalizing filter. Instead, it estimates the sequence of transmitted symbols. The structure of the MLSE is the same as in Fig. 2.8 except that the equalizer $H_{eq}(z)$ is replaced by the MLSE algorithm. Given the channel response $h(t)$, the MLSE algorithm chooses the input sequence $\{d_k\}$ that maximizes the likelihood of the received signal $w(t)$. In the other words, since $w(t)$ depends on d_0, …, d_L , the MLSE decodes this as the symbol sequence d^L that maximizes the likelihood function or the log of this function.

Furthermore, since the derivation of the MLSE is based on the channel output $w(t)$ only (prior to matched filtering), derivation in [41] implies that the receiver matched filter in Fig. 2.8 is optimal for MLSE detection (typically the matched filter is optimal for detecting signals in AWGN, but this derivation shows that it is also optimal for detecting signals in the presence of ISI if MLSE is used). However, it is noted that the complexity of this equalization technique grows exponentially with the channel delay spread.

Although MLSE is the optimal form of equalization, its complexity precludes its widespread use. There has been much work on reducing the complexity of the MLSE [72]. Most of these techniques reduce the number of symbols spanned by the ISI through preprocessing or decision-feedback in the detector. These reduced complexity equalizers have better performance versus complexity tradeoffs than the other equalization techniques, and achieve performance close to that of the optimal MLSE with significantly less complexity.

If the channel is known at the transmitter, then the transmitter can pre-equalize the transmitted signal by passing it through a filter that effectively inverts the channel frequency response. Since the channel inversion occurs in the transmitter rather than the receiver, there is no noise enhancement. It is difficult to pre-equalize in a time-varying channel since the transmitter must have an accurate estimate of the channel, but this approach is practical to implement in relatively static wireline channels. A problem with this approach is that the channel inversion can increase the dynamic range of the transmitted signal, which can result in distortion or inefficiency from the amplifier [73].

Chapter 3 System Models and Analysis Methods

In this chapter, all the analysis models, including the different arranged dual-dipole arrays' models and the arrays with different objects in the system are introduced. The evaluation methods concerning all parameters which are considered throughout this study such as the eigenvalue, spatial correlation, and channel capacity in near-field MIMO, are respectively described.

3.1 Array Elements

Contrary to conventional MIMO systems, near-field MIMO communication systems transfer data in a very short range [74], and the LOS (line-of-sight) paths are the major components [75, 76]. Considering the short distance, the LOS components from each of the Tx elements arrive at the Rx array with a spherical wavefront [21]. Therefore the beamwidth of the antenna element radiation pattern affects not only the receiving gain but also the spatial correlation characteristics. Consequently, the impact of the radiation pattern of each antenna element can't be neglected. Usually, the conventional dipole antennas are used to investigate the MIMO channel capacity. However, the conventional dipoles are omni-directional in the horizontal plane. Therefore, it is very necessary to discuss the effect of the array's elements in the near-field MIMO system.

3.1.1 Conventional Elements of Near-Field MIMO

Before introducing the utilized array element, dual-dipole element, we will make a glance at the conventional array elements used before.

A. Conventional Single Dipole Element

In the existing researches, the most widely used array element is the conventional single dipole element. A dipole antenna is a straight electrical conductor measuring 1/2 wavelength from end to end and connected at the center to a radio-frequency (RF) feed line. As we know, the dipole antenna is one of the simplest types of antenna, and constitutes the main RF radiating and receiving element in various sophisticated types of antennas. The dipole is inherently a balanced antenna, because it is bilaterally symmetrical [78].

Dipoles have a radiation pattern, shaped like a toroid (doughnut) symmetrical about the axis of the dipole, as shown in Fig. 3.1. The radiation is maximum at right angles to the dipole, dropping off to zero on the antenna's axis.

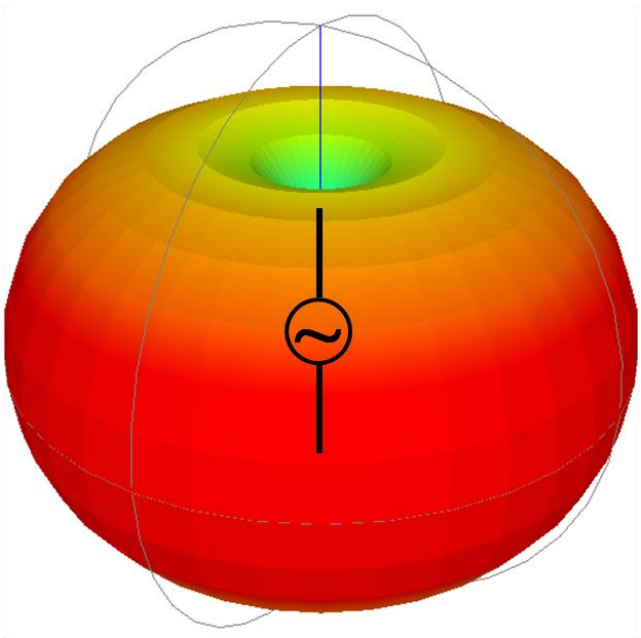

Fig. 3.1. The conventional single dipole and its 3-D radiation pattern.

Obviously, the conventional dipoles are omni-directional in the horizontal plane. Hence, the conventional dipole can be used in the conventional far-field MIMO with confident. However, in the near-field MIMO, the distance between the transmitting antenna and the receiving antenna is very short, then this omni-directional pattern antenna will leak most power on the other directions.

Therefore, the conventional single dipole element is not the proper choice for the near-field MIMO system.

B. Patch Antenna Element

Besides the conventional single dipole antenna, the patch antenna is also very popular to be used in the near-field MIMO system. A patch antenna (also known as a *rectangular microstrip antenna*) [78, 79] is a type of radio antenna with a low profile, which can be mounted on a flat surface. It consists of a flat rectangular sheet or "patch" of metal, mounted over a larger sheet of metal called a ground plane. The assembly is usually contained inside a plastic radome, which protects the antenna structure from damage. Patch antennas are simple to fabricate and easy to modify and customize. They are the original type of microstrip antenna, the two metal sheets together form a resonant piece of microstrip transmission line with a length of approximately one-half wavelength of the radio waves. The radiation mechanism arises from discontinuities at each truncated edge of the microstrip transmission line. The radiation at the edges causes the antenna to act slightly larger electrically than its physical dimensions, so in order for the antenna to be resonant, a length of microstrip transmission line slightly shorter than one-half a wavelength at the frequency is used. A patch antenna is usually constructed on a dielectric substrate, using the same materials and lithography processes used to make printed circuit boards.

Comparing with the conventional single dipole antenna, the radiation pattern of a patch antenna element constrains the gain of the pattern in one side, as shown in Fig. 3.2. Hence, the channel capacity of the near-field MIMO with the patch antenna elements will enhance. However, once the patch antenna is chosen, the beamwidth of the radiation pattern is settled. The purpose of this research is to investigate the effect of the radiation pattern of the array element, therefore, the patch antenna element is also not the appropriate array element.

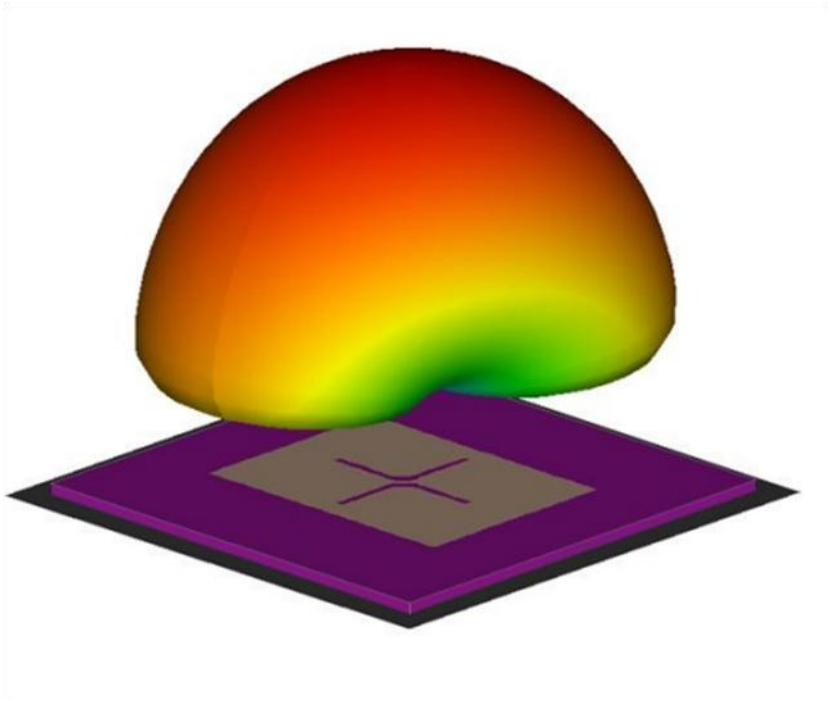

Fig. 3.2. A typical patch antenna and its 3-D radiation pattern.

3.1.2 Dual-Dipole Element

In order to construct a model that enables us to change the beamwidth of the radiation pattern, we arrange two dipoles in parallel on the Tx side as one element as shown in Fig. 3.3. The new element is named as dual-dipole [80] element, which can adjust the beam width of the element radiation pattern by changing the internal distance between two dipoles in one element, denoted as Δd. In addition, the transmission power of each dual-dipole element is constrained as the same as that for a conventional dipole element.

To measure the change of the beam width in the radiation pattern, we use the HPBW (half power beam width) in this research. The HPBW is the angular separation at which the power of the radiation pattern decreases by 50% (or -3 dB) from the peak of the main beam as shown in Fig. 3.4. This research is in the near-field region, but the HPBW [81] can be defined only in the far-field radiation pattern. To explain the definition of the HPBW, the far-field radiation pattern is utilized in this paper.

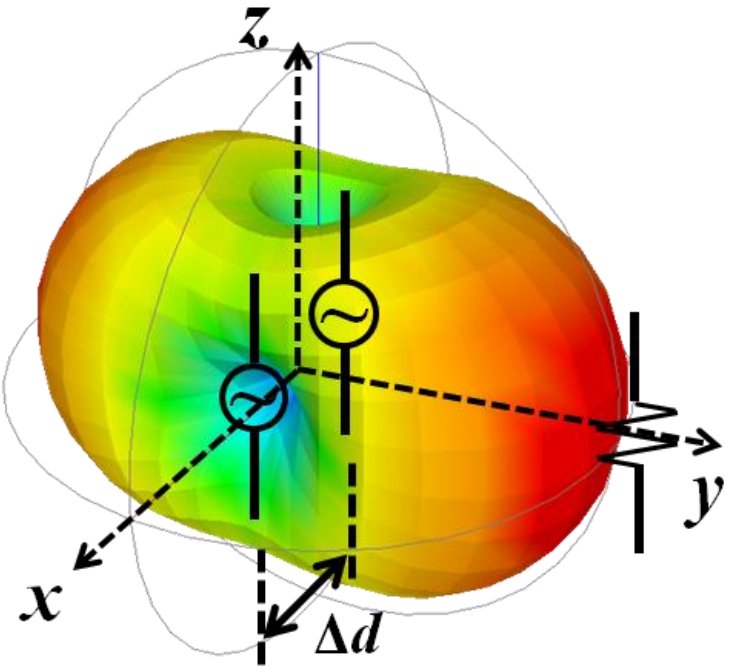

Fig. 3.3. Dual-dipole element and its 3-D radiation pattern.

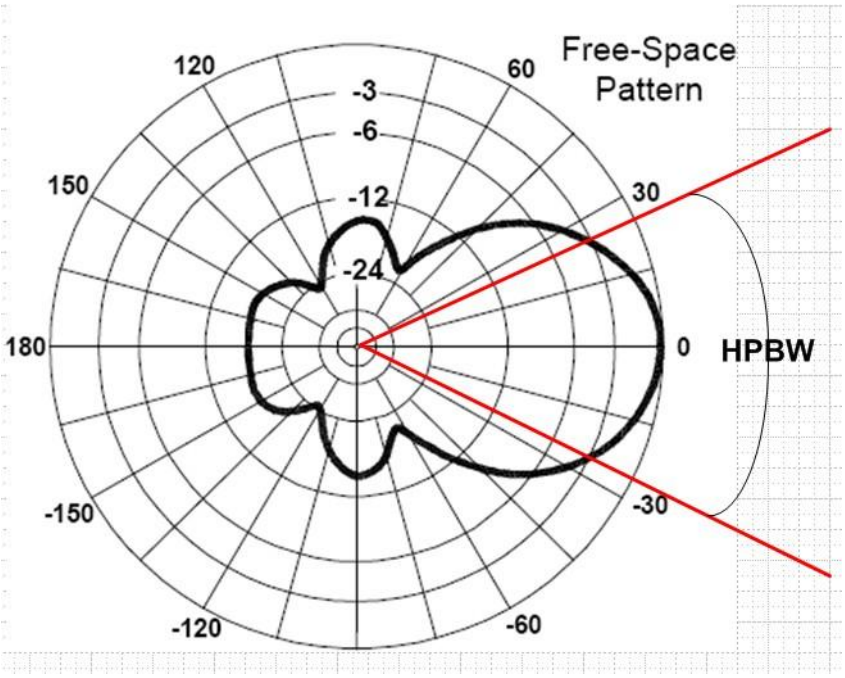

Fig. 3.4. Definition of HPBW.

The 3-D radiation pattern of a dual-dipole element is shown in Fig. 3.3. We note that, the receiver antenna is in the *y* direction, so the *x*-*z* plane pattern does not need to be considered. By changing the distance between the two dipoles in one element, Δd, we find that the *y*-*z* plane pattern hardly changes. The Δd can only control the HPBW of the *x*-*y* plane (horizontal plane) pattern, so we should focus on the HPBW of the *x*-*y* plane pattern. Hereafter, the HPBW of the *x*-*y* plane is used to judge the change in the radiation pattern.

The relation between Δd and the HPBW of the *x*-*y* plane is shown in Fig. 3.5. Generally speaking, as the Δd becomes larger, the HPBW changes smaller. However, when HPBW is less than 50º (the corresponding Δd increases over about $0.6\lambda_0$), the side lobes will occur. The side lobes will carry off some power from the main beam, and lead to more spatial correlation in the horizontal array. To avoid the effect of side lobes, the HPBW in this paper is considered only larger than 50 º(the corresponding Δd is from $0.2\lambda_0$ to $0.6\lambda_0$) when using the dual-dipole arrays. Here, when the radiation pattern has no obvious main beam, we set the HPBW to be 180 º.

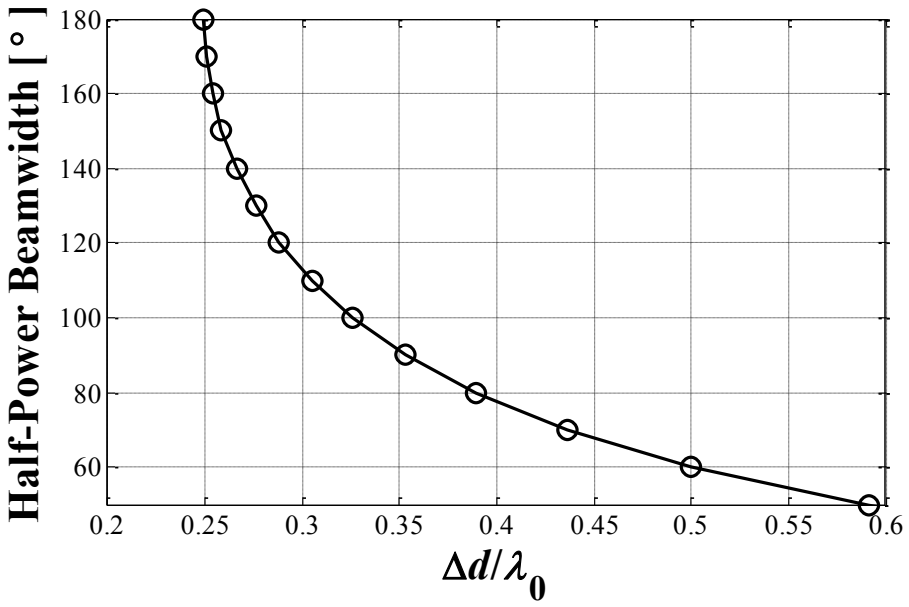

Fig. 3.5. Relation between Δd and HPBW.

3.2 Dual-Dipole Array Models

3.2.1 Array Arrangements

The near-field MIMO analysis models used in this paper are basically consists of dual-dipole elements. Due to the different gain of the *x* and *y* directions in the radiation pattern shown in Fig. 3.3, the different performances when the dual-dipole elements is arranged in different methods are expected. Therefore, the analysis models in this dissertation are considered in two types of arrangements, the horizontal arranged linear array and the vertical arranged linear array.

Two linear arrays consisting of identical half-wavelength dipole antennas are placed parallel face-to-face as the transmitter and receiver. Since the Tx and Rx antennas are placed at a very short distance from each other, the shape of the radiation pattern is a significant component that affects the channel capacity. The numbers of antenna elements on Tx side M_T and on Rx side M_R are set to be the same, i.e., four. The distance between the transmitter and the receiver is defined as antenna distance *D*, the distance between two adjacent antenna elements is denoted as element spacing *d*, and the internal distance between the two dipoles in one transmitter element is defined as Δd. In addition, the transmission power of each dual-dipole element is constrained as the same as that for a conventional dipole element.

A. Horizontal Array

The horizontal arranged linear array is shown in Fig. 3.6. Two linear arrays consisting of identical half-wavelength dipole antennas are placed parallel face-to-face as the transmitter and receiver. The transmitting antenna array consists of dual-dipole elements, in the other hand, the receiving antenna array is composed of conventional single dipole element. The adjacent elements are arranged in a horizontal line.

Since the Tx and Rx antennas are placed at a very short distance from each other, the shape of the radiation pattern is a significant component that affects the channel capacity. The numbers of antenna elements on Tx side M_T and on Rx side M_R

are set to be the same, i.e., four. The distance between the transmitter and the receiver is defined as antenna distance *D*, the distance between two adjacent antenna elements is denoted as element spacing *d*, and the internal distance between the two dipoles in one transmitter element is defined as Δd. In addition, the transmission power of each dual-dipole element is constrained as the same as that for a conventional dipole element.

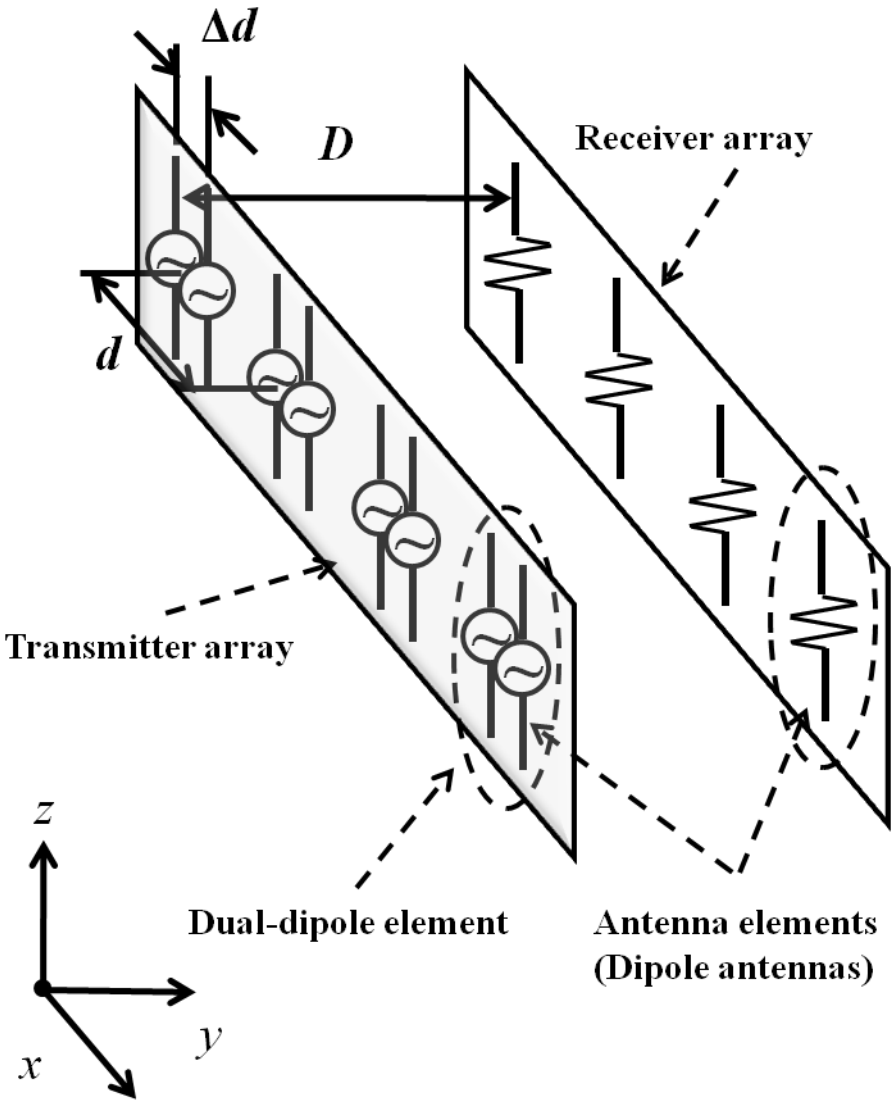

Fig. 3.6. Analysis model of horizontal arranged dual-dipole array.

B. Vertical Array

The horizontal arranged linear array is shown in Fig. 3.7.

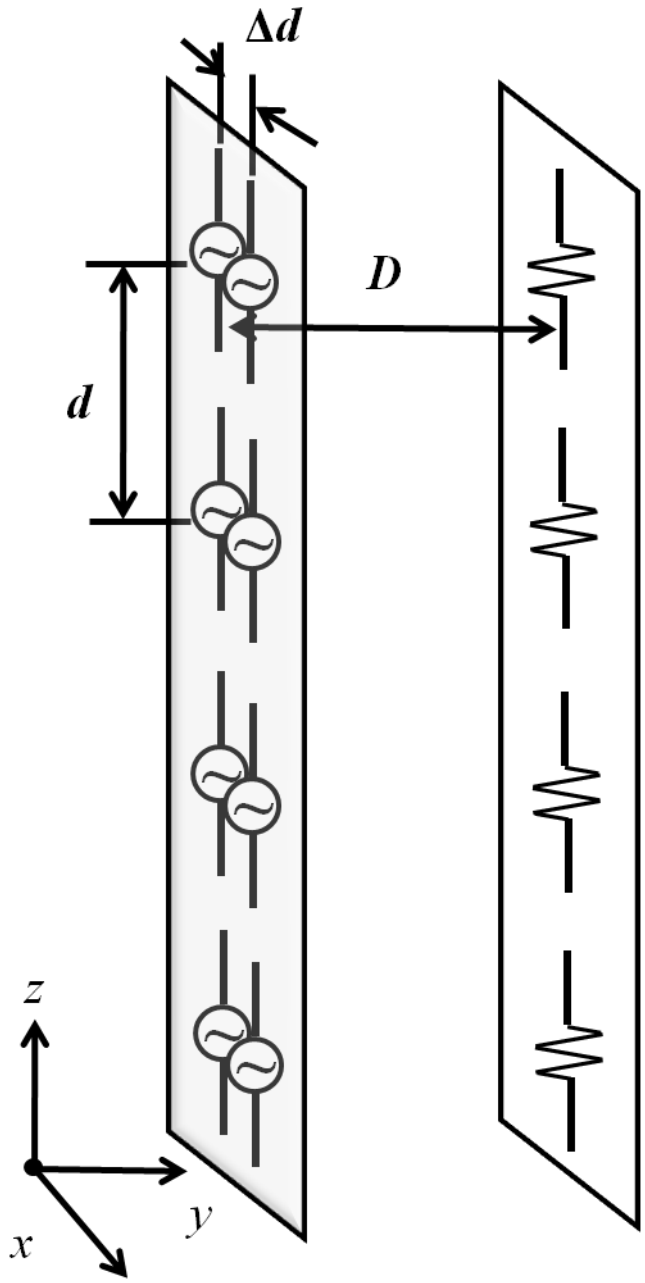

Fig. 3.7. Analysis model of vertical arranged dual-dipole array.

Two linear arrays consisting of identical half-wavelength dipole antennas are placed parallel face-to-face as the transmitter and receiver. The transmitting antenna

array consists of dual-dipole elements, in the other hand, the receiving antenna array is composed of conventional single dipole element. The adjacent elements are arranged in a vertical line. And the measurements of the vertical array are denoted by the same parameters in the horizontal one.

3.2.2 Arrays' Location Errors

In the previous models, the transmission antennas are placed face to face. However, in a practical application the opposing antennas cannot always be placed in the ideal position. Since the antenna distance is fairly short, a slight deviation or bias of the receiver antenna to the transmitter antenna may significantly affect the channel capacity. Therefore, we address the deterioration in the channel capacity caused by antenna location errors in this subsection.

Considering a practical application where the near-field MIMO is used to transmit data through a wall as shown in Fig. 2.2(c), the antenna distance is constant (the thickness of the wall) and the two planes including the transmitter and receiver are parallel to each other. Hence, the antenna location errors are limited considering the offset error in the x and z directions and rotational error around the y axis.

A. Offset Errors

The analysis models of the dual-dipole array with offset error are shown in Fig. 3.8. The horizontal array and the vertical array are shown respectively. The offset error is only considered in the x and z directions because the offset in the y direction can be involved in the change of antenna distance D. In addition, the scenarios of the models are assumed through a wall, so the distance in y direction indicates the thickness of the wall, which is fixed. And the offset errors in the x and z directions are denoted by Δx and Δz, respectively.

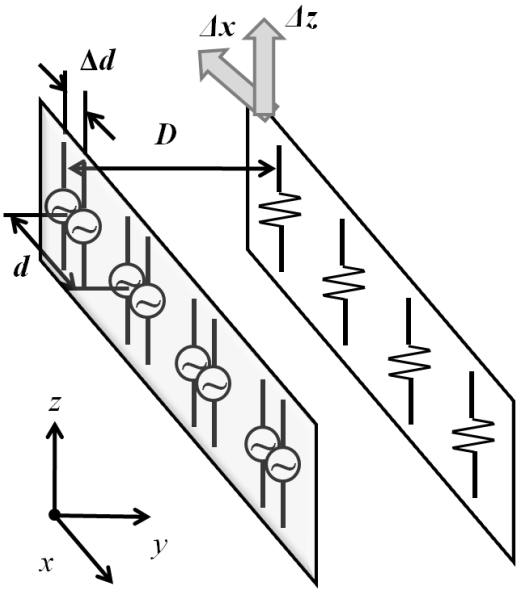

(a) Horizontal array

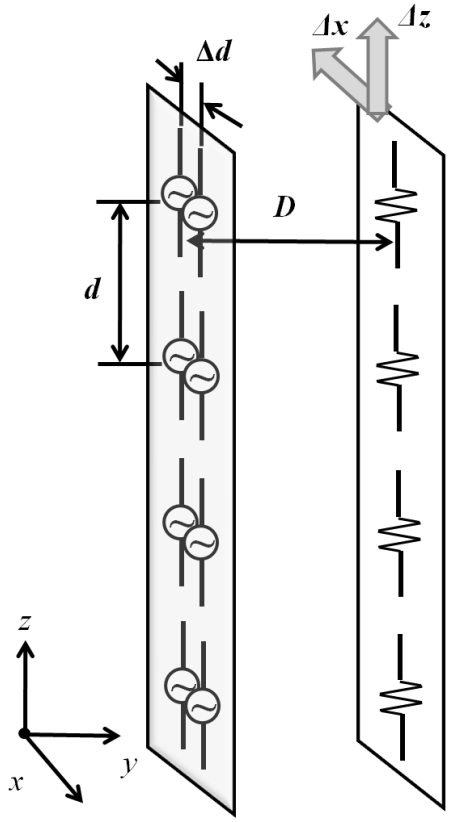

(b) Vertical array

Fig. 3.8. Analysis model of offset errors in dual-dipole array.

B. Rotational Errors

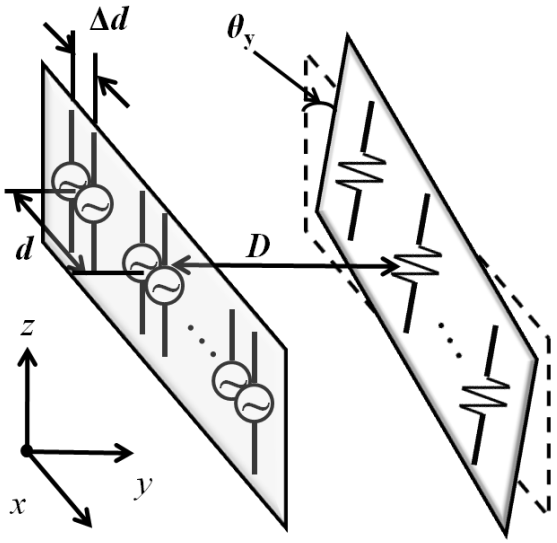

(a) Horizontal array

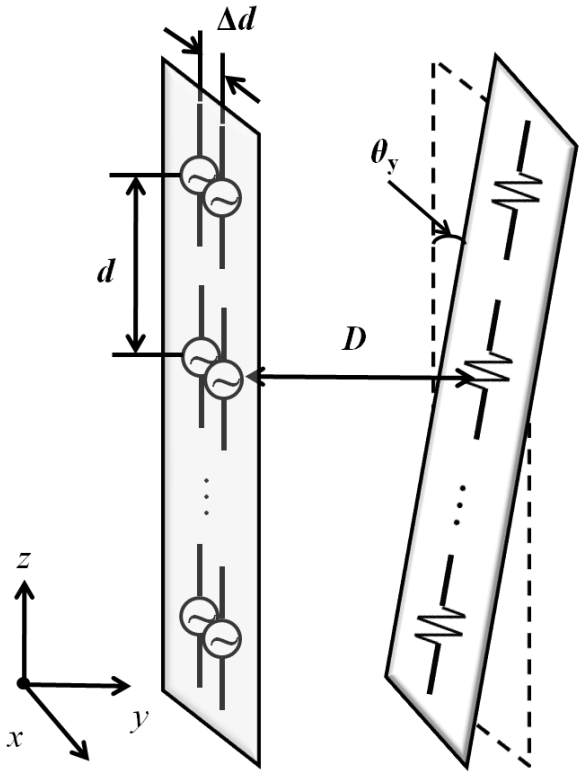

(b) Vertical array

Fig. 3.9. Analysis model of rotational errors in dual-dipole array.

The analysis models of the dual-dipole array with offset error are shown in Fig. 3.9. The horizontal array and the vertical array are shown respectively. The rotational error is only considered in the *y* direction because the array on the wall can't change its rotation in *x* and *z* directions. And the rotational errors in the *y* directions are denoted by θ_y.

3.3 Array with Objects

Due to the short transfer distance of the near-field MIMO, a tiny variation of the channel will lead to a significant difference on the channel capacity. Therefore, we employ objects in the near-field MIMO system to increase the multipath richness and clarify the effect of obstacles in the system.

3.3.1 Array with a Single Metal Wire

In the practical application, the objects between the transmitting antennas and the receiving antennas might be the wall, so the effect of the metal wires in the wall is very necessary to be investigated. For the basic discussion, first of all, only one single metal wire is added in the dual-dipole array near-field MIMO system. Considering the effect of antennas' polarization, only when the metal wire is parallel with the dipoles, the metal wire will affect the system channel capacity most significantly, the analysis models abandon the case when the metal wire is perpendicular to the dipoles. The models of horizontal array and the vertical array with single metal wire are described respectively.

A. Horizontal Array

A model of the horizontal dual-dipole arrays with a metal wire is shown in Fig. 3.10. The antenna parameters are set the same as those in the previous subsections. The metal wire is placed near the opposing arrays, and is parallel to the dipoles. The length for the metal wire, is denoted as *L*. For discussing the effect of the location of the metal wire in the system, the metal wire is moved around the antenna arrays. The terms Δx_{mw} and Δy_{mw} denote the offset in the *x* and *y* directions, respectively.

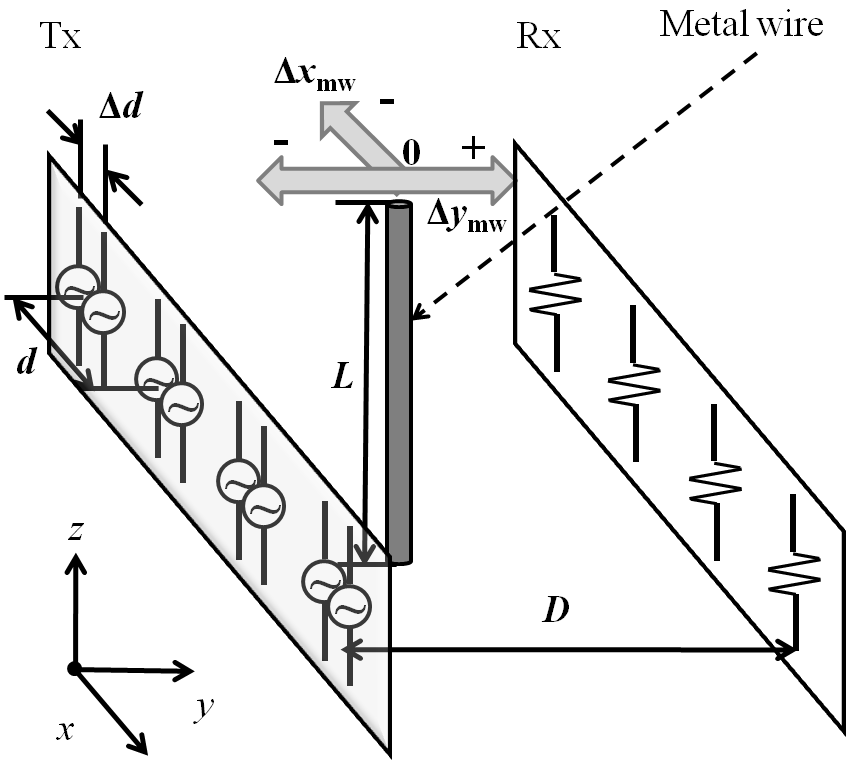

(a) Configuration of model

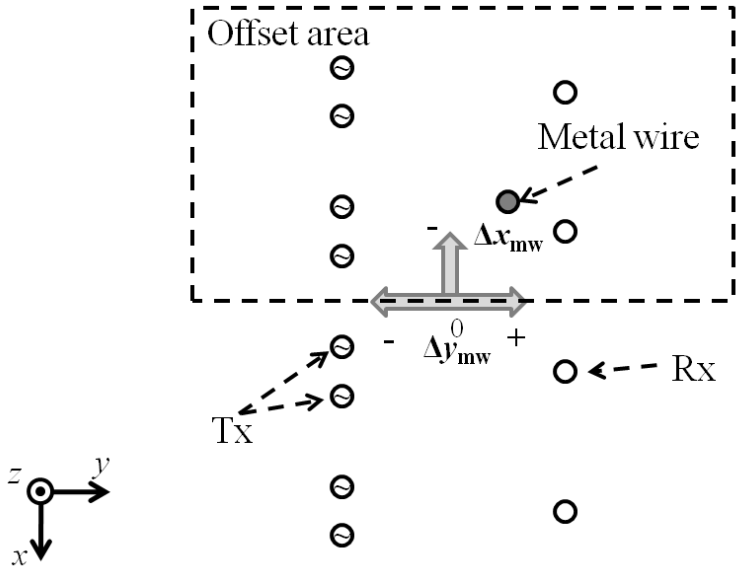

(b) Top view of model

Fig. 3.10. Analysis model of horizontal dual-dipole array with single metal wire.

Since the top view of the horizontal array is symmetrical, the offset area is considered to be only the upper half, as shown in Fig. 3.10(b). The center of the system is set as the origin of the offset for the metal wire. Especially, in the *y* direction, when the metal wire is close to the transmitter array, Δy_{mw} is defined as '-', and when it is close to the receiver array, Δy_{mw} is defined as '+'.

B. Vertical Array

A model of the vertical dual-dipole arrays with a metal wire is shown in Fig. 3.11. The antenna parameters are set the same as those in the previous subsections. Since the top view of the vertical array is also symmetrical, the offset area is considered to be only the upper half, as shown in Fig. 3.11(b).

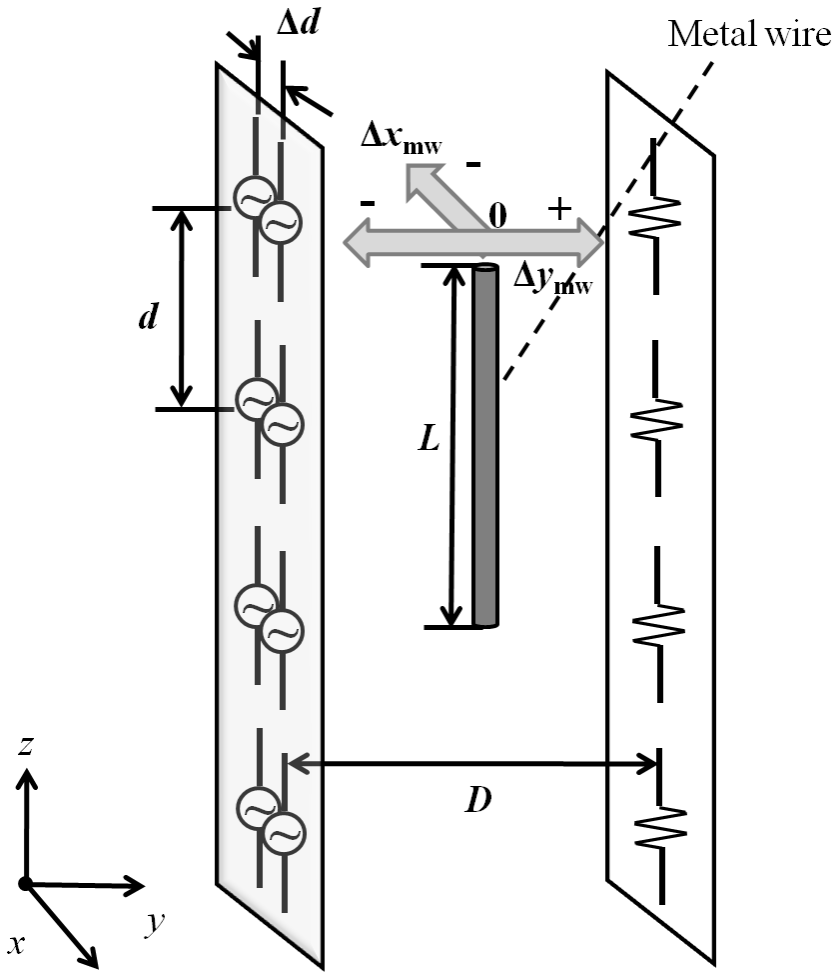

(a) Configuration of model

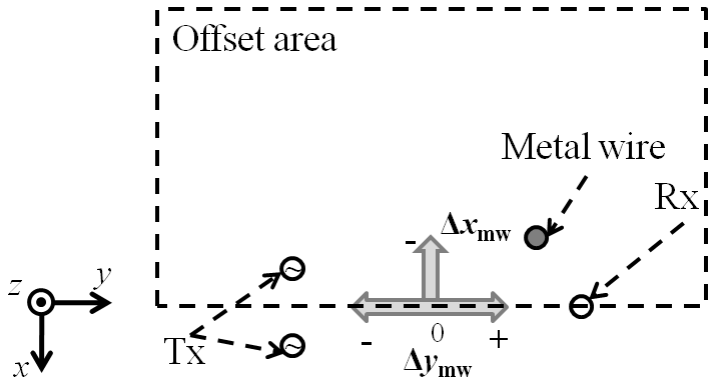

(b) Top view of model

Fig. 3.11. Analysis model of vertical dual-dipole array with single metal wire.

3.3.2 Array with Multiple Metal Wires

For further discussion on the effect of metal wire, the effect of the multiple metal wires on channel capacity in the system is also researched. In this discussion, besides the horizontal and vertical arrays, the square array with dual-dipole elements is also proposed. The reason of utilizing the square array will be explained in Chapter 5 in detail. The models of the arrays with multiple metal wires are shown in Fig. 3.12. All the metal wires are placed in the proper locations of the system.

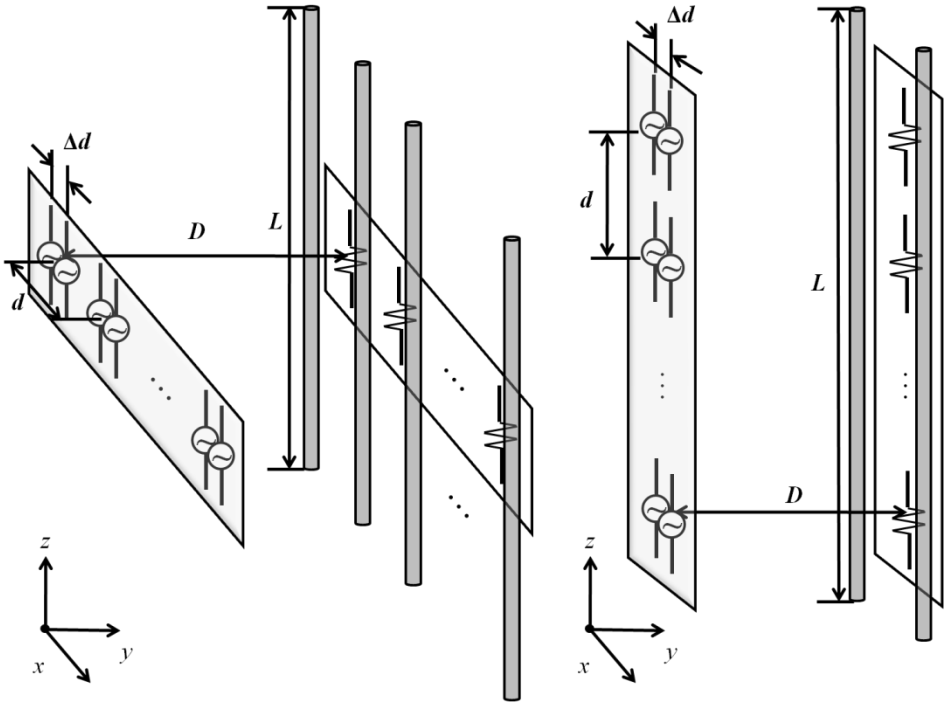

(a) Horizontal array (b) Vertical array

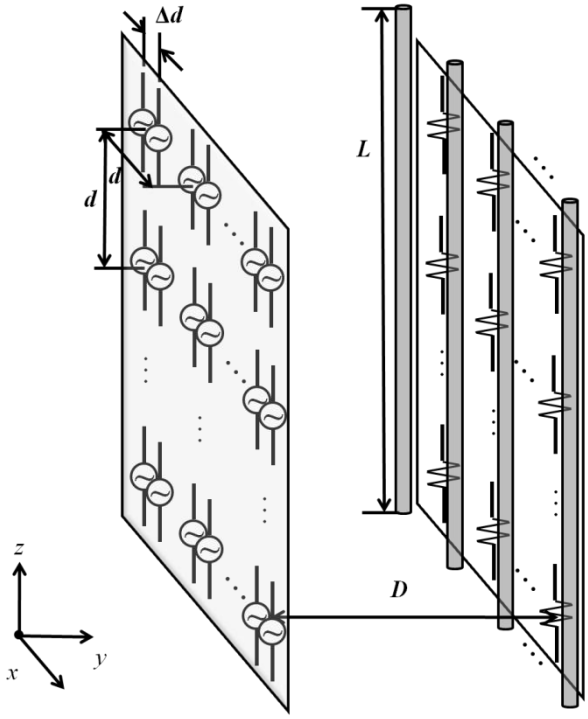

(c) Square array

Fig. 3.12. Analysis model of arrays with multiple metal wires.

3.4 Evaluation Methods

The performance of urban MIMO systems considered throughout this study is dealt with many parameters, such as the SNR, spatial correlation, eigenvalue and finally the channel quality is judged by the channel capacity. For an intuitive understanding of the near-field MIMO channel, the definitions of these parameters are first introduced in this section.

3.4.1 Eigen Value

The Singular Value Decomposition (SVD) is an elegant tool to analyze MIMO systems. It is capable of identifying the independent spatial excitation modes that are intrinsic to the channel. Consider a MIMO channel, $\boldsymbol{H}$, with N_t and N_r antennas at transmitter and receiver respectively. Define $m = \min(N_t;N_r)$, $n = \max(N_t;N_r)$ and $l = n - m$. By using the SVD, $\boldsymbol{H}$ can be expressed as [21, 82]

$$H = U\Lambda V^{\dagger} \tag{3.1}$$

where $U \in C^{N_r \times N_r}$ and $V \in C^{N_t \times N_t}$ are unitary matrices, and $[\cdot]^{\dagger}$ represents Hermitian transpose. Λ is a diagonal matrix whose diagonal elements $s_1 \geq s_2 \geq \cdots \geq s_m$ are the positive *singular values* of the channel matrix *H*. The non-diagonal elements of Λ are all zero and *m* is the rank of *H*. It is easy to show that the squared singular values, s_i^2, are the eigenvalues of the instantaneous correlation matrix $HH^{\dagger}$, since

$$HH^{\dagger} = U\Lambda\Lambda^{\dagger}U^{\dagger} \tag{3.2}$$

Moreover, the columns of *U* are eigenvectors of $HH^{\dagger}$ and the columns of V are eigenvectors of $H^{\dagger}H$.

In terms of pure mathematics, the rank of matrix *H* is said to be *m* as there are *m* positive singular values with probability one. In the context of MIMO communication engineering, however, the rank of *H* is usually defined as the number of significant singular values. In general, the Rayleigh i.i.d channel is anticipated to be "full rank" as the average magnitude of all *m* singular values are reasonably high.

The components of the diagonal matrix Λ represent the square roots of the eigenvalues [83, 84], and can be expressed as,

$$\Lambda = \begin{pmatrix} \sqrt{\lambda_1} & \cdots & 0 \\ \vdots & \ddots & \vdots \\ 0 & \cdots & \sqrt{\lambda_m} \end{pmatrix} \tag{3.3}$$

When decomposed in this manner, the propagation path for a MIMO channel can be represented as in Fig. 3.13 where (a) shows the equivalent circuit representing channel matrix, and (b) is the equivalent circuit represented in SVD. It is clear that the MIMO channel comprises a maximum of *m* independent transmission paths. In this context, the term "maximum" refers to the maximum possible number of actual paths. If there are multiple paths for which the eigenvalue is 0, the number of paths will be reduced even further. Such virtual paths are referred to as eigenpaths. The amplitude gain for each unique path is $\sqrt{\lambda_i}$, and it varies according to its eigenvalue. Thus, the MIMO channel possesses the capacity to transmit *m* independent streams of signals without cross-talk. Figure 3.14 shows the specific configuration of an eigenmode transmission scheme [15].

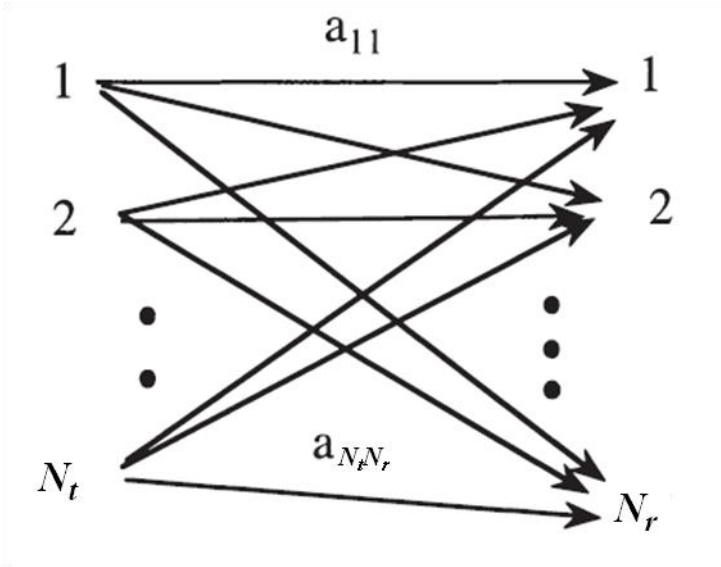

(a) Channel response matrix

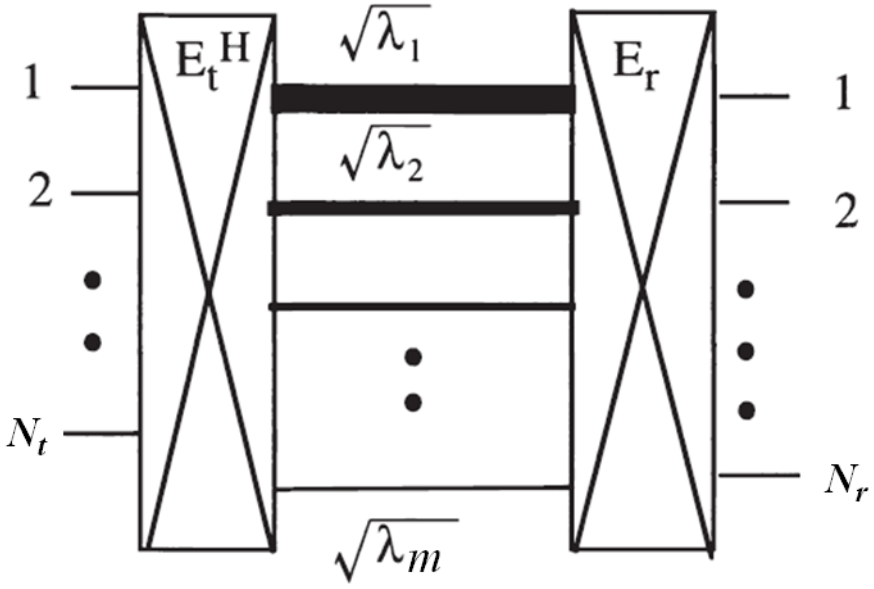

m=min(N_t;N_r)

(b) Equivalent circuit based on SVD

Fig. 3.13. Equivalent circuit of MIMO channel based on SVD.

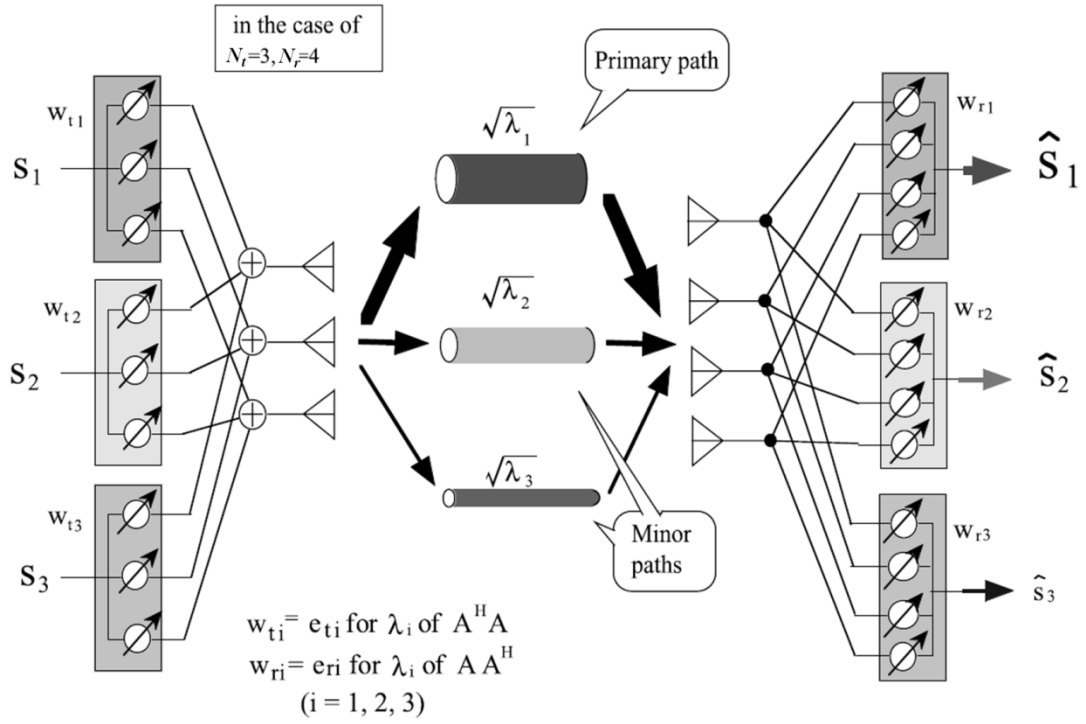

Fig. 3.14. Parallel data transmission scheme through each eigenpath.

3.4.2 Spatial Correlation

In multi-element antenna systems, spatial correlation is a measure of relationship between two antennas' signals. The ideal huge capacity anticipated by a MIMO system can be realizable if there is no spatial correlation. However, in real propagation environments, MIMO channels are correlated due to low scattering and reduced spatial selectivity. Correlated channels of MIMO reduce the high-capacity potential considerably, suggesting that MIMO systems should be designed with low or no correlation [85-87].

Design of systems with low correlation requires a full investigation of underlying parameters that strengthen spatial correlation. The analysis in this article presents spatial correlation as a function of an antenna's spatial structure, AoA distribution, mutual coupling, and antenna patterns. Each of these parameters play a decisive role in the analysis.

Mathematically, the spatial correlation coefficient between two antennas can be expressed as

$$\rho_{ij} = \left| \frac{\sum_{m=1}^{M} h_{im} h_{jm}^{*}}{\sqrt{\sum_{m=1}^{M} |h_{im}|^2} \sqrt{\sum_{m=1}^{M} |h_{jm}|^2}} \right|. \quad (3.4)$$

where h_{ij} is a component of channel matrix $\boldsymbol{H}$, and the channel response between the j-th transmitting antenna and the i-th receiving antenna. It is noted that i, j = 1,2,3,4 in the case of 4×4 MIMO.

MIMO channels can bear spatial correlation due to low scattering and reduced spatial selectivity. The impact of correlation on the capacity of a MIMO system is usually analyzed through the eigenvalues of $\boldsymbol{HH}^{\mathbf{H}}$**.** The eigenvalues reveal the degree of independence between channels or the effective number of parallel channels.

Analyses show that the capacity of a MIMO system is greatly diminished by the spatial correlation [88]**.** Due to spatial correlation, the number of independent channels is reduced. In the extreme case, when all the channels are correlated, the capacity reduces to that provided by a single transmit and receive antenna. Hence, systems with lower spatial correlation are highly desired. Although mutual coupling reduces the correlation, it also causes a lower SNR by decreasing the effective gain of antennas.

In the near-field MIMO communications, the facing Tx and Rx antennas can transfer multiple streams without any degeneracy since the two antenna elements directly communicated with each other. This topology forms, in effect, as many parallel transmission channels as there are antennas. Then channels are not perfectly parallel because of leakage, but the signals from non-facing antenna elements have different phases and amplitudes from that of the facing one since the optical path differences between them are not negligible. For this reason, we can expect low spatial correlation characteristics even without multipath components.

3.4.3 Channel Capacity

The Eigen-mode Transmission System (EMTS), which is MLSE-like algorithm and has been employed in many studies about MIMO systems [89, 90], is herein considered as an optimal equalization. As mentioned in Section 2.4, the decoding complexity of this MLSE-like algorithm can be reduced by using a linear filter to separate the transmitted data streams and then decode each stream independently. Hence, the linear MMSE equalization, which is used to mitigate the intersymbol interference (ISI) and noise enhancement, is also considered herein.

Assume that the Channel State Information (CSI) between the transmitting and receiving antennas is not known by the transmitting antenna. Referring back to Sections 2.3 and 2.4, in such a case, when the adaptive control for the weight coefficients is MMSE, the channel capacity can be obtained in units of bit/second/Hertz (bps/Hz) using [91]

$$C_{MMSE} = -\sum_{m=1}^{M} \log_2 \left(1 - \mathbf{h}_m^H \left(\mathbf{H}\mathbf{H}^H + \frac{M}{\gamma_0} \mathbf{I}_N \right)^{-1} \mathbf{h}_m \right). \qquad (3.5)$$

The upper subscript H denotes the Hermitian transposition, and $\mathbf{h}_m$ denotes the m-th column of $\mathbf{H}$.

By using EMTS with equal power control, the channel capacity of MIMO can be obtained using [92]

$$C_{EMTS} = \sum_{m=1}^{M} \log_2 \left(1 + \frac{\gamma_0}{M} \lambda_m \right), \qquad (3.6)$$

or simply in terms of $\mathbf{H}$ as

$$C_{EMTS} = \log_2 \det \left[\mathbf{I} + \gamma_0 \mathbf{H}\mathbf{H}^H \right]. \qquad (3.7)$$

The term λ_m represents the eigenvalue that is obtained by the matrix of $\mathbf{H}\mathbf{H}^H$. The channel response matrices are determined from the matrices of amplitude and phase

of the received signal at each receiving antenna from each transmitting antenna, and obtained by tracing the ray into the propagation model. The channel capacity is then obtained by deriving the average SNR.

Chapter 4 Channel Capacity Characteristics of Near-Field MIMO Systems

In this chapter, the impact of the radiation pattern of each antenna element in near-field MIMO system is researched. The dual-dipole arrays are utilized to investigate the effect of HPBW (half-power beamwidth) on channel capacity. The HPBW can be changed by varying the internal distance between two dipoles in one element. With a proper HPBW of the antenna element, the channel capacity of a dual-dipole array is improved obviously from a conventional dipole array. And the optimum HPBW is found to be approximately 50°. In addition, we also address the deterioration in the channel capacity caused by antenna location errors in this chapter.

4.1 Effect of HPBW on Channel Capacity in Near-Field MIMO Systems

Considering the very short distance between transmitter and receiver in the near-field MIMO system, the impact of the radiation pattern of each antenna element is not neglectable. Contrary to conventional MIMO systems, near-field MIMO communication systems transfer data in a very short range [19], and the LOS paths are the major components [20, 21]. Therefore the beamwidth of the antenna element radiation pattern affects not only the receiving gain but also the spatial correlation characteristics. Consequently, the impact of the radiation pattern of each antenna element can't be neglected. Usually, the conventional dipole antennas are used to investigate the MIMO channel capacity. However, the conventional dipoles are omni-directional in the horizontal plane. Therefore, it is very necessary to discuss the effect of the elements radiation pattern in the near-field MIMO system. The effect of HPBW on channel capacity will be clarified very well in the section.

4.1.1 Channel Capacity Characteristics in Conventional Single Dipole Arrays

Before investigating the channel capacity of the dual-dipole arrays, we will make a briefly research at the conventional single dipole arrays. For comparing the different performances on channel capacity in the near-field MIMO system with different antenna elements, and also for highlighting the advantages of the utilization of dual-dipole elements, the models of near-field MIMO system with conventional single dipole elements are applied.

The conventional single dipole arrays' analysis models used in this chapter are shown in Fig. 4.1. Two linear arrays consisting of identical half-wavelength dipole antennas are placed parallel face-to-face as the transmitter and receiver, respectively. The number of antenna elements in both ends are set the same as $M_T=M_R=M$. The distance between two adjacent antenna elements is denoted as element spacing d, and the distance between the transmitter and the receiver is defined as antenna distance D.

Considering that the dipole antenna has an omni-distributional radiation pattern rather than an isotropic pattern [99-103], the array antennas are arranged in two types, horizontal and vertical. They are placed in the same arrangements as the model in Figs. 3.6 and 3.7. At the transmitting array, the equal transmitting power is fed on each antenna element, respectively.

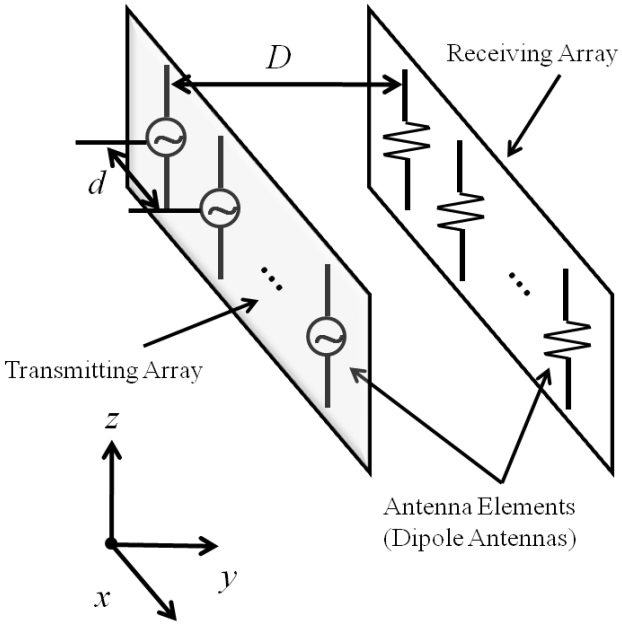

(a) Horizontal array

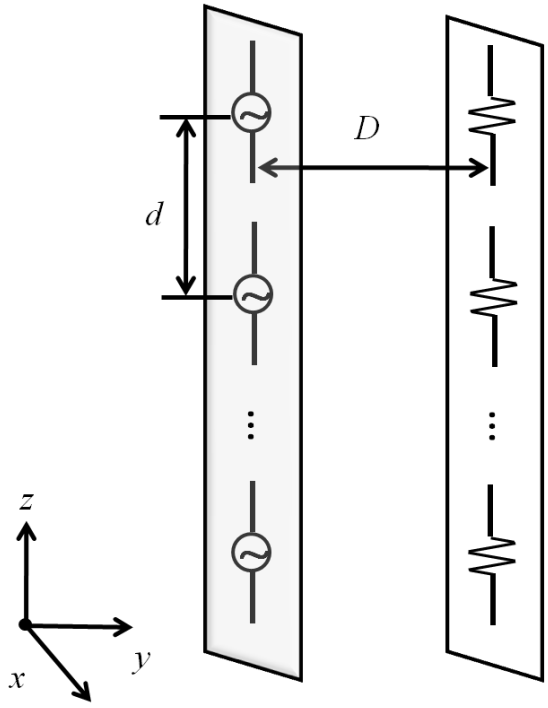

(b) Vertical array

Fig. 4.1. Analysis models of conventional single dipole arrays.

A. Effect of Antenna Parameters on Channel Capacity

In this simulation, the two type arranged linear dipole arrays with antenna element number M_T=M_R=4 are simulated. And the antenna distance *D* and element spacing *d* changes at the same time. The channel capacity at each situation is plotted in the Fig. 4.2.

We can find that obviously in the Fig. 4.2, the channel capacity is affected significantly by the antenna distance *D*. That means in the near-field MIMO, the distance between the transmitting antennas and the receiving antennas plays the most important role. However, we should notice that as the antenna distance *D* is changing, the maximum channel capacity will appear with different element spacing *d*.

In fact, in a near-field MIMO system, the spatial correlation and SNR play significant roles in channel capacity performance. Furthermore, the spatial correlation and SNR are both conditioned strongly by the element spacing *d*, so the element spacing *d* need to be discussed carefully in antenna designing of near-field MIMO system. N. Honma mentioned that, there was an optimal element spacing with certain antenna distance and certain number of the antenna elements, and the situation of using two facing squarely arranged dipole array was analysed in detail [21].

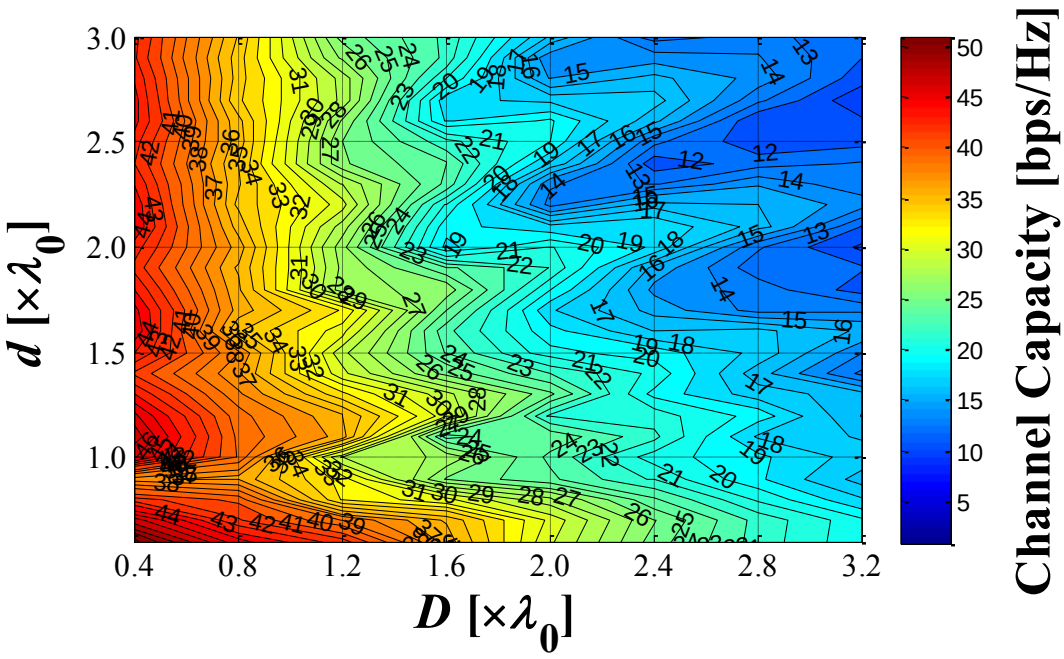

(a) Horizontal array

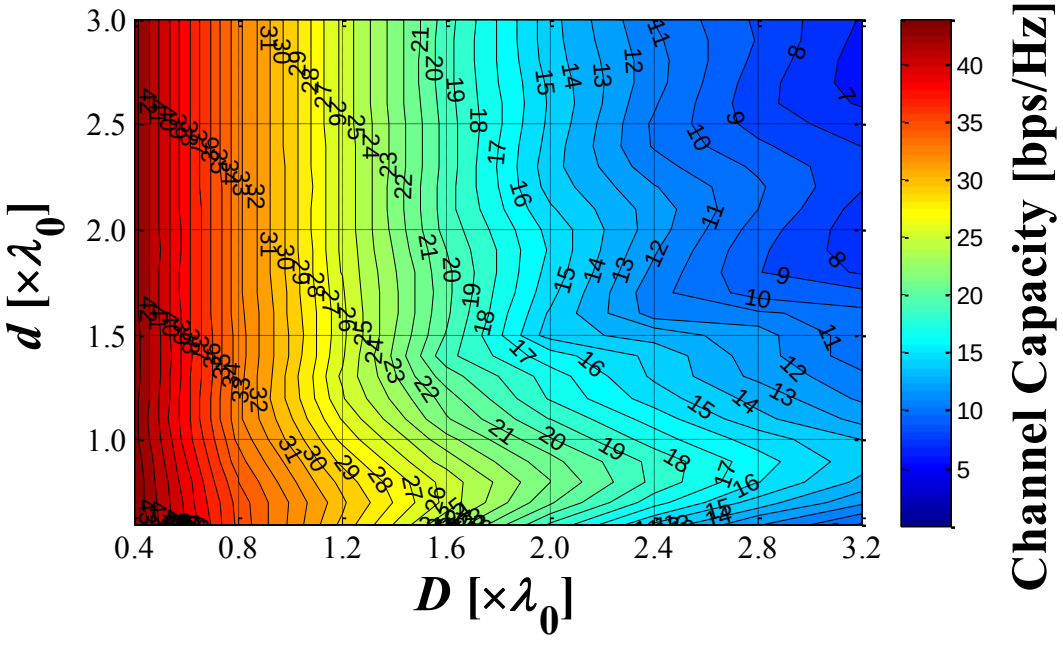

(b) Vertical array

Fig. 4.2. Effect of antenna parameters in the conventional single dipole arrays.

B. Optimum Element Spacing *d*

In this section, the two type arranged linear dipole arrays with antenna element number M_T=M_R=4 are simulated. The antenna distance D normalized by λ_0 (λ_0 is the wavelength in free space) is changed, and the optimal element spacing d_{opt} (d_{opt} is defined as the element spacing that derive the highest channel capacity at a certain D) and the channel capacity approached at d_{opt} are plotted in Fig. 4.3. Figure 4.3 indicates that we obtain almost the same trend of d_{opt} as squarely arranged arrays in [21], that is, d_{opt} increases with D. However, the linearly arranged arrays can obtain smaller d_{opt} than the squarely arranged ones, especially the horizontal type array. It also can be seen in Fig.3 that, the horizontal linear array can obtain higher channel capacity than vertical one at the same spacing.

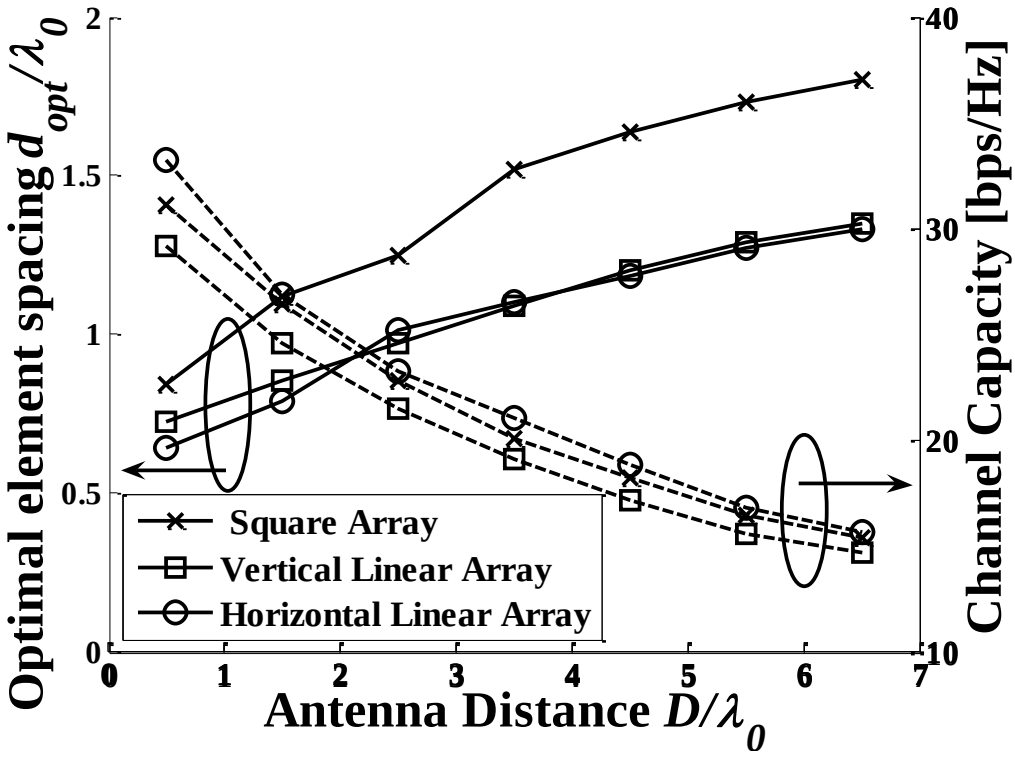

Fig. 4.3. Optimal element spacing d_{opt} at certain antenna distance.

4.1.2 Effect of HPBW in Dual-Dipole Arrays

The effects of the basic antenna parameters on channel capacity in near-field MIMO were descript in detail in the previous section. Finally, the protagonists of this research, the impact of the dual-dipole arrays are going to come on the stage. For comparing the different performances on channel capacity in the near-field MIMO system with the conventional single dipole arrays, the total exciting power for the transmitting antenna is constrained the same as the previous simulation.

A. Channel Capacity Improvement by the Optimum HPBW

To investigate the effect of the HPBW of the dual-dipole array, the analysis models in Figs. 3.6 and 3.7 are used. And the basic antenna parameters are fixed, that is antenna distance D is fixed at $1.6\lambda_0$ and element d is fixed at λ_0. The HPBW is the only various parameter.

In Fig. 4.4, we can see the relationship of the HPBW versus the channel capacity. The straight dashed lines indicate the channel capacity when conventional dipole arrays are used on both sides in the same situation. Fig. 4.4 indicates that the beamwidth of the radiation pattern has a great impact on the channel capacity. General speaking, when the HPBW becomes narrower, the dual-dipole MIMO system achieves a higher channel capacity than that for a conventional dipole antenna. As the HPBW changes, the channel capacity achieves a peak. The highest channel capacity is obtained when the HPBW is approximately 50º. The corresponding Δd for the optimal HPBW is approximately $0.6\lambda_0$ (λ_0 is the wavelength).

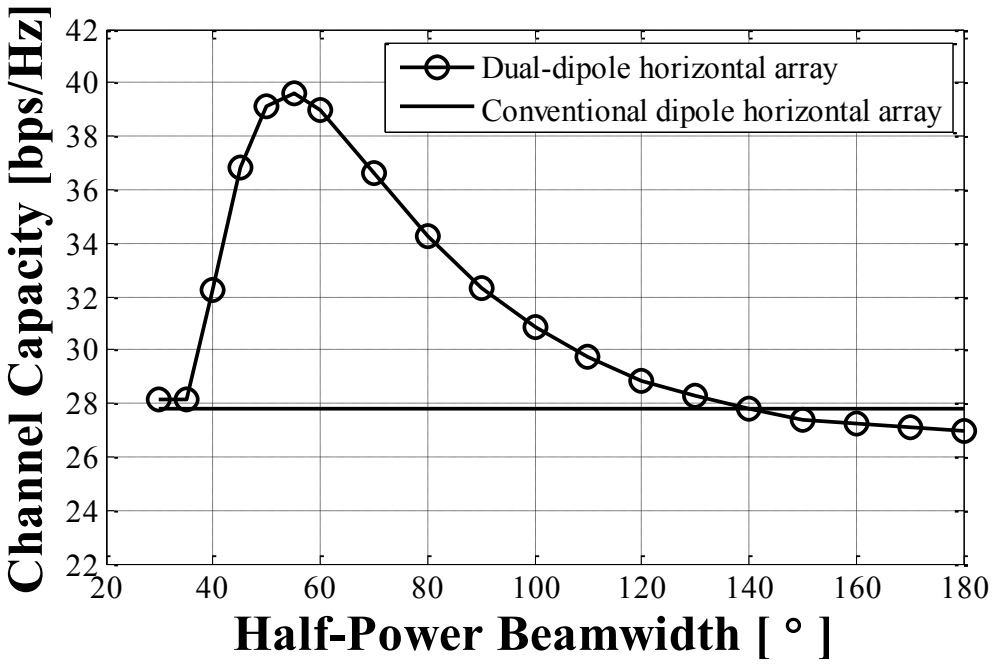

(a) Horizontal array

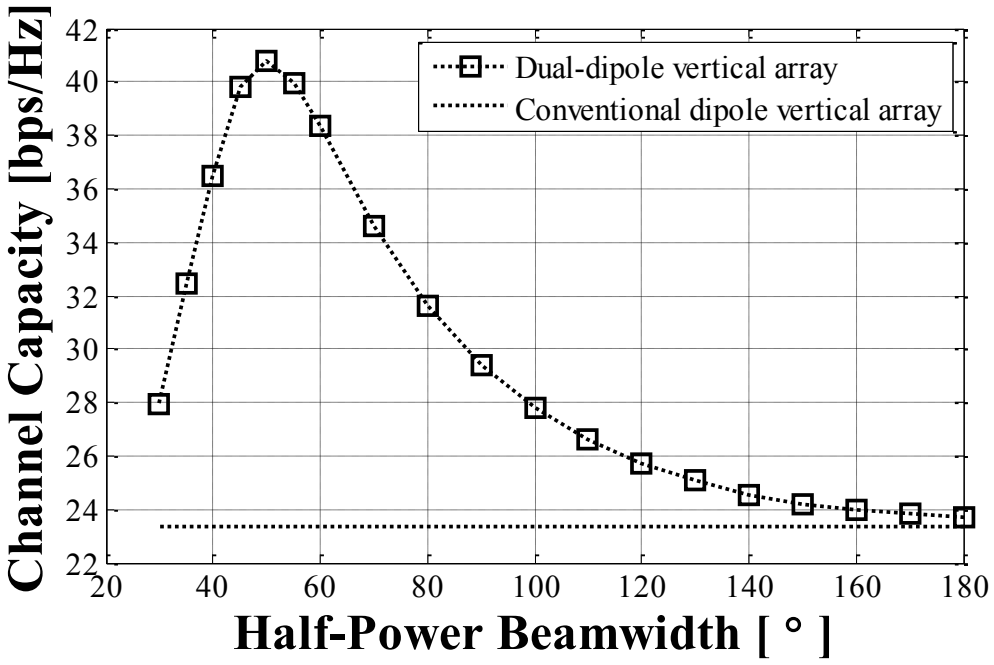

(b) Vertical array

Fig. 4.4. Effect of HPBW on channel capacity in near-field MIMO.

It is obvious that, when the HPBW is larger than 50 º, the improvement in the vertical array is much considerable than that in the horizontal array. The different performances of the two types of arrangements are caused by the different spatial correlation and the different receiving SNR in each non-facing Rx element branch. The spatial correlation can be ignored in the vertical array but important in the horizontal array. Especially when the HPBW is near 180 º, the spatial correlation in the dual-dipole horizontal array is larger than that of the conventional dipole array. Because the dipoles number in Tx increases from 4 to 8. Therefore, the tiny increase on SNR can't cancel off the effect of the spatial correlation increment. Furthermore, in the horizontal array, as the HPBW in *x*-*y* plane becomes narrower, the power received by the non-facing elements (especially the ones further from the facing one) will not increase as much as the facing one. On the other hand, in the vertical array the beamwidth in the *y*-*z* plane affects the SNR in each non-facing Rx element branch. The beamwidth in the *y*-*z* plane will not change with the Δd, but the gain of the radiation pattern in the *y*-*z* plane will increase. Therefore, besides the facing element, the SNR in the other Rx branches will also increase as Δd increases. That's why the improvement in the vertical array is larger.

The reduction of the channel capacity when HPBW is less than 50 º (the corresponding Δd increases over about $0.6\lambda_0$), is caused by the occurrence of the side lobes. The side lobes will carry off some power from the main beam, and as the HPBW becomes narrower the side lobes become larger, which leads to more spatial correlation in the horizontal array. That's why the channel capacity in the horizontal array decreases earlier than that in the vertical array. Especially in the dual-dipole horizontal array, when the HPBW is near 30 º, the side lobes are so large that the negative impact of the spatial correlation exceeds the positive impact of SNR increment. So the channel capacity for the dual-dipole horizontal array becomes less than the results for conventional dipole hereafter. To avoid the effect of side lobes, the HPBW should be considered only larger than 50º (the corresponding Δd is from $0.2\lambda_0$ to $0.6\lambda_0$).

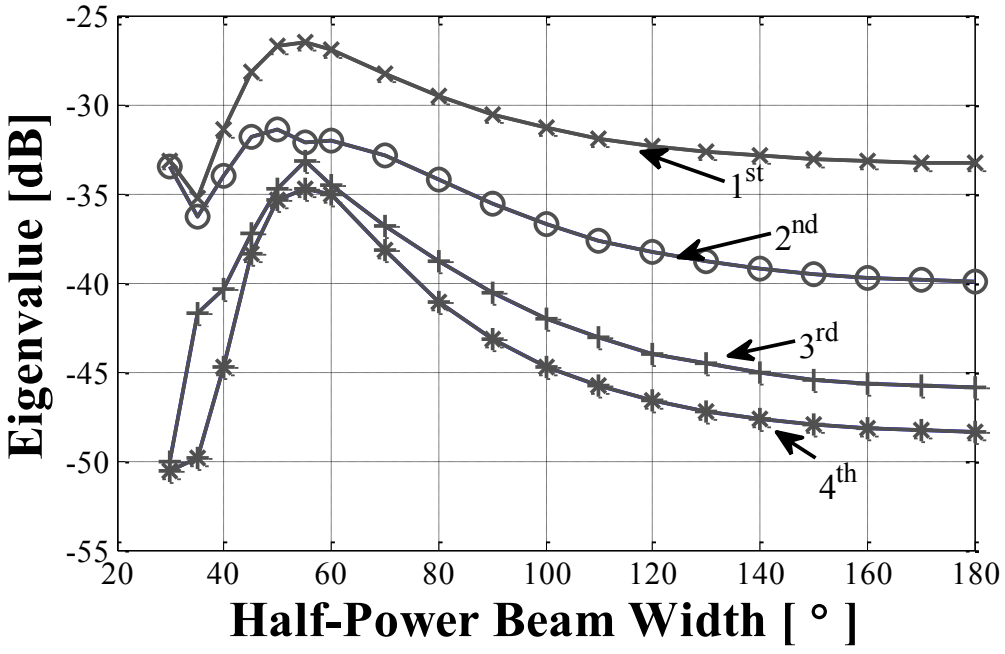

(a) Horizontal array

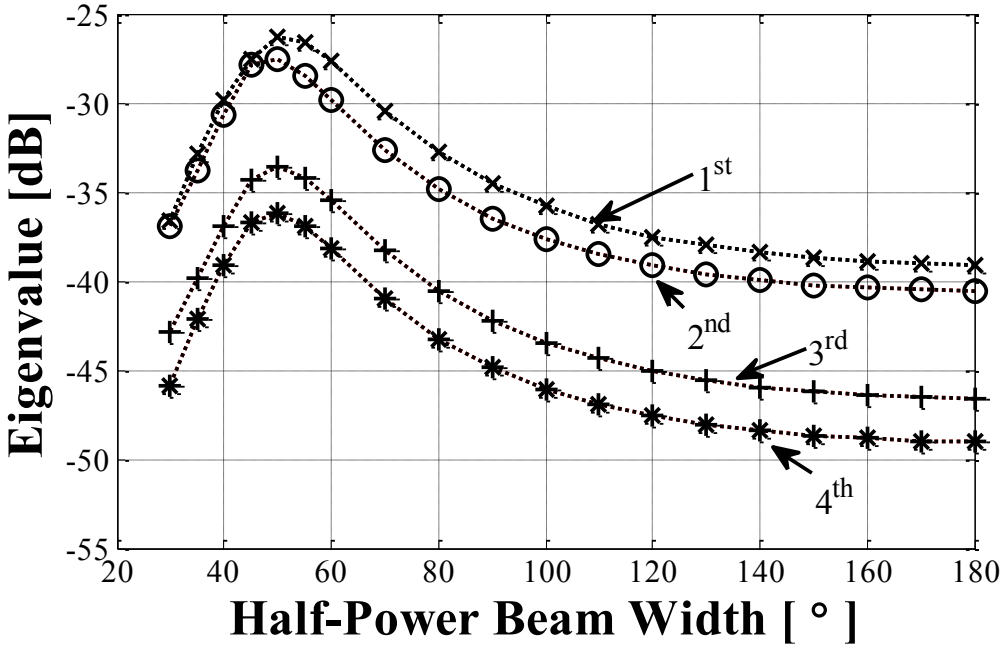

(b) Vertical array

Fig. 4.5. Effect of HPBW on eigenvalue in near-field MIMO.

The theoretic explanation can be made by the change of eigenvalues. The effect of HPBW on eigenvalues in near-field MIMO is shown in Fig. 4.5. From Fig. 4.5, the effect of the HPBW on eigenvalue distributions is plotted. When the HPBW is larger than 50°, we can see that in the horizontal array, although the 3rd and 4th eigenvalues change very obviously, the 1st and 2nd eigenvalues those are the principal components of channel capacity vary gently. On the other hand, all the eigenvalues in the vertical array are affected by the HPBW seriously. Hence, we can find in Fig. 4.4 that the improvement of channel capacity in the vertical array is much more significant than that in the horizontal array. When the HPBW is larger than 50°, the trends of all 4 eigenvalues curves of vertical array are similar. But the trends of horizontal array are distinctly different. The vertical eigenvalues have an obvious steeper decreasing slope than the 2nd horizontal eigenvalue, but a little gentler slope than the 1st and 4th horizontal eigenvalues and a similar slope as the 3rd one. The differences among every horizontal eigenvalue will cancel out the impact of each other, and finally it shows the similar trend of channel capacity slope as that of the vertical one in Fig. 4.4. Therefore, the improvement of channel capacity can be explained well by the variation of eigenvalues.

B. Generality of Optimum HPBW

The effect of antenna distance D and element spacing d on the channel capacity in the near-field MIMO systems was clarified in previous section. The channel capacity will simply decrease with D enlarges. However, an optimum element spacing d_{opt} could be obtained at each certain D, because that the variation of d will affect not only the SNR in each Rx element branch but also the spatial correlation. To verify the generality of the optimum HPBW mentioned previously, we will check the channel capacity when the HPBW changes with D at the same time, or when the HPBW changes with d at the same time. The generality of the optimum HPBW will be verified in this section.

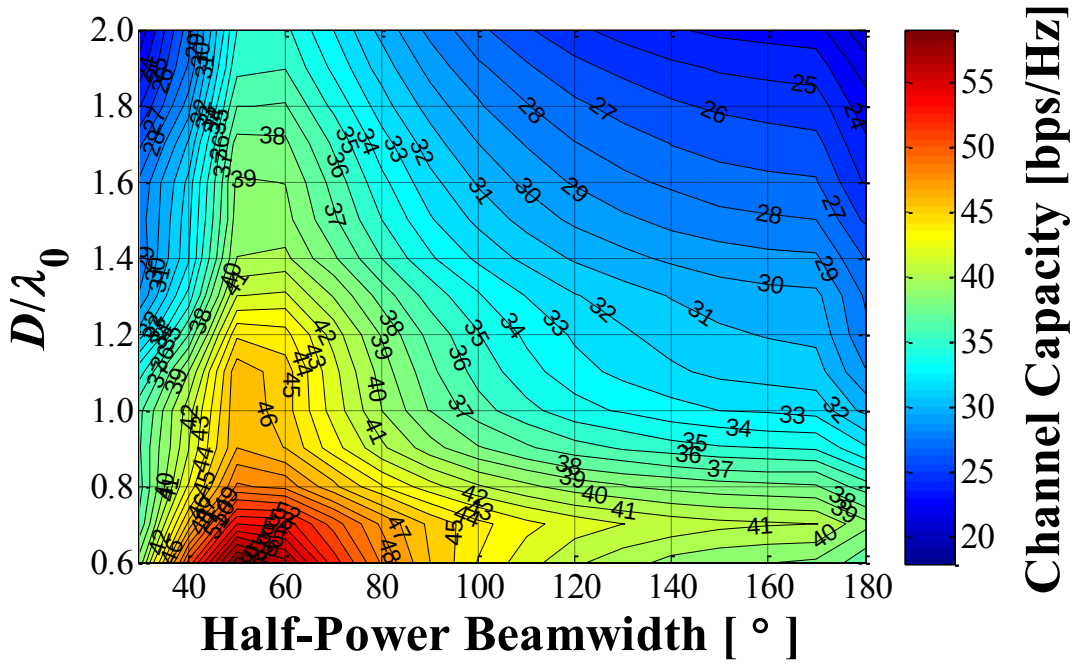

(a) Horizontal array

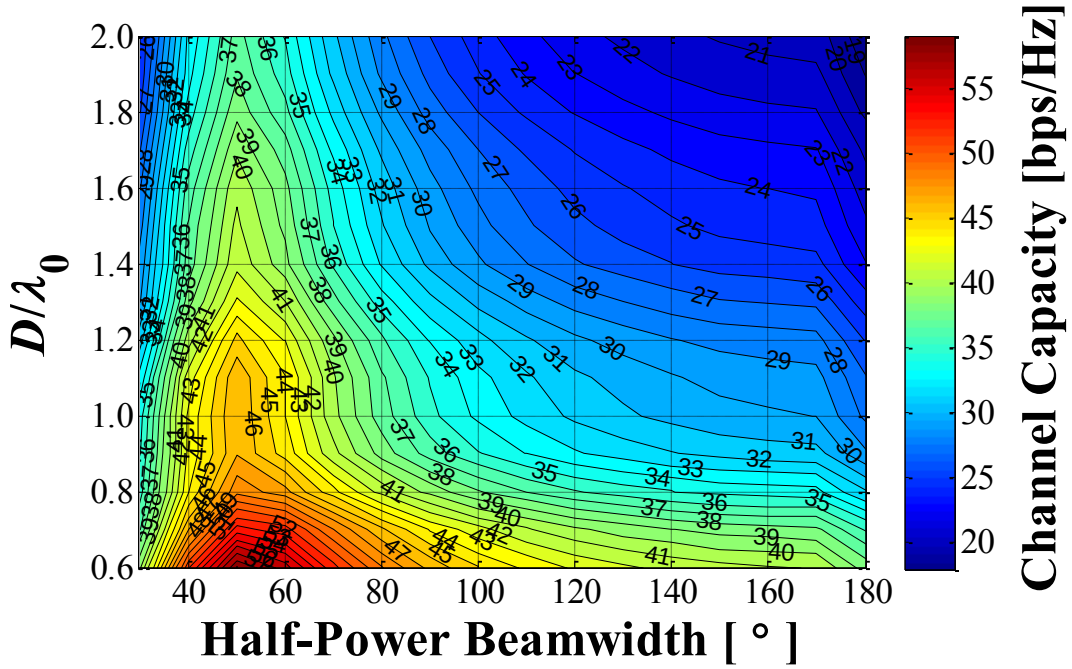

(b) Vertical array

Fig. 4.6. Effect of D and HPBW on channel capacity when d is λ_0.

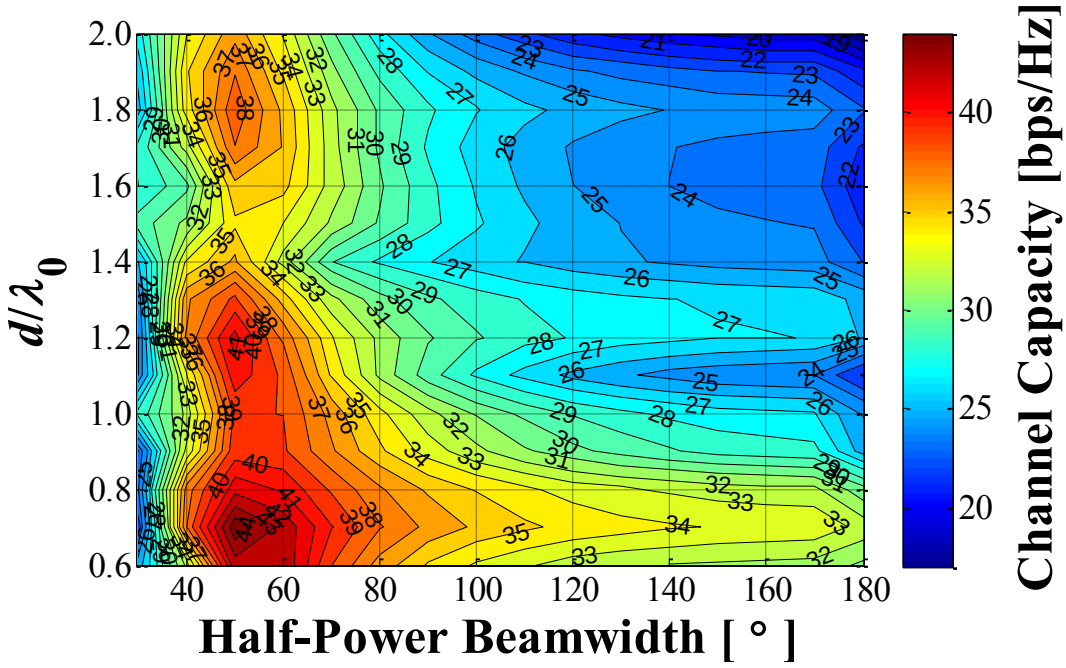

(a) Horizontal array

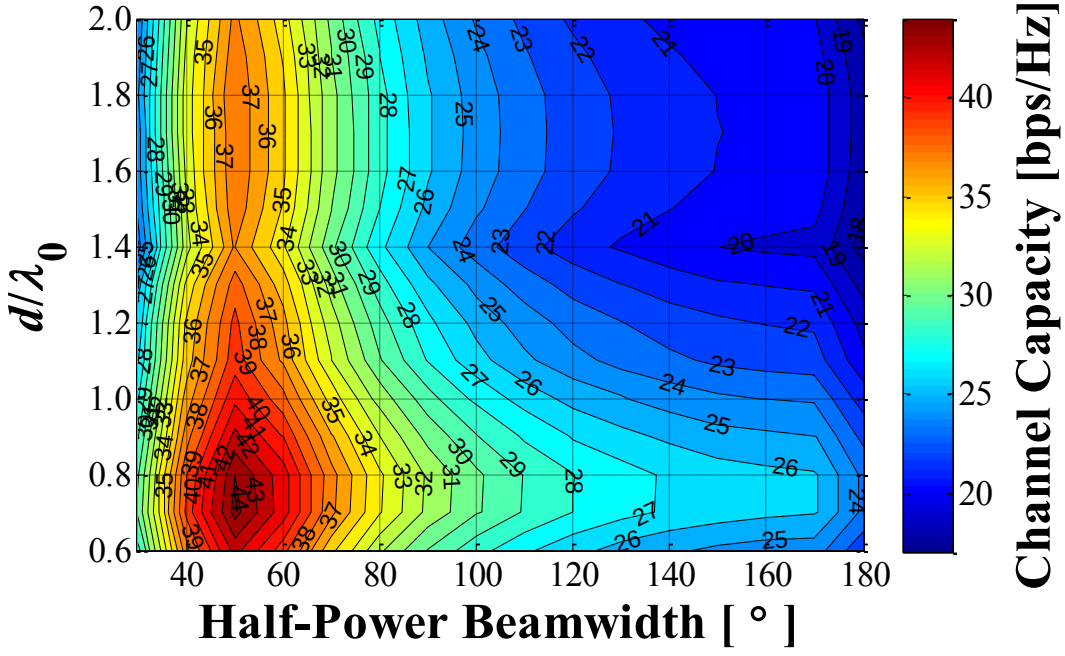

(b) Vertical array

Fig. 4.7. Effect of *d* and HPBW on channel capacity when *D* is $1.6\lambda_0$.

Figure 4.6 shows the situation when d is fixed at λ_0 and the HPBW and D are variable. We can find that as the conventional single dipole arrays, the antenna distance D still affects the channel capacity very significantly. In addition, the effect of the HPBW is also very considerable. And whatever D changes, the optimum HPBW is always found to be approximately 50 º. That means the channel capacity improvement caused by adjusting HPBW is independent from D changes.

Figure 4.7 indicates that the d_{opt} still exists whatever Δd changes, and the d_{opt} is $0.7\lambda_0$ as the same as mentioned in [21]. However, the effect of d is much less than HPBW, especially in the vertical array. In addition, the channel capacity improvement caused by adjusting HPBW is independent from d changes. The optimum HPBW can be found to be approximately 50 º.

Therefore, we can say that the effect of the HPBW in near-field MIMO system is independent, and the generality of the optimum HPBW is clarified.

4.2 Effect of Antenna Location Errors on Channel Capacity in Near-Field MIMO System

In the previous discussion, we clarified the effects of the radiation pattern of the dual-dipole array. In those cases, the transmission antennas are placed face to face. However, in a practical application the opposing antennas cannot always be placed in the ideal position. Since the antenna distance is fairly short, a slight deviation or bias of the receiver antenna to the transmitter antenna may significantly affect the channel capacity. Therefore, we address the deterioration in the channel capacity caused by antenna location errors in this subsection.

Considering a practical application where the near-field MIMO is used to transmit data through a wall as shown in Fig. 2.2(c), the antenna distance is constant (the thickness of the wall) and the two planes including the transmitter and receiver are parallel to each other. Hence, the antenna location errors are limited considering

the offset error in the x and z directions as shown in Fig. 3.8, and rotational error around the y axis, as shown in Fig. 3.9.

In this simulation, both the horizontal and vertical arrays are simulated to clarify the deterioration in the channel capacity. Antenna distance D is fixed at $1.6\lambda_0$, and element spacing d is fixed at λ_0. The distance between the two dipoles in one element, Δd, is variable, which means that the corresponding HPBW is also variable.

4.2.1 Effect of Antenna Offset Errors on Channel Capacity

In the offset error model, the offsets of the receiving antenna in both the x and z directions are considered. The relationship between the offset error and channel capacity for a different case of HPBW (caused by Δd) is shown in Fig. 4.8 and Fig. 4.9. Generally speaking, in all cases, as the offset errors increases, the channel capacity decreases. In addition, we find that the highest channel capacity is obtained when $\Delta d=0.5\lambda_0$ or $0.6\lambda_0$, with the corresponding HPBW from 49 ºto 60 º. These results support the conclusion in Section 4.1.

A. Offset Errors in the x direction

To verify the effect of the offset error only in the x direction, the Δz is considered as 0. The simulation results are shown in Fig. 4.8. Each curve indicates a situation with a different HPBW (Δd). It is clear that when Δx increases, the deterioration in the channel capacity in the horizontal array is less than that in the vertical array. This means that the offset error in the x direction has a more significant effect on the vertical array than on the horizontal array. Especially when the HPBW is narrower, the deterioration in the channel capacity is more pronounced. Furthermore, there are fluctuations in the curves when the HPBW is narrow. This is because when the HPBW becomes very narrow, the side lobes of the radiation pattern in the x direction become larger. As Δx increases, although the receiver array will miss the signal from the main beam, it can receive the signal from the side lobes. Therefore, the channel capacity will increase again. In the case of the horizontal array, in

addition to the contribution from the side lobes of the opposite transmitter element, the radiation pattern of the adjacent transmitter element can increase the channel capacity. This is the reason why there are multiple fluctuations in the horizontal array but only one in the vertical array.

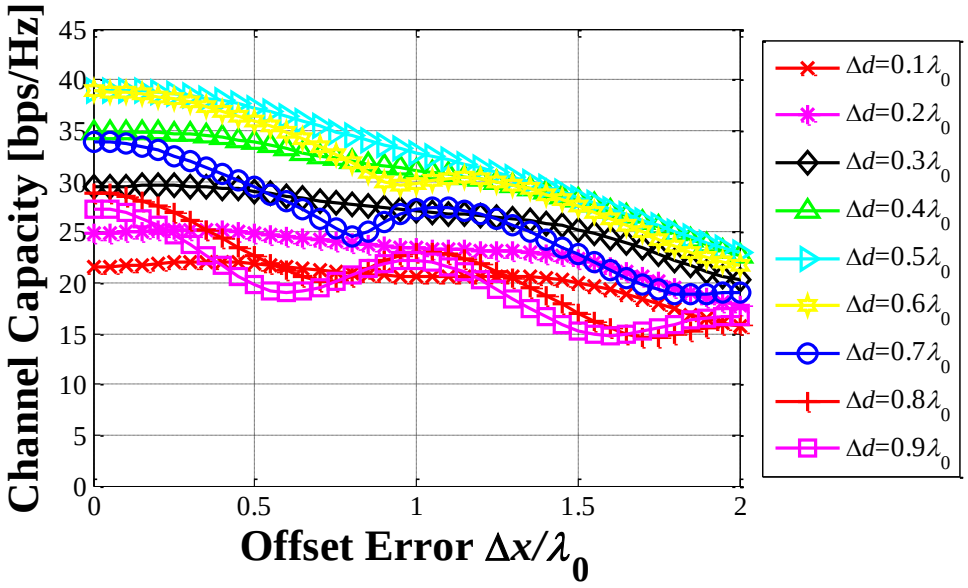

(a) Horizontal array

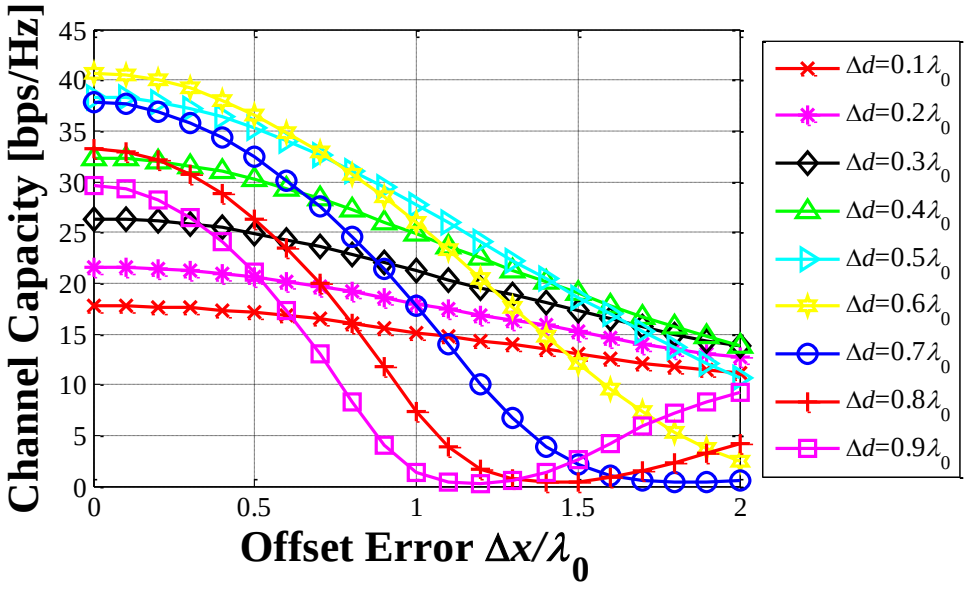

(b) Vertical array

Fig. 4.8. Effect of offset error in *x* direction with different HPBWs.

B. Offset Errors in the *z* direction

Figure 4.9 shows the effect of the offset error only in the *z* direction. Conversely to Fig. 4.8, the offset error in the *z* direction has a more pronounced effect on the horizontal array than the vertical array. The tendency of the channel capacity curves in Fig. 4.9 is a straightforward decline as Δz increases, which is much simpler than that in Fig. 4.8. Furthermore, we find the same tendency for Δx, i.e., the HPBW affects the channel capacity for the vertical array more than that for the horizontal array.

4.2.2Effect of Antenna Rotational Errors on Channel Capacity

Rotational error is only considered when the receiver antenna rotates around the *y* axis by θ_y from 0 to 45°. The simulation results are shown in Fig. 4.10. The effects on both the horizontal and vertical arrays are almost the same. As rotational error θ_y increases, the channel capacity becomes worse slowly and continuously. In addition, the best channel capacity is still obtained when Δd=0.5λ_0 or 0.6λ_0 (HPBW is from 49°to 60°).

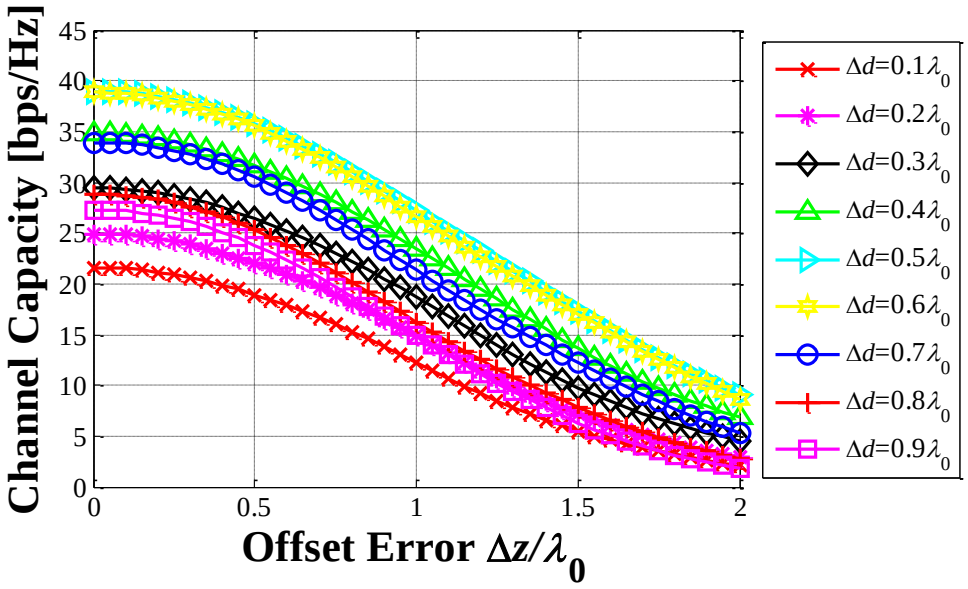

(a) Horizontal array

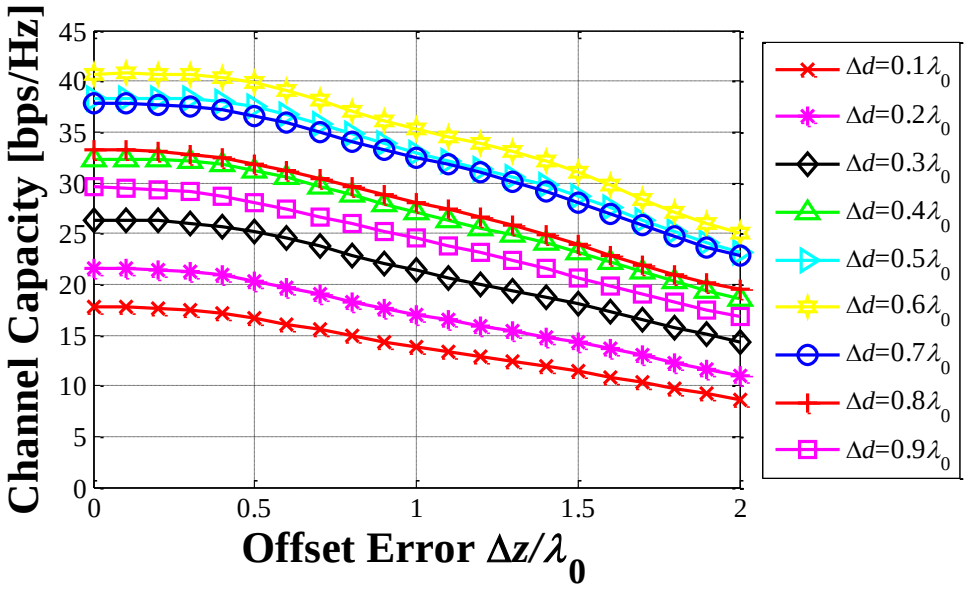

(b) Vertical array

Fig. 4.9. Effect of offset error in *z* direction with different HPBWs.

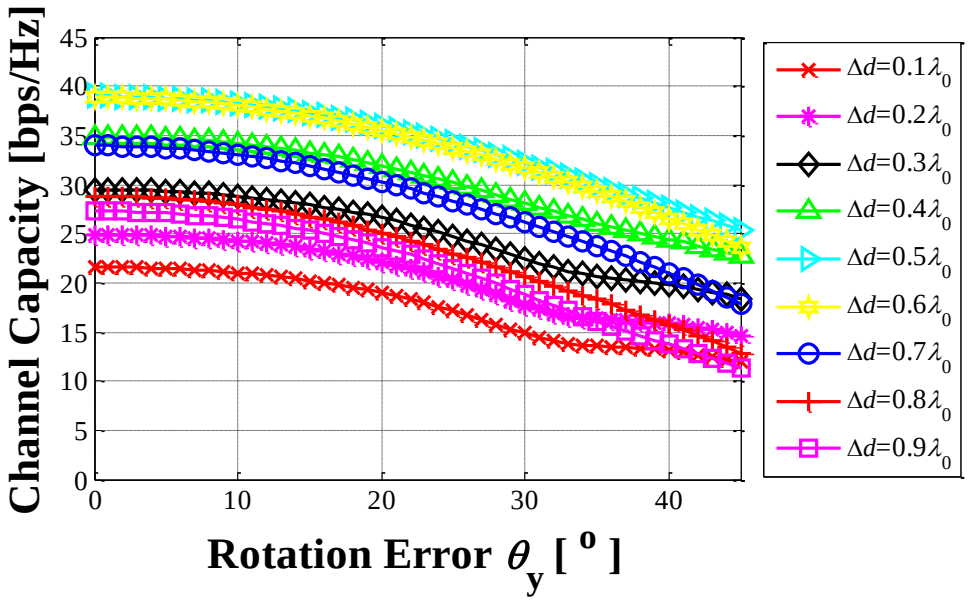

(a) Horizontal array

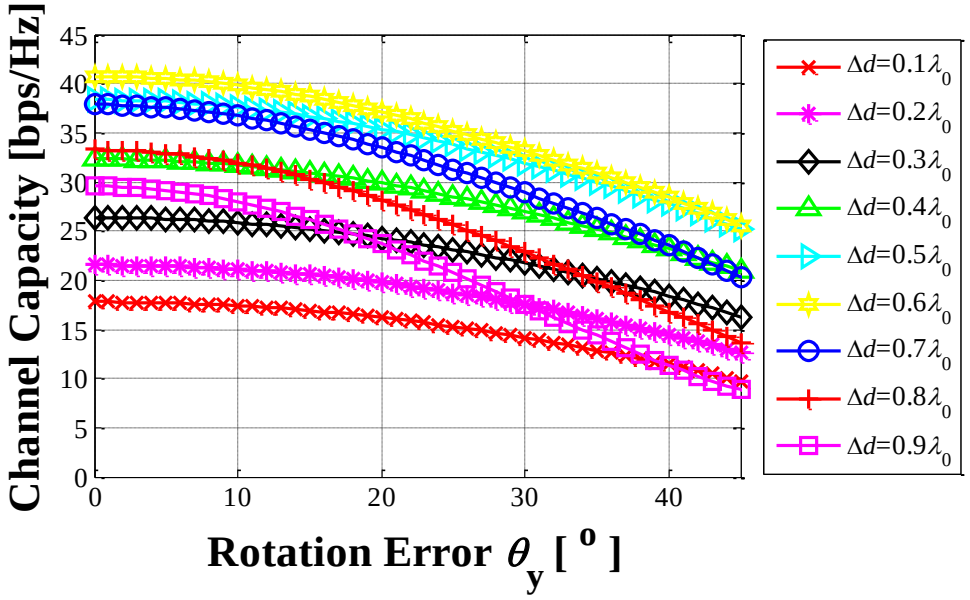

(b) Vertical array

Fig. 4.10. Effect of rotational error around *y* axis with different HPBWs.

4.2.3 Effect of HPBW on Stability of Deterioration in Channel Capacity

The previous subsections showed the direct effect of the HPBW on the antenna location error based on the channel capacity. The performance of the system in every situation can be compared easily. In this subsection, the stability of the system in different situations is discussed using an average unit for deterioration in the channel capacity. The unit of deterioration indicates the percentage that the channel capacity deteriorates when the location error increases one unit. In the case of the offset error, one unit represents a step of $0.1\lambda_0$, and in terms of the rotational error, one unit represents a step of 1 º. Since the unit of deterioration is variable, we use the average value of all the units in location error areas to evaluate the stability of the system at different HPBWs. Hence, when the absolute value of the average unit of deterioration is large, this means that the channel capacity of the system decreases quickly, which indicates that the system is unstable. On the contrary, when the absolute value is smaller, the stability of the system is better.

Figure 4.11 shows the effect of the HPBW on the stability of the system. All the location error situations are plotted in the figure. The solid lines represent the horizontal array and the dashed lines represent the vertical array. Figure 11 shows that when the HPBW becomes wider, its effect on the system stability is less important. In the case of rotational error, the levels of stability for both the horizontal and vertical arrays are almost the same. As the HPBW exceeds 50 º, the average unit of deterioration remains at approximately -0.8% per degree. When considering the offset errors, the horizontal array is more stable than the vertical array for an offset in the *x* (horizontal) direction, and the vertical array is more stable for an offset in the *z* (vertical) direction.

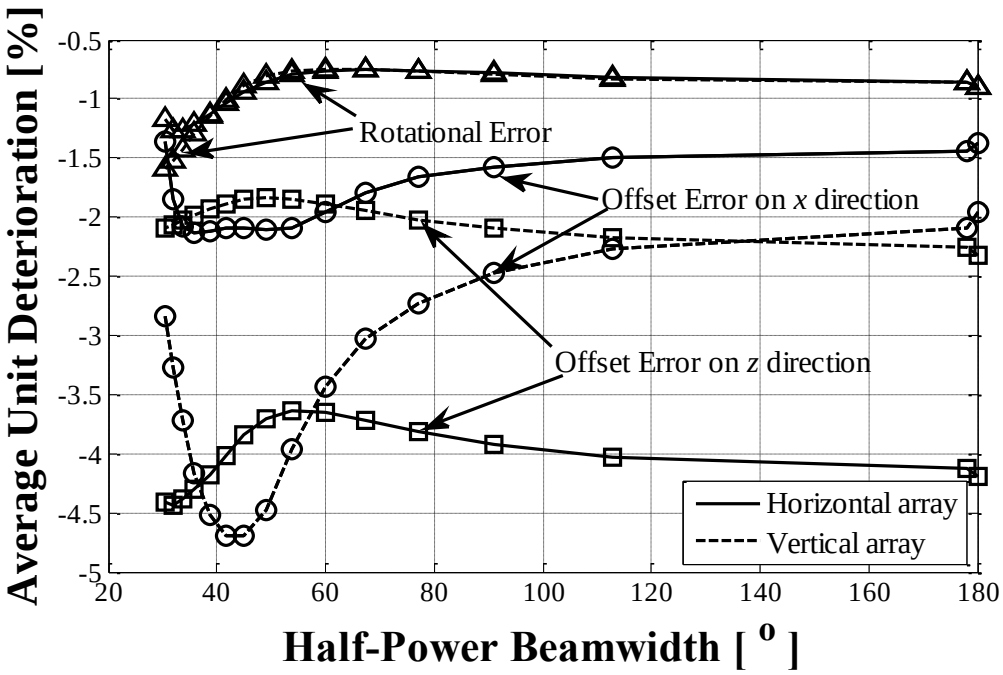

Fig. 4.11. Effect of HPBW on stability of deterioration in channel capacity.

Chapter 5 Effect of Objects in Near-Field MIMO Systems

Basically two factors determine the capacity of a MIMO system—the path loss and the multipath richness [25, 93, 94]. The dual-dipole arrays lead to much lower path loss than the conventional dipole arrays, hence, the channel capacity improves significantly. However, the multipath richness rarely exists in the near-field MIMO. So far, all the researches on the near-field MIMO are in the free space without any obstacle. However, due to the short transfer distance of the near-field MIMO, a tiny variation of the channel will lead to a significant difference on the channel capacity. Therefore, we employ metal wire [97, 98] in the near-field MIMO system to increase the multipath richness and clarify the effect of obstacles in the system.

In this chapter, the metal wires are chosen as the objects between the transmitting antennas and the receiving antennas for the fundamental research. First of all, one single metal wire is investigated to confirm the effects of metal wire's length, radius and polarization. Especially, the effect of the metal wire's location is verified clearly, the proper locations in the system for the metal wire are pointed out. In addition, the effect of multiple metal wires placed at the proper locations in the system is also described in detail.

5.1 Effect of Single Metal Wire in Near-Field MIMO Systems

In the expected practical application, the objects between the transmitting antennas and the receiving antennas might be the wall, so the effect of the metal wires in the wall is very necessary to be investigated. Hence, for the basic discussion, first of all, only one single metal wire is added in the dual-dipole array near-field MIMO system.

5.1.1Effect of the Basic Characters of the Single Metal Wire

Before investigating the effect of the metal wire's location on the channel capacity of the dual-dipole arrays, we will choose the appropriate basic characters of the single metal wire for normalize the simulation results.

A. Effect of the Length of the Metal Wire

In this simulation, the antenna distance D is fixed at $1.6\lambda_0$, the element spacing d is fixed at λ_0, and the distance between two dipoles in one element Δd is fixed at $0.6\lambda_0$. The length of the metal wire L changes from 0 (no wire) to $20\lambda_0$. The simulation results are shown in Fig. 5.1.

Figure 5.1 indicates that the general tendency of the channel capacity fluctuates and decreases as L increases. And when L is larger enough, the channel capacity will converge to a constant.

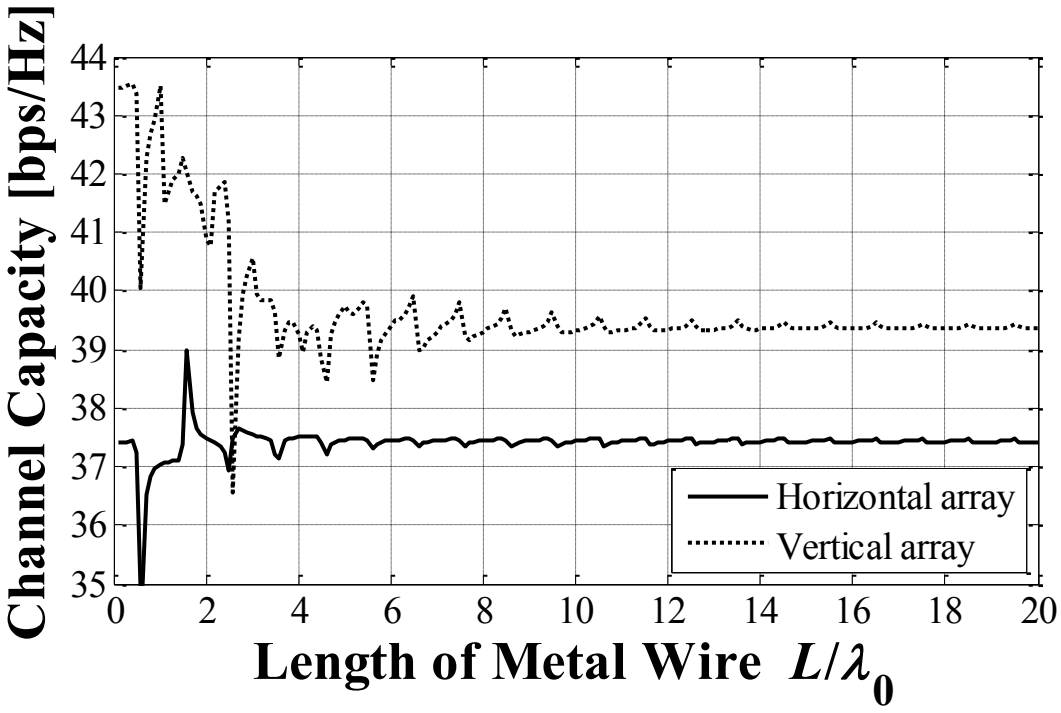

Fig. 5.1. Effect of the length of the metal wire.

To avoid instability from diffraction caused by a short metal wire, and to avoid the mass calculation caused by long length of metal wire, a suitable length for the metal wire, L, is selected as $10\lambda_0$ (λ_0 is the wavelength) and used hereafter.

B. Effect of the Radius of the Metal Wire

In this section, we try to find out the effect of the radius of the metal wire in the system. In this simulation, we set the metal wire in the vertical array system and the radius of the metal wire is denoted as R, as shown in Fig. 5.2. The other parameters are all the same as previous research: the antenna distance D is fixed at $1.6\lambda_0$, the element spacing d is fixed at λ_0 and the distance between two dipoles in one element Δd is $0.6\lambda_0$, the length of the metal wire L is $10\lambda_0$. The offset of the metal wire in x direction Δx_{mw} is from 0 to $2\lambda_0$, in y direction Δy_{mw} is from $-2\lambda_0$ to $2\lambda_0$.

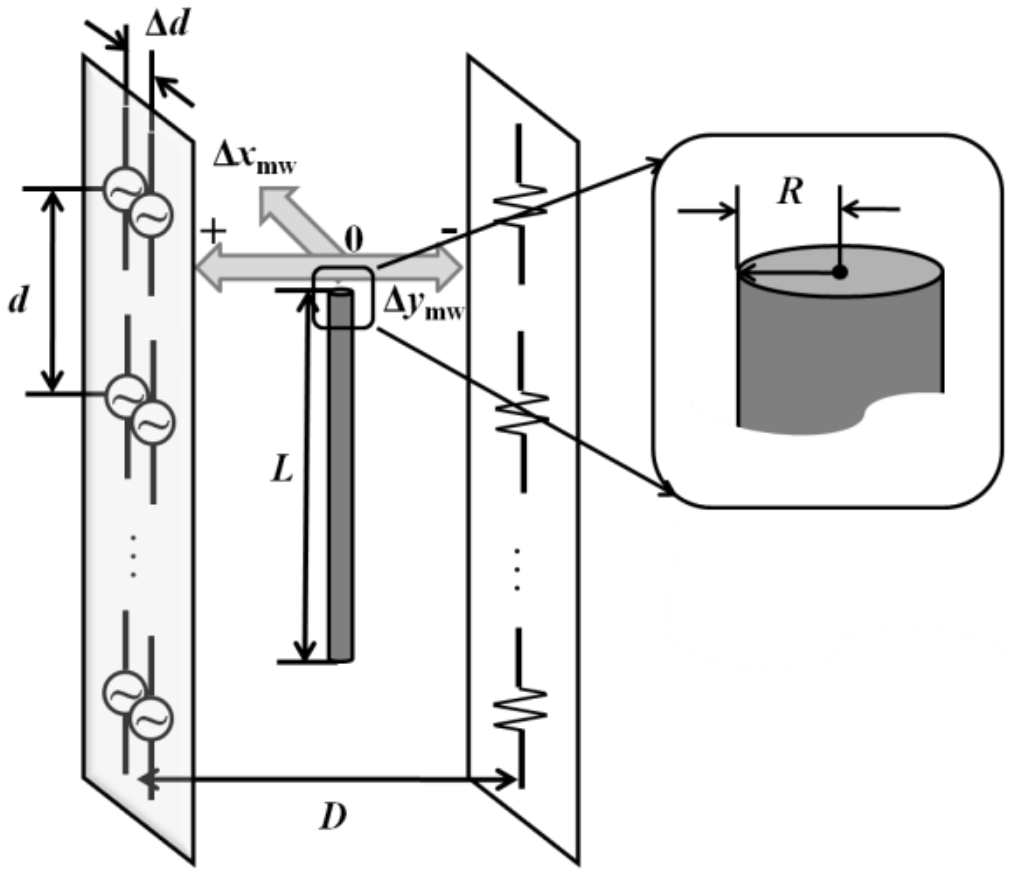

Fig. 5.2. Analysis model of metal wire radius.

The effect of the radius of the metal wire on the maximum channel capacity is shown in the following figure. We can see that as the *R* increases, the maximum channel capacity becomes larger. Therefore, we can say that the larger radius can affect the system more significantly.

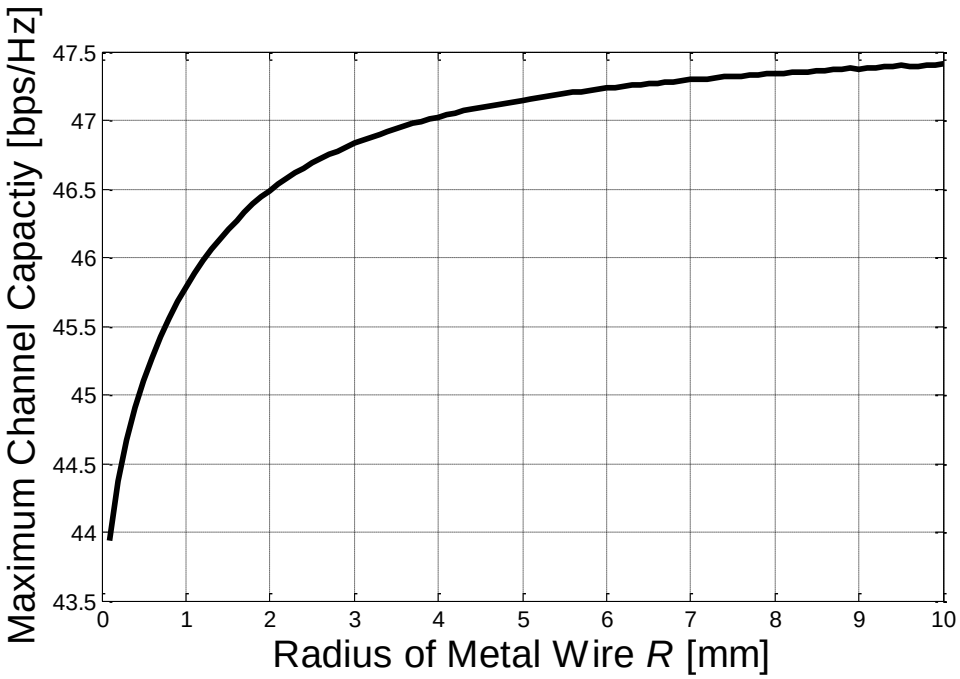

Fig. 5.3. Effect of Radius of Metal Wire on Maximum Channel Capacity.

C. Effect of the Rotation of the Metal Wire

Considering the effect of antennas' polarization, only when the metal wire is parallel with the dipoles, the metal wire will affect the system channel capacity most significantly, the analysis models mentioned in Chapter 3 are all with the parallel metal wires to the dipoles. In this subsection, the simulation results will improve that the reason of abandoning the case when the metal wire is perpendicular to the dipoles.

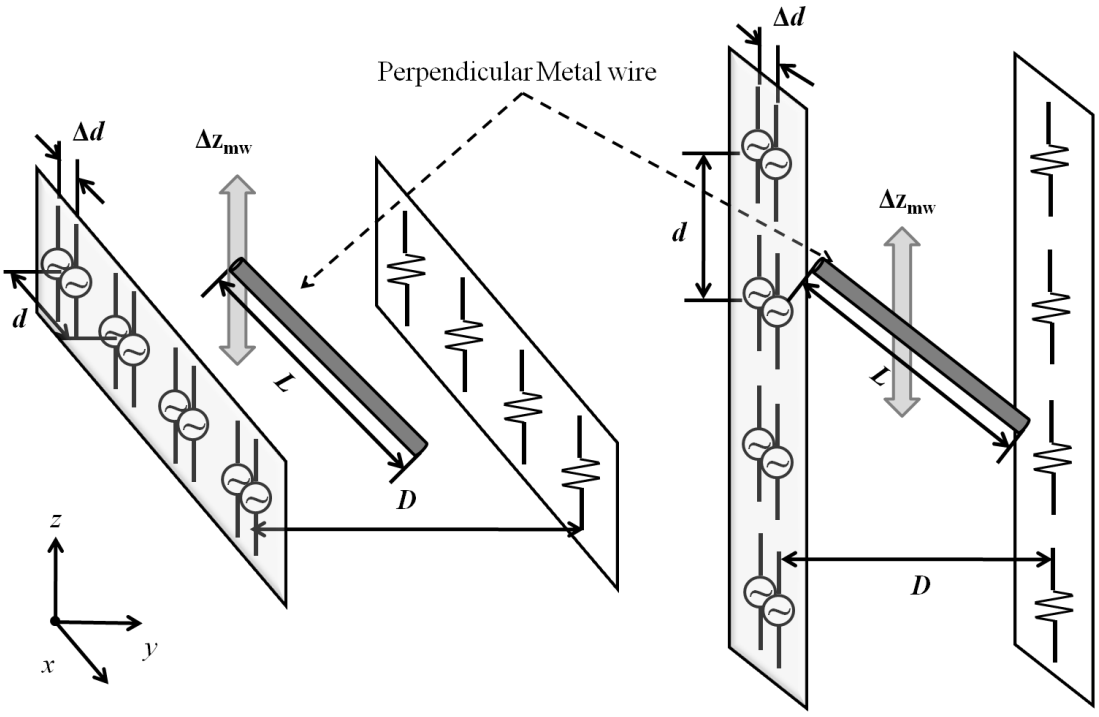

(a) Horizontal array (b) Vertical array

Fig. 5.4. Analysis models of dual-dipole arrays with perpendicular metal wires.

The models of horizontal array and the vertical array with perpendicular metal wire are described respectively in Fig. 5.4. To verify the effect of the perpendicular metal wire on the channel capacity, it is moved in the *z* direction, which is denoted as Δz_{mw}. The effect of the perpendicular metal wire in the system is shown in Fig. 5.5(a). We can see that the perpendicular metal wire can rarely affect the system channel capacity. On the contrary, the systems with parallel metal wires are shown in Figs. 3.10 and 3.11, and the effects of the offset in *x* direction in these systems are shown in Fig. 5.5(b). The effect of the parallel in the system is considerable. Therefore, the metal wires in the system are chosen as the parallel ones in this research hereafter.

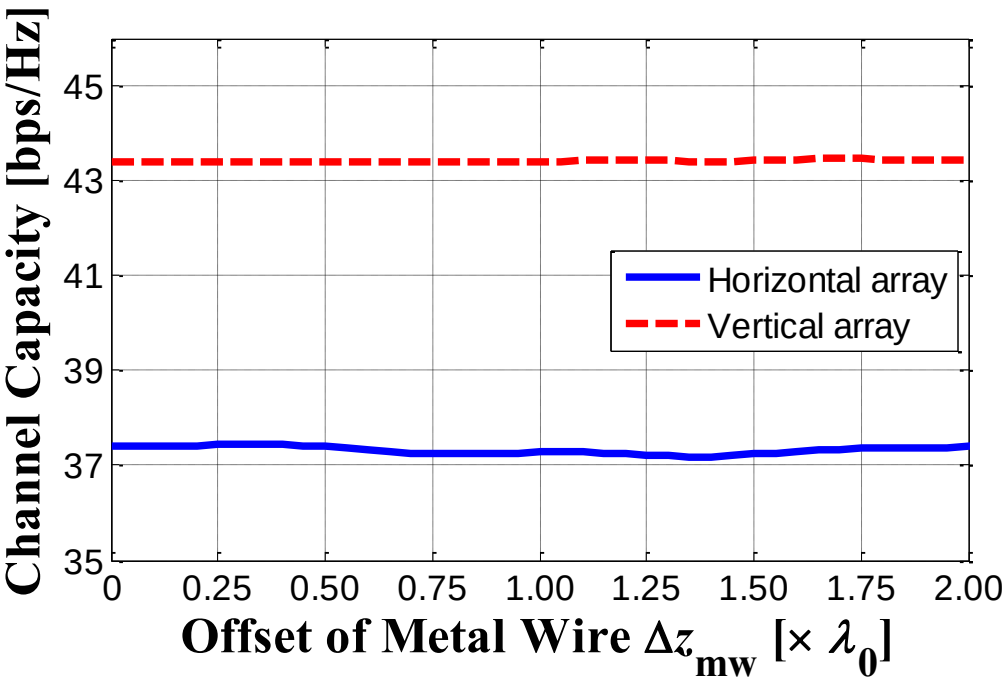

(a) Perpendicular metal wire

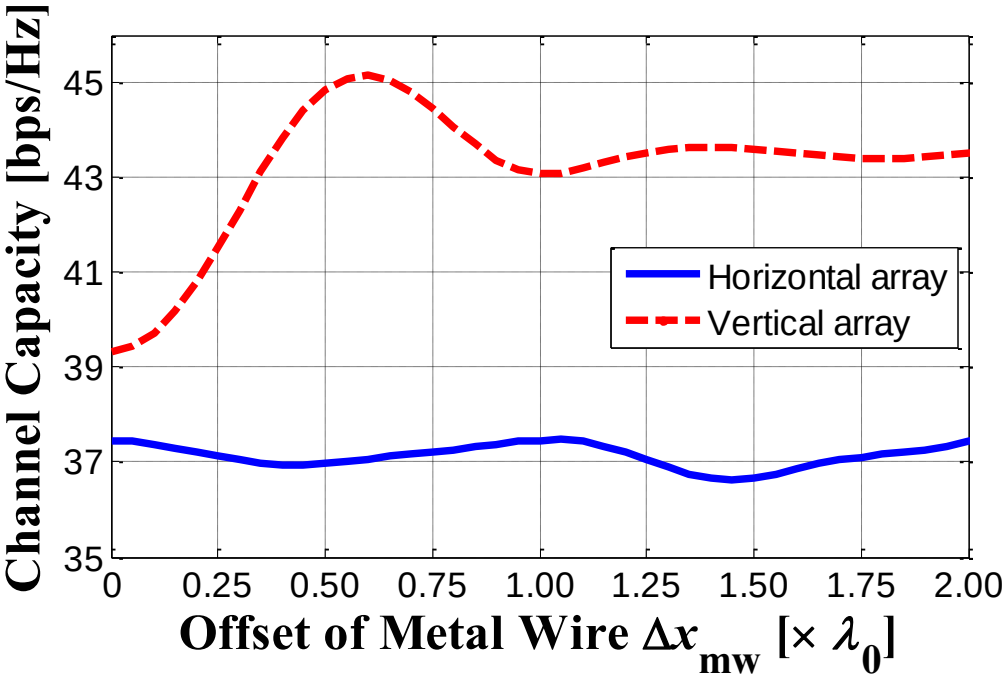

(b) Parallel metal wire

Fig. 5.5. Effect of rotation of metal wire.

5.1.2 Effect of the HPBW

The effect of the HPBW on channel capacity in the system without a metal wire has been verified in [10]. And in this simulation, we set the metal wire placed in the centre between the transmitter and receiver. Figure 5.6 plots the relationship of the HPBW versus the channel capacity when D is fixed at $1.6\lambda_0$ and d is fixed at λ_0. The variation of channel capacity for the system without a metal wire is also plotted in the same figure used as a comparison. The horizontal and vertical arrays are considered respectively.

Figure 5.6 indicates that the beamwidth of the radiation pattern has a great impact on the channel capacity. We find that as the HPBW decreases the channel capacity achieves a peak. The highest channel capacity is obtained when the HPBW is approximately 50°, the same as the system without a metal wire [10]. Due to the significant improvement on channel capacity, the HPBW is set 50° in the following discussion.

It should be noted that although the metal wire is placed in the centre of either the horizontal array or the vertical array, the influences of the metal wire are different. As shown in Fig. 5.6(a), in the horizontal array, the two curves are almost the same, which means the influence of the metal wire can be ignored. However, as shown in Fig. 5.6(b), in the vertical array, the metal wire reduces the channel capacity distinctly. It is because the centre of the vertical array is between the Tx and Rx. When the metal wire is placed in this location, it will obstruct the signal transmission and enlarge the path loss. On the other hand, the centre of the horizontal array is out of the main transmission path, thus the influence of the metal wire is insignificant. Therefore, not only the HPBW but also the array arrangement and metal wire location will affect the system channel capacity.

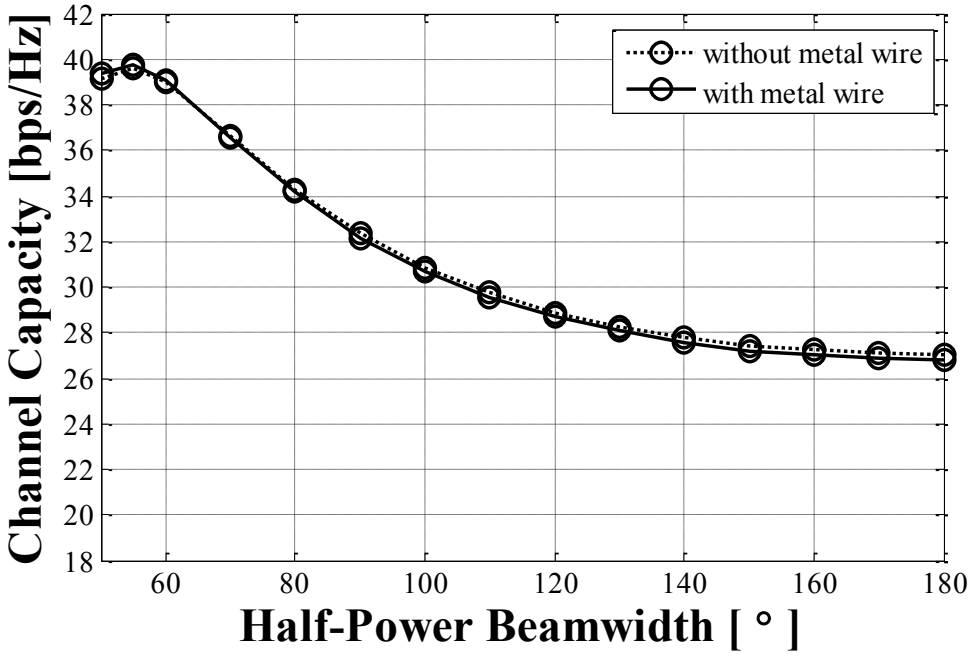

(a) Horizontal array

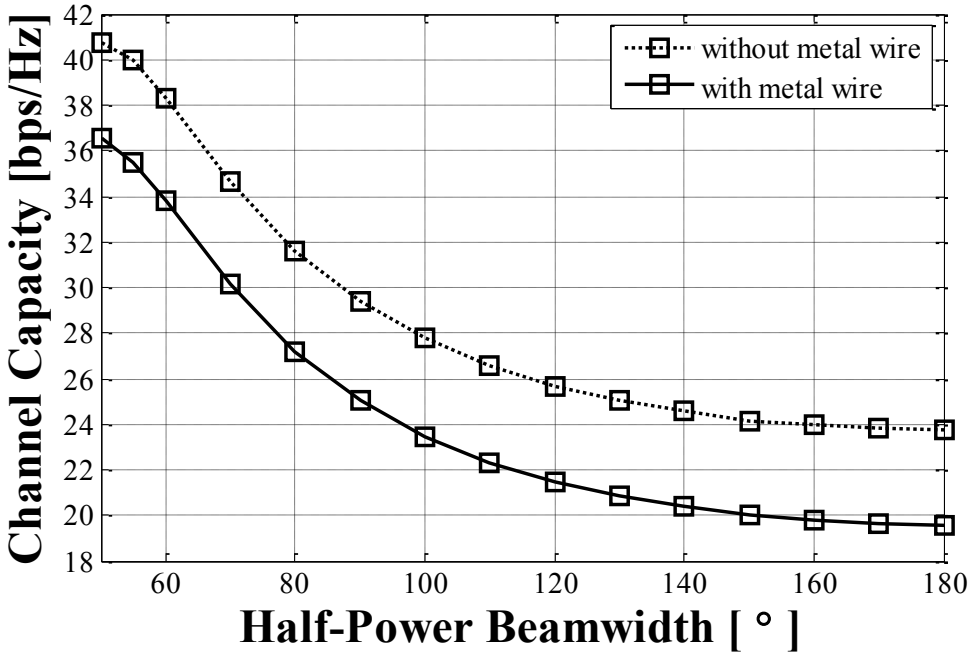

(b) Vertical array

Fig. 5.6. Effect of HPBW on channel capacity in the system with metal wire.

5.1.3 Effect of the Location of the Metal Wire

Since the distance between Tx and Rx arrays is very short, a slight offset of the metal wire location will significantly affect the channel capacity. To verify the effect of the metal wire location, the metal wire is simulated at different locations in the offset area, as shown in Fig. 3.10 and Fig. 3.11. We fix antenna distance D at $1.6\lambda_0$, element spacing d at λ_0 and the HPBW at 50 º. Since the top views of the arrays are symmetrical, the offset area is considered to be only the upper half. The center of the system is set as the origin of the offset for the metal wire. The terms Δx_{mw} and Δy_{mw} denote the offset in the x and y directions, respectively. Especially, in the y direction, when the metal wire is close to the Tx array, Δy_{mw} is defined as '-', and when it is close to the Rx array, Δy_{mw} is defined as '+'.

The effect of the metal wire location in the offset area on the channel capacity is shown in Fig. 5.7. The level curves of the channel capacities when the system is without any metal wire are drawn as the white lines and denoted by $CC_{\mathrm{w/o}}$. The locations where the channel capacities are much higher than $CC_{\mathrm{w/o}}$ are defined as the proper locations, and they are marked as stars. And the location of the lowest channel capacity is marked by a square. The locations of the Tx and Rx antennas are indicated by '⊳' and '⊲', respectively.

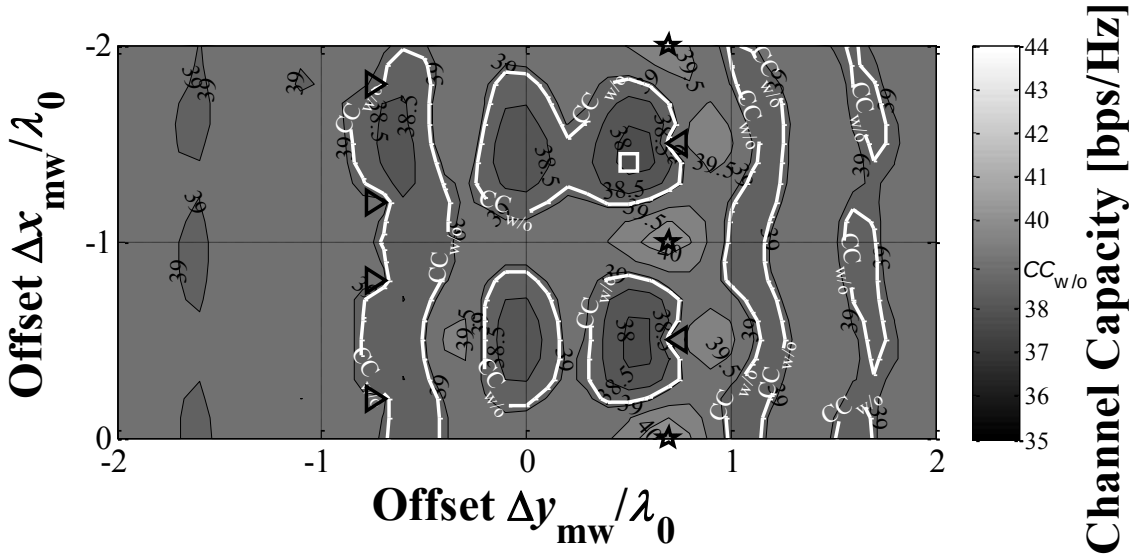

(a) Horizontal array

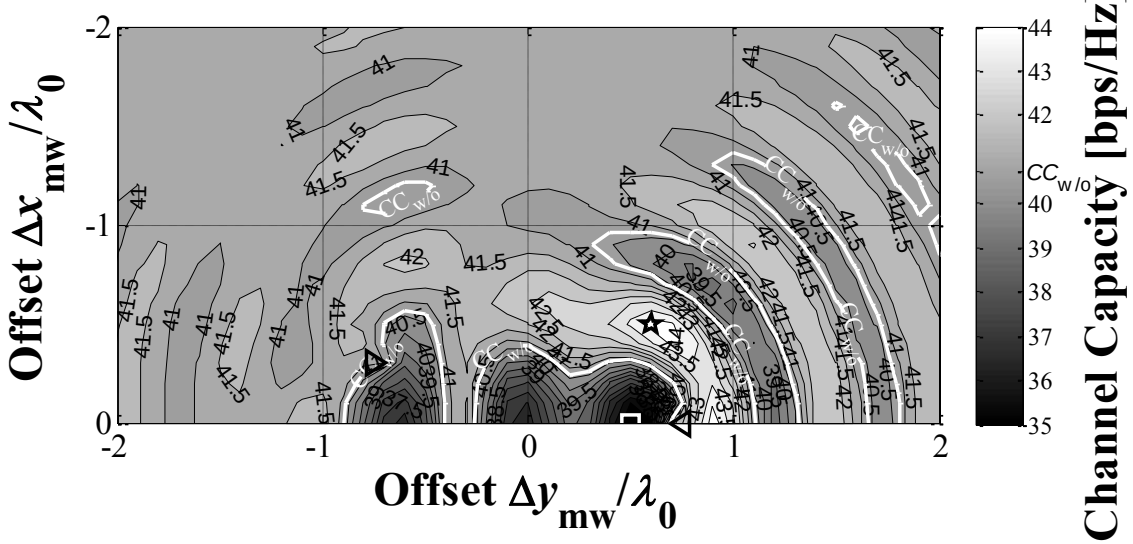

(b) Vertical array

Fig. 5.7. Effect of metal wire location on channel capacity.

Figure 5.7 shows that when the location of the metal wire changes, the channel capacity of the system changes greatly. Especially, when the metal wire is placed between the Tx and Rx elements in one pair, the channel capacity decreases significantly, as shown by the dark areas. When the metal wire is far from the arrays the effect of the metal wire can be ignored. Furthermore, it should be noted that when

the metal wire is placed in certain locations as the bright areas shown in Fig. 5.7, we can obtain a high channel capacity which is even higher than that in the system without a metal wire. We named the kind of areas as the proper locations. The proper locations distribute on both sides of each Rx element, and the Δy_{mw} is found at $0.65\lambda_0$. As shown in Fig. 5.7(a), the proper locations in the horizontal array can be found between every two adjacent Rx elements and another two proper locations can be found beyond the two outer Rx elements. That means in the horizontal array, the number of proper locations will increase with the number of elements increases. And we only considered upper half of the total offset area as shown in Fig. 3.10(b), therefore, there are $M_R + 1$ proper locations in the system when using the horizontal array. On the other hand, in the vertical array, we can observe only one Rx element from the top view as shown in Fig. 3.11(b). So no matter how many elements are there in the arrays, the number of proper locations is always only 2 in the system when using the vertical array.

For observing the effect of the metal wire on channel capacity more clearly, we fix Δy_{mw} at $0.65\lambda_0$ (the offset of the proper locations in y direction) and change Δx_{mw}. The variation of the channel capacity with Δx_{mw} is shown in Fig. 5.8. The channel capacities of the systems without metal wires are also plotted in the figure as straight lines. Figure 5.8 indicates that when the metal wire is placed at the proper locations, the improvement of the channel capacity is considerable. Especially, in the vertical array, the maximum channel capacity increases more than 3bps/Hz from the system without a metal wire. In the horizontal array, the improvement of channel capacity is not so obvious, but there are several proper locations. At the meanwhile, we can see that when the metal wire is placed at some locations that can decrease the channel capacity, the degradation in the vertical array is much more serious than that in the horizontal array. Because the metal wire is placed parallel with the dipoles, it will exert the same influence on all the elements at the same time in the vertical array. However, in the horizontal array, due to the distances from each element to the metal wire are different, the effects of the metal wire to each element are different, and they may weaken the effects by each other. That is the reason why the effect of metal wire in the vertical array is more obvious.

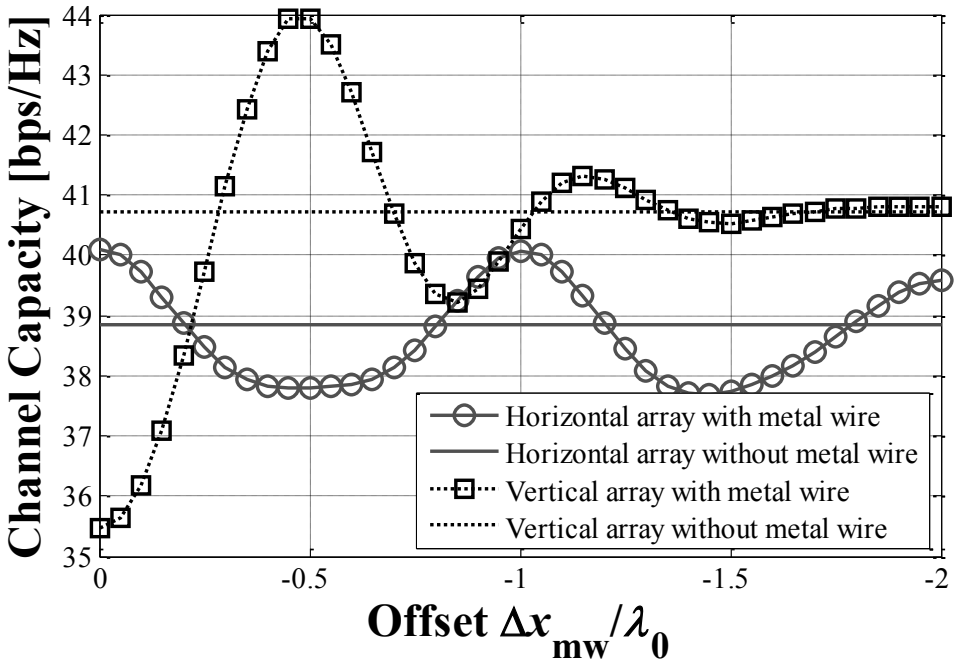

Fig. 5.8. Comparison in effect of metal wire location on channel capacity (D=1.6λ_0 d=λ_0 Δd=0.6λ_0 Δy_{mw}=0.65λ_0).

To explain the variation of the channel capacity caused by the metal wire in Fig. 5.8, the variation of the eigenvalues is shown in Fig. 5.9. In the horizontal array, the 1st eigenvalue changes only a little, and the significant improvement is caused by the 2nd and 3rd eigenvalues, and the reduction of the 4th one is the worst. That makes the gentle variation of the channel capacity in the horizontal array as shown in Fig. 5.8. In the vertical array, the 4 eigenvalues almost change in the same step. They increase or decrease in the same time and with the same degree. That's the reason why the channel capacity improvement is more in the vertical array.

Generally, an object placed between the Tx and Rx antennas will decrease the channel capacity of the system. Here, we try to determine the optimal location of the object between the Tx and Rx antennas. We expect that the optimal location will alleviate the deterioration in the capacity caused by the object. However, the simulation results indicate that if the metal wire is placed in a proper location, a channel capacity which is even higher than the one of the system without a metal wire can be obtained. And we find there are plural different proper locations in the system.

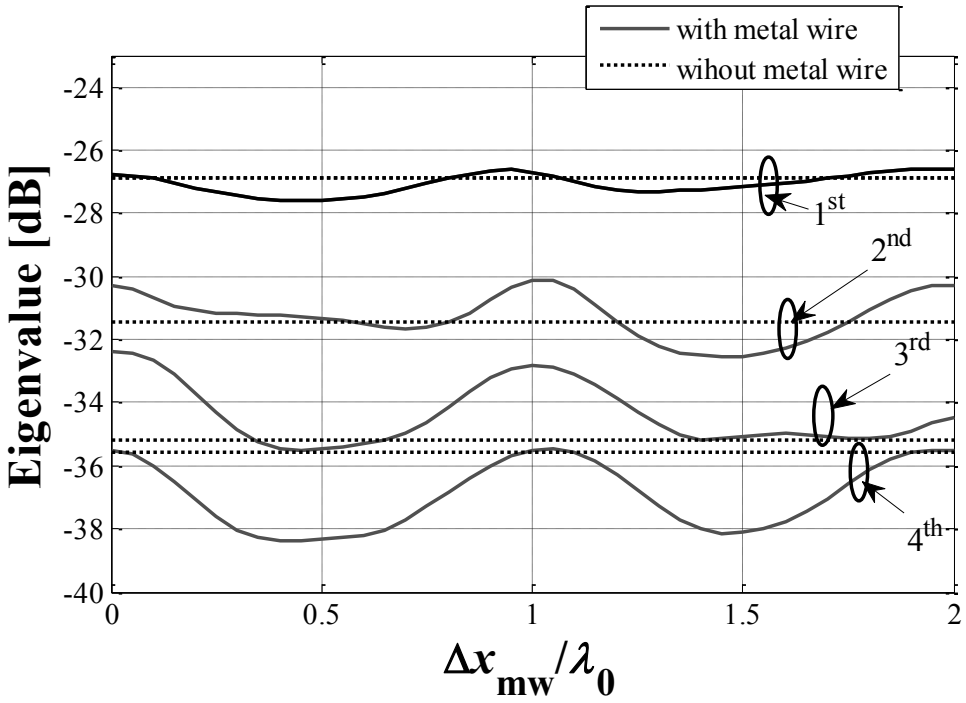

(a) Horizontal

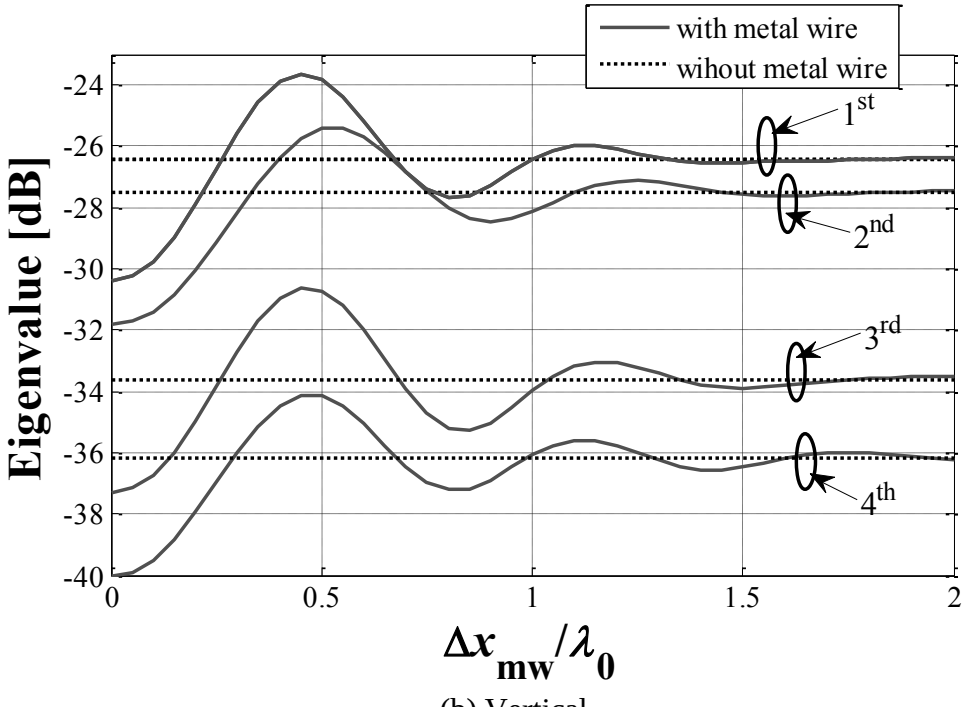

(b) Vertical

Fig. 5.9. Effect of metal wire location on eigenvalue (D=1.6λ_0 d=λ_0 Δd=0.6λ_0 Δy_{mw}=0.65λ_0).

5.1.4Generality of Improvement by Metal Wire

The effect of the metal wire was investigated only upon one specific situation in previous section. To clarify the generality of the improvement on channel capacity caused by the metal wire, we fix the element spacing d at λ_0 and change the antenna distance D and the HPBW at the meanwhile of moving the metal wire in the offset area.

The channel capacity of the system without a metal wire is denoted as $CC_{w/o}$ and the maximum channel capacity of the system affected by a metal wire is denoted as CC_{max}. Then, the difference between the maximum channel capacity and the channel capacity without a metal wire can be defined as

$$CC_{\Delta} = CC_{max} - CC_{w/o}. \quad (5.1)$$

We use the CC_{Δ} to evaluate the improvement of the channel capacity caused by the metal wire.

The value of CC_{Δ} in every specific situation is plotted in Fig. 5.10. And the highest CC_{Δ} is marked as a star. From Fig. 5.10, we can find that all the values of CC_{Δ} are larger than 0. It implies that no matter how the antenna distance or the HPBW change, as long as the metal wire is placed in the proper location, the channel capacity in the near-field MIMO will improve. Therefore, the generality of the improvement by a metal wire is verified. In addition, Fig. 5.10 indicates that the D makes the larger influence than the HPBW on the CC_{Δ}. Once the D is determined, the CC_{Δ} will hardly change with different HPBW. The maximum CC_{Δ} in the horizontal array is found at the situation when D=0.6λ_0 and HPBW=150°, and in the vertical array is found at the situation when D=0.7λ_0 and HPBW=180°.

The effects of the metal wire location at both maximum situations are shown in Fig. 5.11 in horizontal array and vertical array respectively. In these cases, the metal wires are placed in the center of the Tx and Rx. Corresponding to the expected application image, if the relative location between the MIMO antennas and the metal wire in the wall is set properly, the channel capacity will improve.

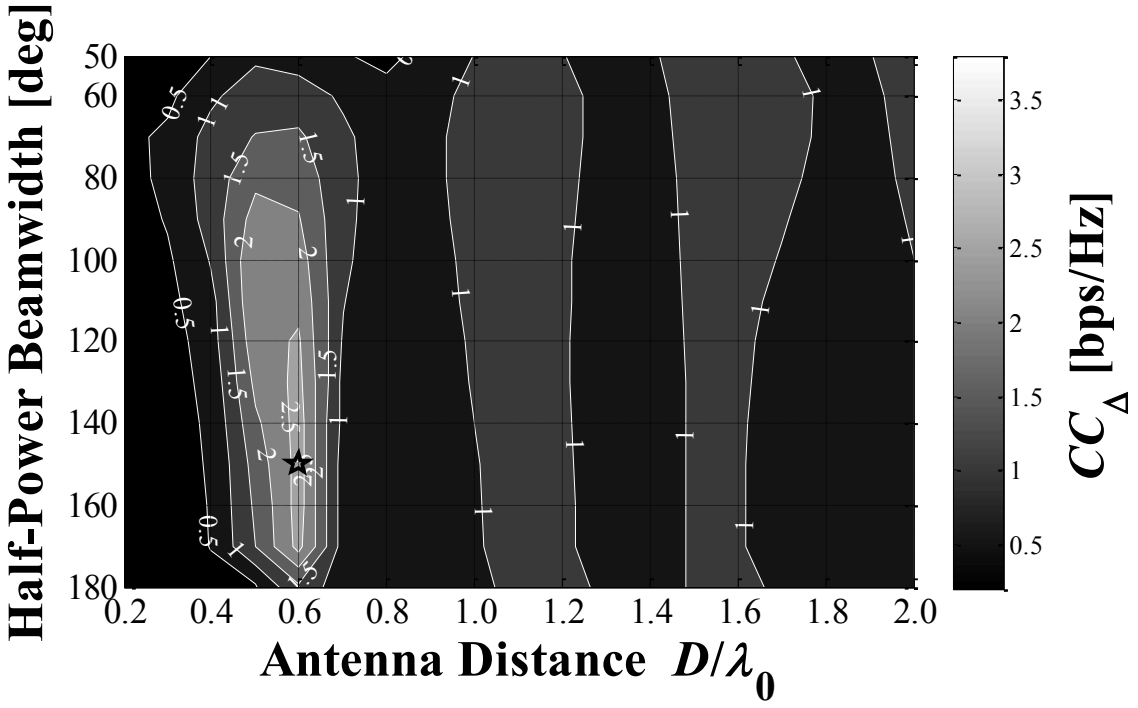

(a) Horizontal array

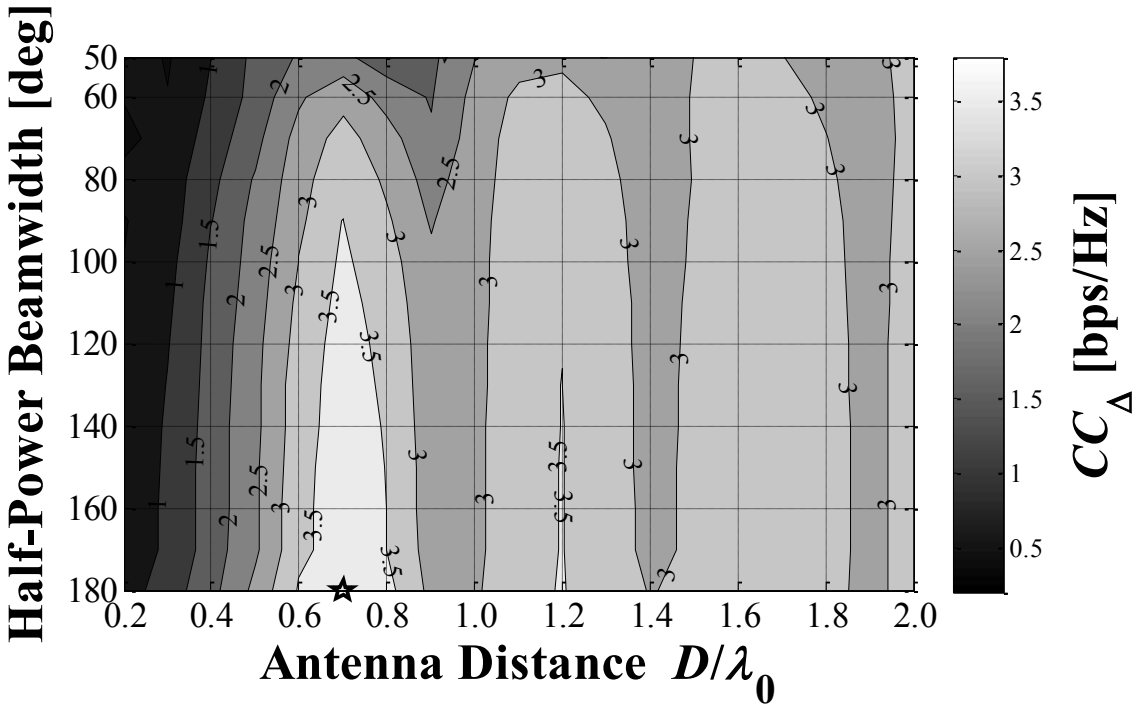

(b)Vertical array

Fig. 5.10. Generality of channel capacity improvement.

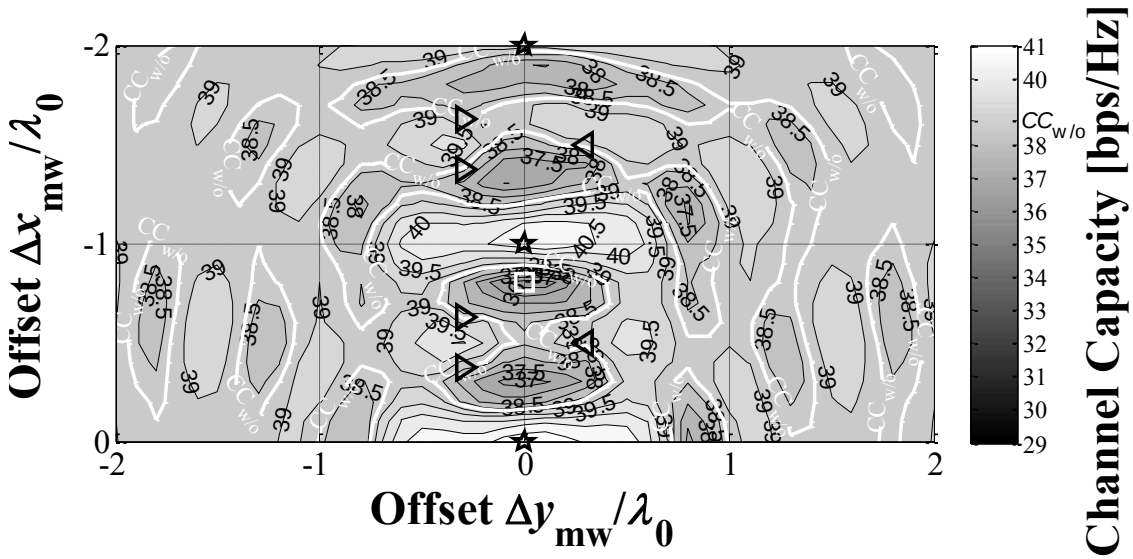

(a) Horizontal array (D=0.6λ_0, d=λ_0, HPBW=150 ℃)

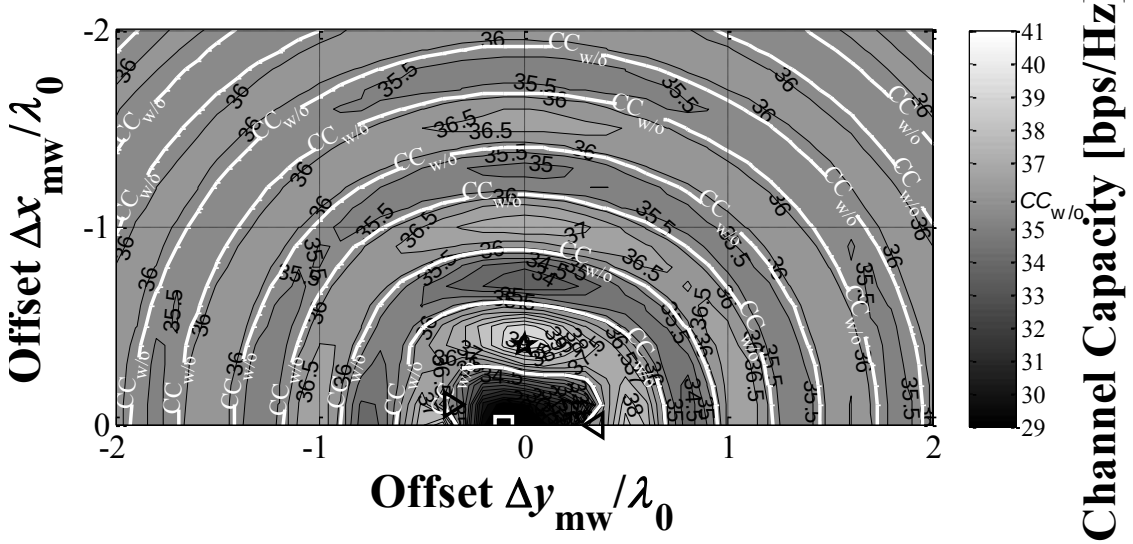

(b) Vertical array (D=0.7λ_0, d=λ_0, HPBW=180 ℃)

Fig. 5.11. Effect of metal wire location at the situation of the maximum CC_{Δ}.

5.2 Effect of Multiple Metal Wires in Near-Field MIMO System

The effect of only one metal wire in the near-field MIMO system was clarified in the Section 5.1, and we can notice that there are plural proper locations in the system. Hence, it is expected that the channel capacity will increase with multiple metal wires. The analysis models of different arranged arrays with multiple metal wires are shown in Fig. 3.12. The metal wires are placed at the proper locations. The antenna distance D is fixed at $1.6\lambda_0$, the element spacing d fixed at λ_0, and the HPBW is fixed at 50 °.

The performance of the metal wire placed in the horizontal or the vertical array is depicted very clearly in Figs. 5.7 and 5.8. In the vertical array, although the effect of an individual metal wire in the channel capacity is much better than that in a horizontal array, the proper locations in which the metal wire could improve channel capacity are only 2, not as many as in the horizontal array. Therefore, to combine the advantages of the horizontal and vertical arrays, we choose the square arrays to investigate the effect of multiple metal wires in the near-field MIMO system. In the square arrays, as shown in Fig. 3.12(c), the antenna elements are arranged the same in the both horizontal and vertical dimensions, and with the same element spacing d fixed at λ_0.

5.2.1 Proper Locations for Multiple Metal Wires

The effect of single metal wire in near-field MIMO systems was clarified in the Sec. 5.1, and we can note that there are plural proper locations in the system.

In this subsection, 2 metal wires are employed in the system to clarify the proper locations for the multiple metal wires. The parameters of the system are entirely the same as the system discussed in Sec. 5.1.3. Except that an additional metal wire is fixed at the proper location on the opposing side of the offset area. The other metal wire moves in the same offset area as shown in Figs. 3.10 and 3.11. The effect of the location of the mobile metal wire in the offset area on the channel capacity is shown in Fig. 5.12. The level curves of the channel capacities when the system is with only one metal wire at the proper location are drawn as the white lines and denoted by $CC_{1\mathrm{mw}}$.

Comparing Fig. 5.7 and Fig. 5.12, we can see that the proper locations for a single metal wire and for 2 metal wires are exactly at the same place. Thus, we can say that the proper locations for one wire are also effective for plural wires. In addition, the channel capacities in Fig. 5.12 are obviously larger than the ones in Fig. 5.7, and the differences are just the same as the improvement caused by the fixed metal wire in the proper location. So it is clarified that the effects of multiple metal wires can be accumulated together. Therefore, we can expect that the channel capacity will increase with multiple metal wires placed in the plural proper locations simultaneously.

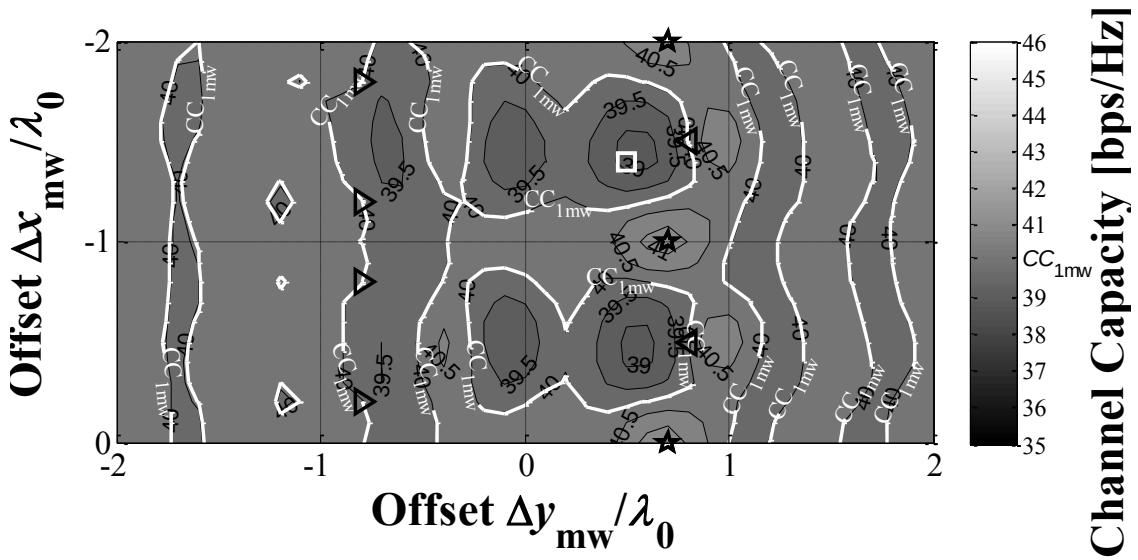

(a) Horizontal array

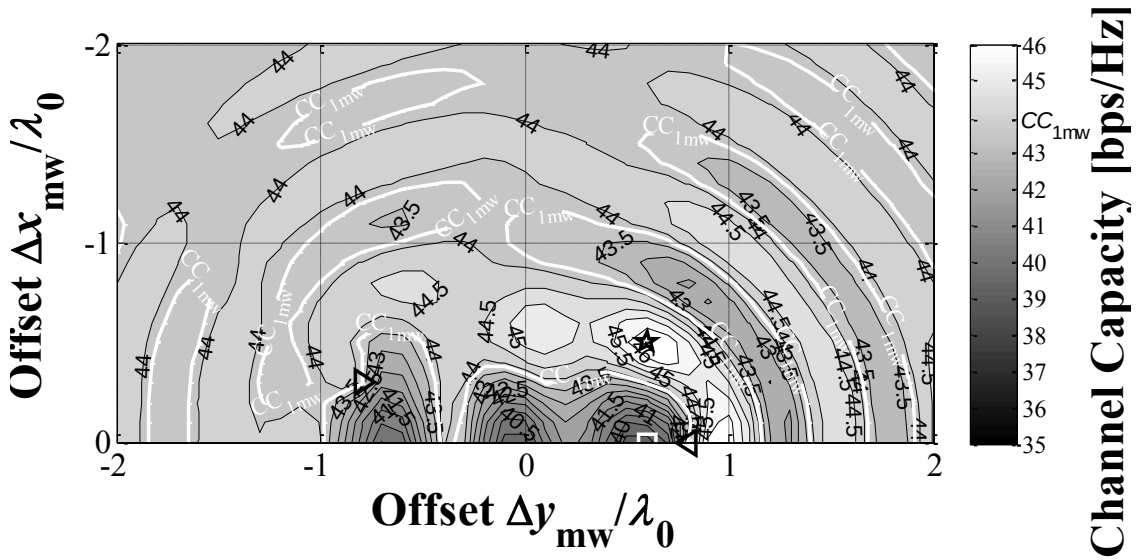

(b) Vertical array

Fig. 5.12. Proper locations for 2 metal wires.

5.2.2 Effect of Array Arrangement

Figure 5.13 shows the comparison of using different array arrangements. We can find that the numbers of the proper locations are limited and related to the different array arrangements. As mentioned in Sec. 5.1.3, there are $M_R + 1$ proper locations in the horizontal array and only 2 proper locations in the vertical array. In addition, in a square array with $n \times n$ elements, the number of proper locations is $n + 1$. When the number of antenna elements is fixed, even if more metal wires are placed in the system, the channel capacity will hardly improve. From Fig. 5.13 we can find that the vertical array is affected by the metal wire most. And the square array would achieve the same channel capacity by utilizing more additional metal wires placed in different proper locations. According to the different array arrangements, the speed of channel capacity improvement is different. The vertical array is the fastest, however, no matter how many antenna elements are there in the vertical arranged array, there are only two proper locations. Obviously, two is not enough to investigate the effect of multiple metal wires. In the square array and horizontal array, the number of proper locations increases when the number of antenna elements increases. And in the square array, the effect of the metal wires is more significant. Therefore, the square arrays are selected to clarify the effect of multiple metal wires.

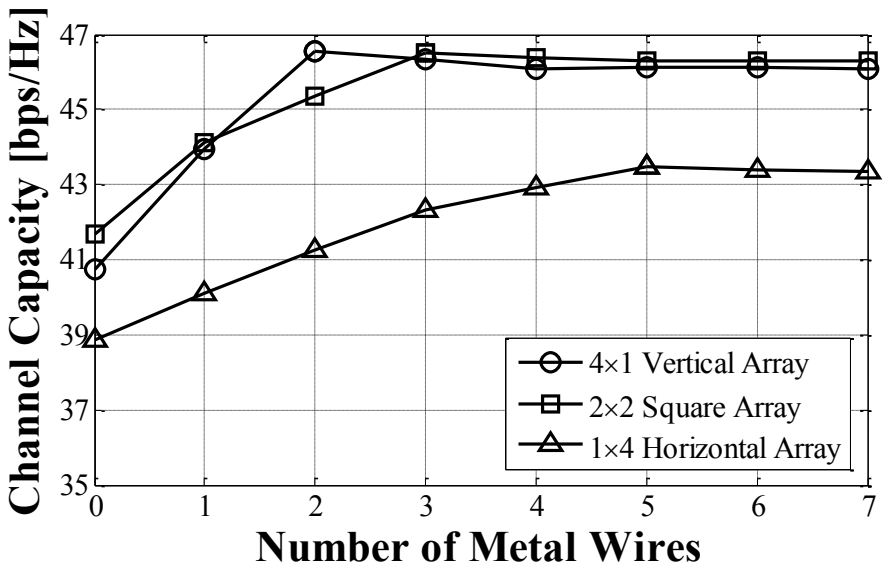

Fig. 5.13. Comparison of different array arrangements.

5.2.3 Effect of the Number of Metal Wires

Figure 5.14 shows the effect of the number of metal wires on the improvement of channel capacity when the square arrays are used. From Fig. 5.14 we can see that as the number of antenna elements increases, we can set more metal wires in the system to improve the channel capacity. And as the number of metal wires increases, the maximum channel capacity of the system will enhance. The effects of multiple metal wires can accumulate together. The improvement of channel capacity is approximately proportional to increase with the number of metal wires.

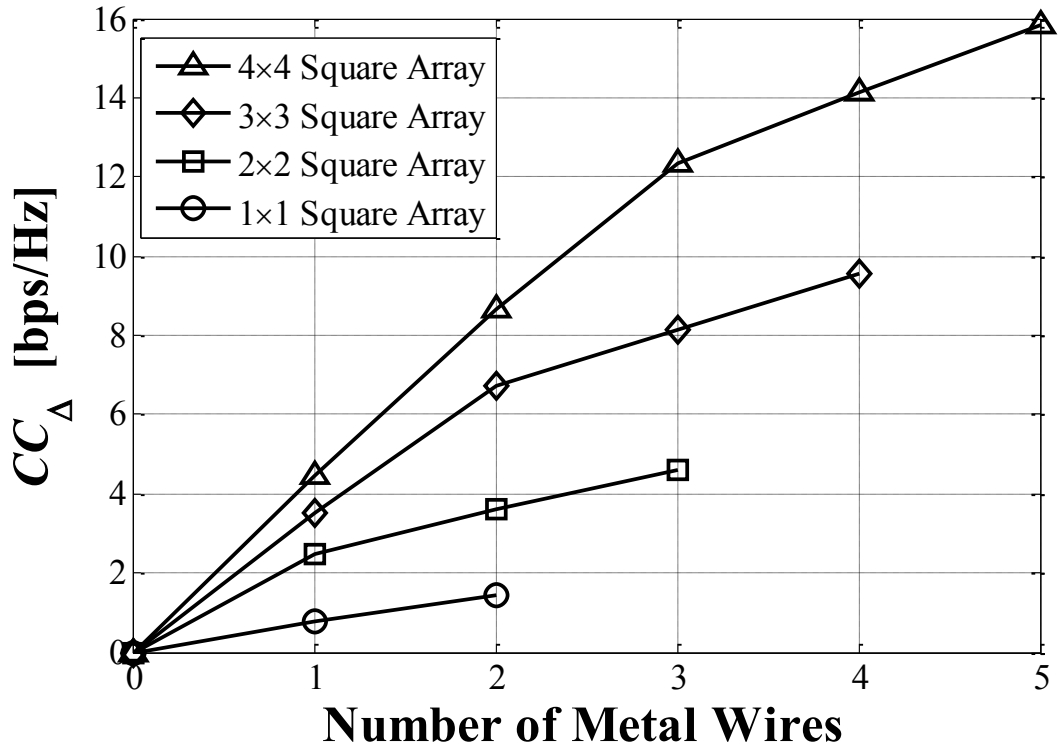

Fig. 5.14. Effect of number of metal wires on CC_Δ.

Chapter 6 Frequency Dependency of Channel Capacity in Near-Field MIMO System with Metal Wire

Recently, a novel scheme of applying Multiple-Input-Multiple-Output (MIMO) technology for the near-field communication has been proposed. Contrary to conventional MIMO systems, near-field MIMO communication systems transfer data over very short ranges, and the line-of-sight (LOS) paths are the major components. Hence, the contribution of the multipath components will not appear in near-field MIMO systems. However, the channel capacity might be higher than the ergodic capacity since the near-field MIMO system has a high similarity with a parallel data transmission. One of the expected applications for near-field MIMO systems is a wireless repeater, which can connect networks in two adjacent rooms through a wall. The metal wires in the wall are considered as the major obstacles in the system. The improvement on channel capacity by metal wire and the proper location for the obstacle metal wire in near-field MIMO system have been verified in. However, in actual applications, the system might work within various wireless communication standards with different specific frequencies. Therefore, this paper applies the near-field MIMO system with metal wire in different frequencies to study the effect of frequency on channel capacity.

6.1 Configuration of analysis model

The Near-field MIMO analysis model used in this paper is shown in Fig. 6.1(a). Two linear vertical arrays consisting of identical half-wavelength dipole antennas are placed parallel face-to-face as the transmitter (Tx) and receiver (Rx), respectively. The numbers of antenna elements on the Tx side, M_T, and on the Rx

side, M_R, are set to the same value, i.e., four. The distance between two adjacent antenna elements is denoted as element spacing *d*, and the distance between the transmitter and receiver is defined as antenna distance *D*. The operating frequency of the system is variable, so the length of the dipoles changes with the frequency varying. But *D* and *d* are fixed while changing the frequency. A metal wire is placed near the arrays. Considering the polarization direction, the impact of the metal wire is negligible when the metal wire is set perpendicular to the dipoles. Hence, the metal wire is set parallel to the dipoles. Term *L* indicates the length of the metal wire. To avoid instability from diffraction caused by a short metal wire, and to avoid a heavy calculation load caused by a long metal wire, 1000mm is selected as a suitable length for the metal wire and used hereafter.

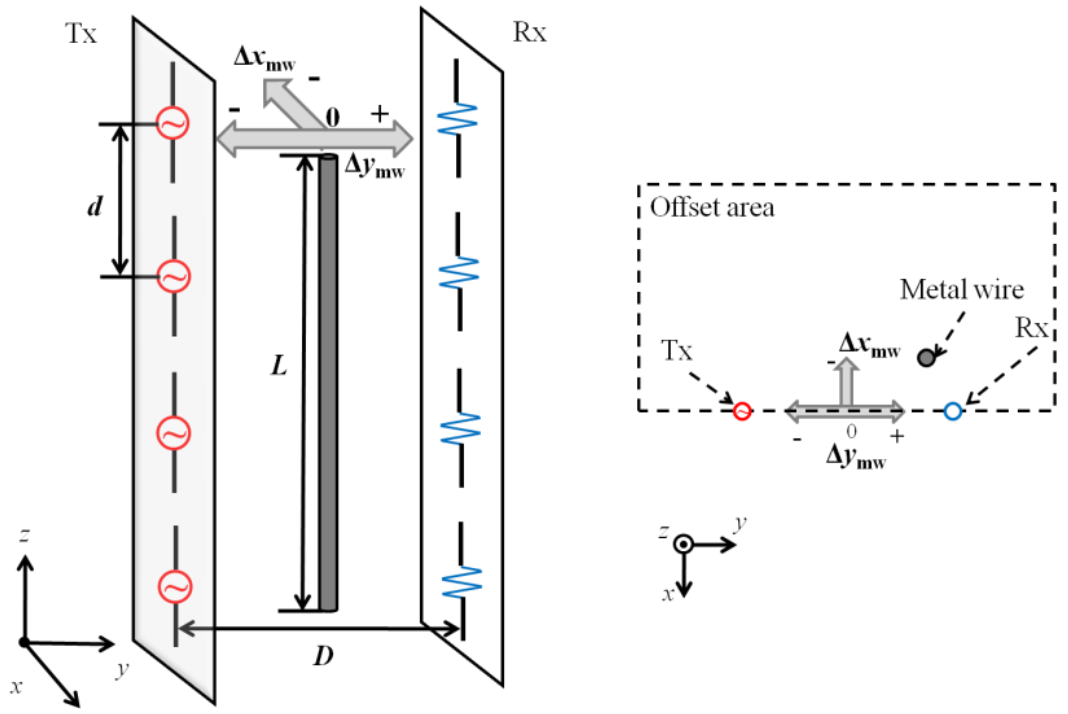

(a) Configuration of analysis model. (b) Top view of analysis model.

Fig. 6.1. Analysis models of near-field MIMO with metal wire.

To verify the effect of the location of the metal wire, the metal wire is simulated at different locations in the offset area, as shown in Fig. 6.1(b). Since the top view of the array is symmetrical, the offset area is considered to be only the upper

half. The center of the system is set as the origin of the offset for the metal wire. Terms Δx_{mw} and Δy_{mw} denote the offset in the x and y directions, respectively. Especially, in the y direction, when the metal wire is close to the Tx array, Δy_{mw} is defined as '-', and when it is close to the Rx array, Δy_{mw} is defined as '+'.

The SNR in this study is constrained at 20dB. All of the results in this paper are calculated using the Method of Moments (by EEM-MOM).

6.2 Effect of frequency on metal wire's proper location

The channel capacity of the system without a metal wire is denoted as $CC_{w/o}$ and the channel capacity of the system affected by the metal wire in each specific location is denoted as CC_{mw}. Then, the difference between the channel capacity of the system with a metal wire and that without a metal wire can be defined as

$$CC_{\Delta} = CC_{mw} - CC_{w/o}. \tag{6.1}$$

CC_{Δ} can be used to evaluate the improvement in the channel capacity due to the metal wire. The effect of the metal wire location in the offset area with different frequencies is shown in Fig. 6.2. In this simulation, D and d are fixed at 160mm and 100mm, respectively. The locations of the Tx and Rx antenna elements are indicated by '⊳' and '⊲', respectively. The level curves of the channel capacities when the system is without a metal wire are marked by '0'. The location with the highest channel capacity is defined as the proper location, and it is marked by a star. The location of the lowest channel capacity is marked by a circle.

From Figs. 6.2(a-c), we can find that although the offset area of the metal wire is exactly the same, the effects of the metal wire on channel capacity with respective frequencies are different. As the frequency increases, the coverage of the metal wire's effect becomes smaller. Especially, when using 10GHz, once the offset in x direction, Δx_{mw}, is larger than 100mm, the effect of the metal wire is negligible. In addition, the effects of the metal wire on the Tx side and on the Rx side are similar, the figures are almost symmetric, but the effect on the Tx side is slightly greater. Both the best and the worst points are found on the Tx side. Furthermore, the proper location is closer to

the antenna element when the frequency becomes larger. The distance between the proper location and the Tx element is denoted as d_{pl}. The relationship between frequency and d_{pl} is shown in Fig. 6.2(d). d_{pl} in each specific frequency is marked by a red circle, and the corresponding half wavelength of every specific frequency, $0.5\lambda_0$, is also ploted by a dotted line in the same figure. Comparing the d_{pl} and the corresponding half wavelength, we can find that no matter how the frequency changes, the proper location can be found nearly $0.5\lambda_0$ from the Tx element. In addition, once the frequency is decided, d_{pl} will hardly change with different D.

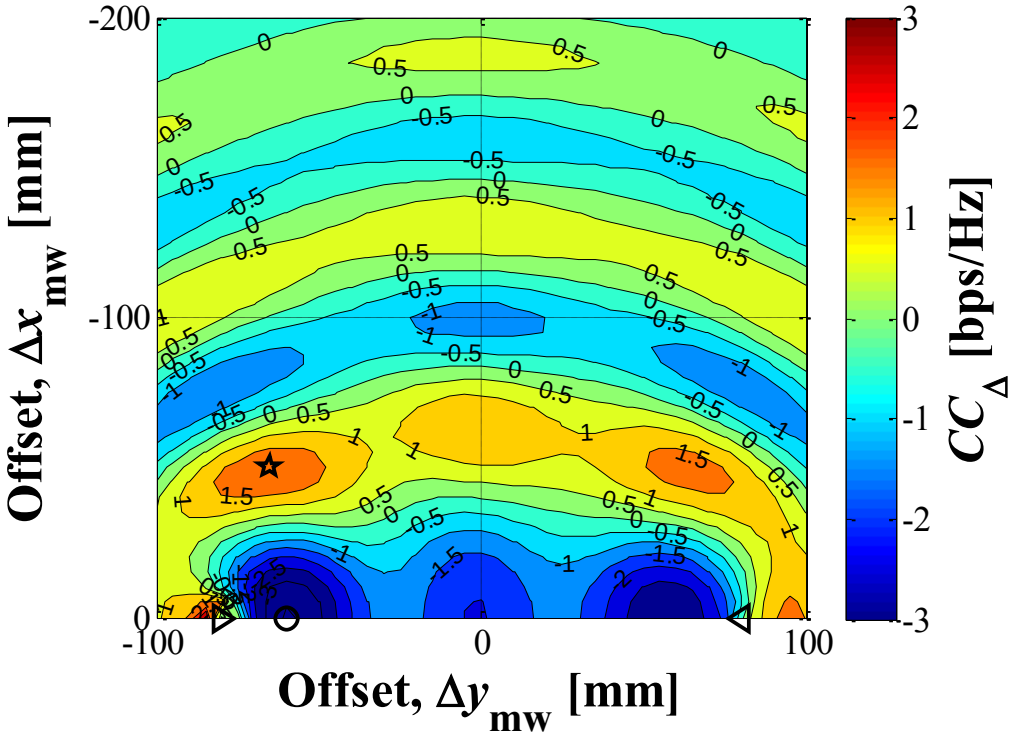

(a) 3GHz

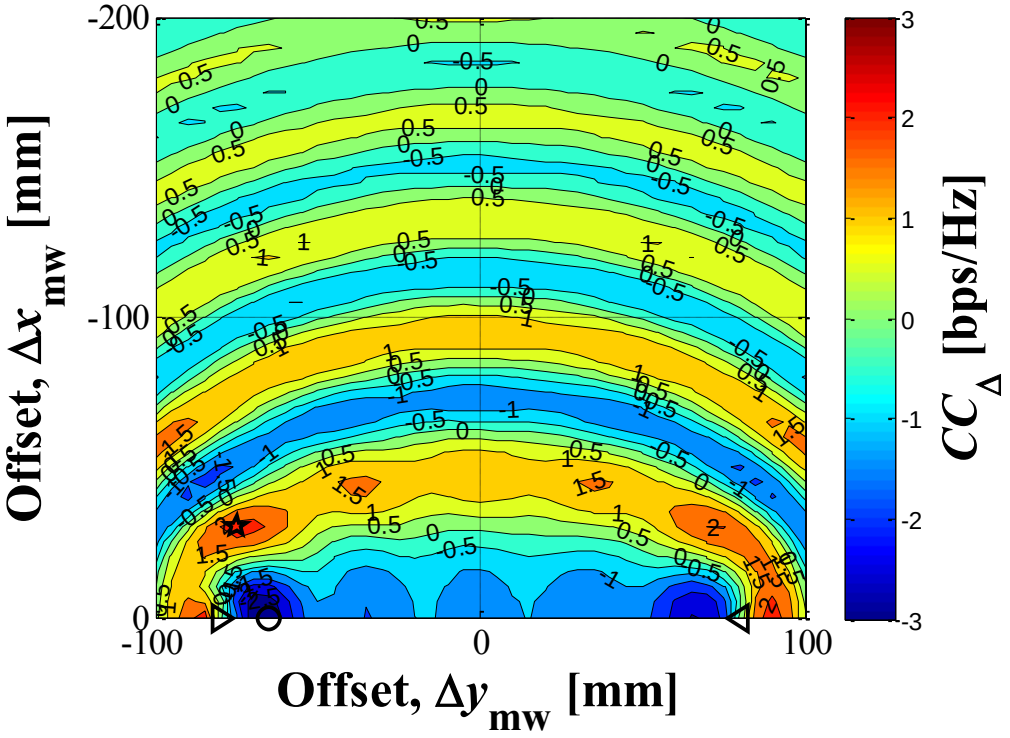

(b) 5GHz

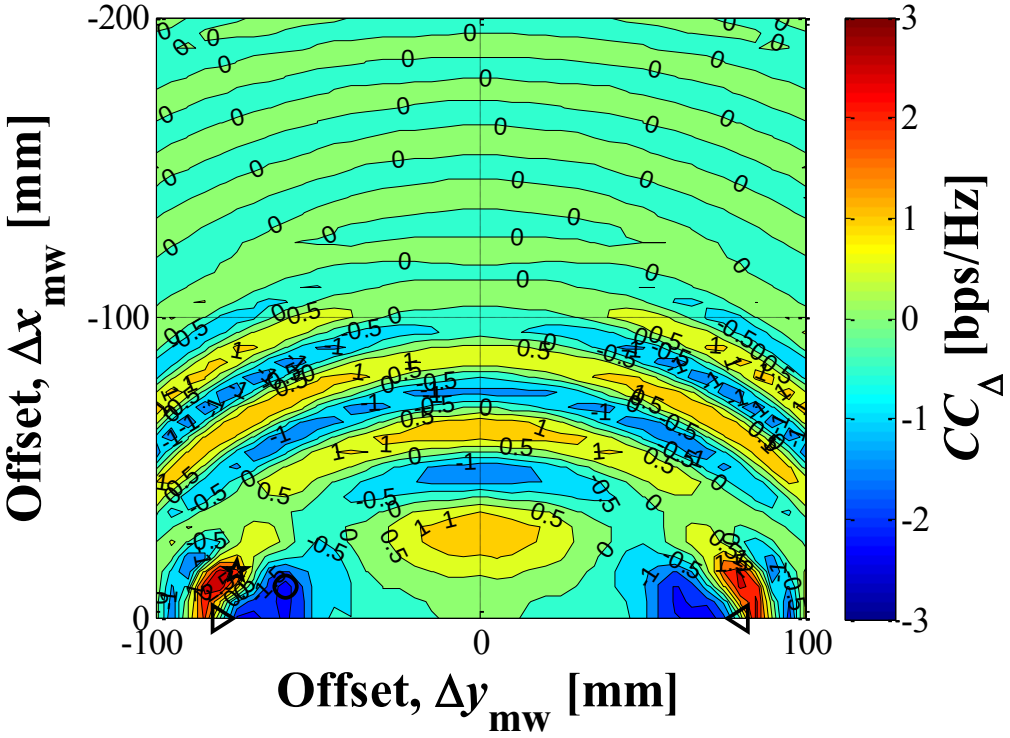

(c) 10GHz

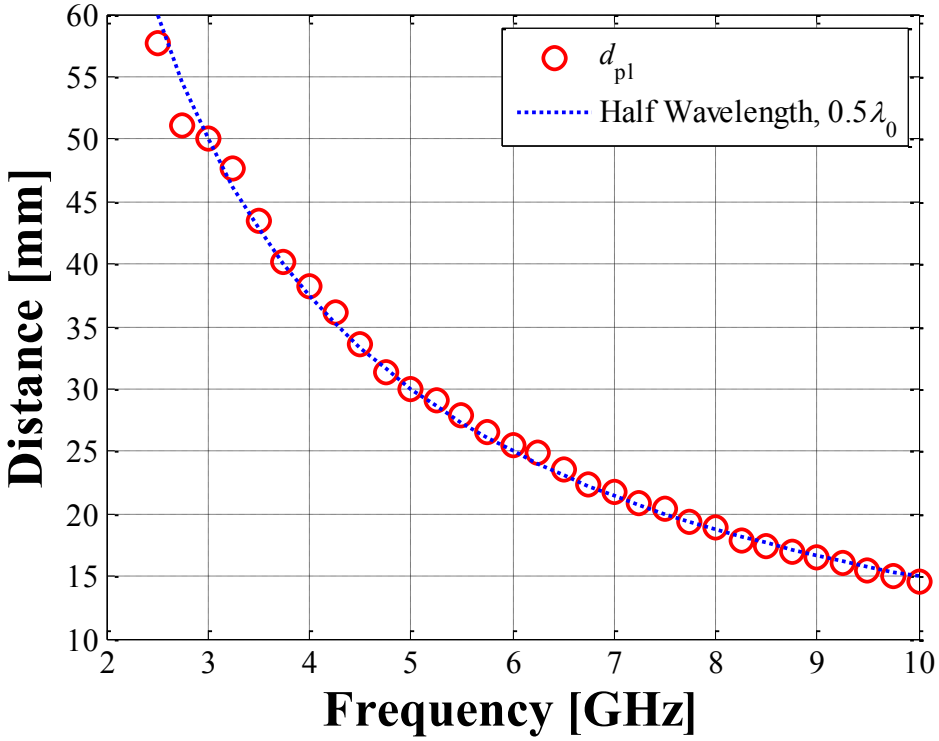

(d) Relationship between frquency and d_{pl}.

Fig. 6.2. Effect of frequency on metal wire's proper location.

6.3 Frequency dependency of channel capacity improvement

The change of the channel capacity caused by frequency is shown in Fig. 6.3. In this figure, the maximum channel capacities of the systems with a metal wire are plotted by the solid lines, and the channel capacities of the systems without a metal wire are plotted by the dot lines. Considering the thickness of the wall can be chosen as different value, various antenna distances, *D*, are concerned. And the element spacing, *d*, is still fixed at 100mm.

Figure 6.3 indicates that when the frequency increases, the channel capacity decreases. However, the reduction of the channel capacity is not smooth. The reason of the fluctuated curves of the channel capacity is that when frequency changes the corresponding wavelength, λ_0, changes, then the relative values of *d* and *D* with

respect to λ_0 are variable. Element spacing, d, affects not only the receiving SNR but also the spacial correlation [21], therefore, the channel capacity is fluctuated with the frequency.

From Fig. 6.3, we can see that the channel capacity improvement appears with every frequency. Especially, in the range from 5GHz to 25GHz, the improvement is very consideralbe. However, the improvement becomes smaller as the frequency becomes larger. When the frequency is larger than 30GHz, the improvement on channel capacity by a metal wire is negligible.

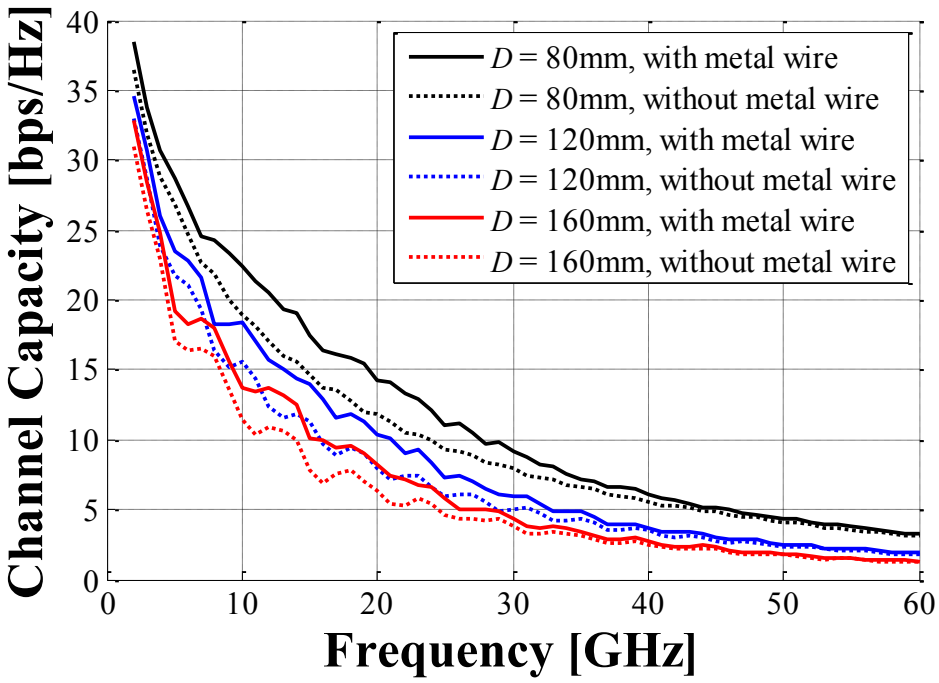

Fig. 6.3. Frequency dependency of channel capacity change.

The relationship between the frequency and the maximum channel capacity improvement is shown in Fig. 6.4. The maximum channel capacity can be found at the proper location indicated in Fig. 6.2 and denoted as $CC_{\Delta max}$. Considering the thickness of the wall can be chosen as different value, various antenna distances, D, are concerned. And the element spacing, d, is still fixed at 100mm. As discussed in the previous subsection, d_{pl} is only depended on the frequency, so the proper location

of the metal wire will change as frequency changes. Hence, the metal wire's location in Fig. 6.4 is varied depending on the frequency to maintain the optimum condition.

From Fig. 6.4, we can see that the channel capacity improvement appears with every frequency. When the frequency is less than 10GHz, $CC_{\Delta max}$ increases as the frequency increases. And when the frequency is larger than 20GHz, $CC_{\Delta max}$ decreases as the frequency increases. Especially, the maximum value of the channel capacity improvement is found in the range from 10GHz to 20GHz. In addition, as the antenna distance, D, increases, $CC_{\Delta max}$ becomes smaller, and the curve of $CC_{\Delta max}$ declines earlier.

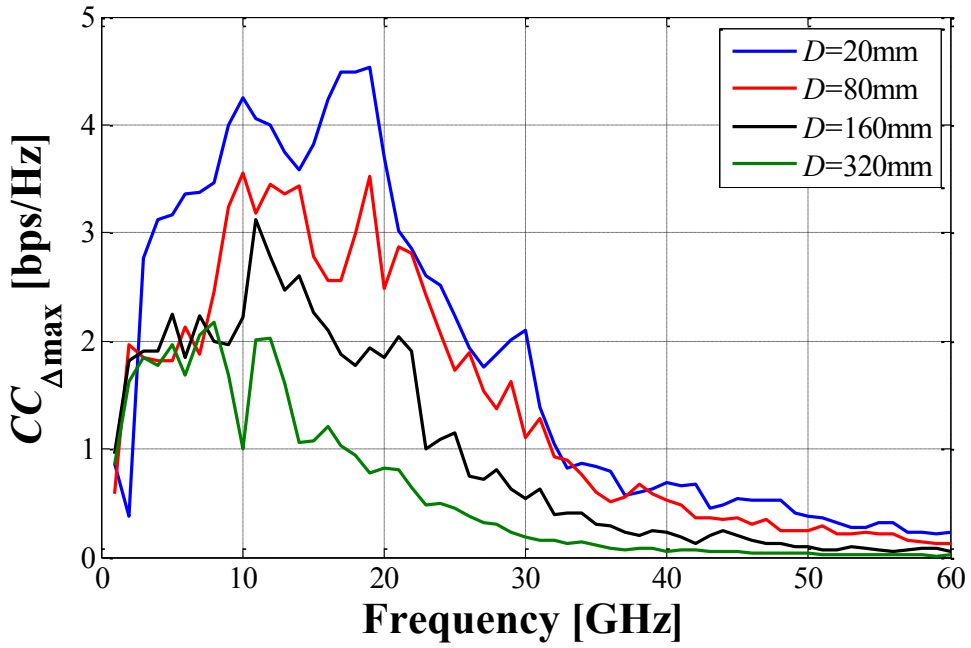

Fig. 6.4. Frequency dependency of channel capacity improvement.

Chapter 7 Conclusions

In this chapter, the contributions of this dissertation are concluded. It is summarized how the HPBW affect channel capacity in the near-field MIMO systems, and how the metal wire improve the channel capacity. The metal wire that was supposed as the obstacle in the system but with the proper location will improve the channel capacity.

In this study, the channel capacity characteristics in near-field MIMO system were exhaustively researched. Two methods of improving the channel capacity in the near-field MIMO systems were proposed and verified. The first one was the utilization of the dual-dipole array and by adjusting the beamwith of the radiation pattern, and then the channel capacity would increase considerably with the proper HPBW. And the second method was adding the metal wires between the transmitting antennas and the receiving antennas to increase the multipath richness of the system. When the metal wires were settled in the proper locations in the near-field MIMO system, the channel capacity exceeded that without a metal wire.

First, after showing the overview of near field communication and MIMO system, the system models and analysis methods employed in this study were introduced. Especially, the characteristics and advantages of dual-dipole element were declared in detail. The beamwidth of the radiation pattern of the dual-dipole element could be adjusted by the internal distance between the two dipoles in one element. The relationship between the HPBW and the internal distance Δd was clarified.

Second, the horizontal and vertical dual-dipole arrays were introduced to near-field MIMO system in this research. General speaking, when the HPBW became narrower, the dual-dipole MIMO system achieved a higher channel capacity than that for a conventional dipole antenna. As the HPBW changed, the channel capacity achieved a peak. The highest channel capacity was obtained when the HPBW was

approximately 50º. The corresponding Δd for the optimal HPBW was approximately $0.6\lambda_0$. The theoretic explanation was made by the change of eigenvalues.

Third, the effect of the receiver array location error, including offset error and rotational error, were also clarified in this research. The change in the HPBW in terms of the location error affected not only system channel capacity, but also how quickly the channel capacity deteriorates, which represents the stability of the system. The maximum channel capacity was obtained when the HPBW was approximately 50 º, regardless of the location error. As the HPBW became wider, the system became more stable in terms of the location error.

Forth, this study also clarified the channel capacity improvement in near-field MIMO systems, by employing the metal wires placed on the proper locations near the MIMO arrays. Horizontal and vertical dual-dipole arrays were introduced to the near-field MIMO system with the metal wires placed parallel to the dipoles. The basic characters of the metal wire were discussed. The metal wires which were parallel to the dipoles and with the length of $10\lambda_0$ were fit for the investigation. The location of the metal wire near the transmitter array and receiver array affected the system channel capacity significantly. We could obtain different channel capacity by adjusting the relative position between the metal wire and the arrays. In addition, this paper verified that when a metal wire was placed at the proper location in the near-field MIMO system, the channel capacity exceeded that without a metal wire. The improvement with one single metal wire in the vertical array was more considerable, but there were more proper locations in the horizontal array. And the generality of the channel capacity improvement by a single metal wire was verified.

Then, to research the effect of multiple metal wires, the square array was chosen to combine the advantages of both the horizontal and vertical arrays. As the number of antenna elements increased, the square array could contain more metal wires set in proper locations. The effects of multiple metal wires could accumulate together, and the improvement of channel capacity was approximately proportional to increase with the number of metal wires.

Finally, this study investigated the frequency dependency of channel capacity improvement in near-field MIMO system with metal wire. A vertical arranged near-field MIMO array model with fixed antenna distance and element spacing was built. The frequency was varied while moving the metal wire in the offset area. The proper location for the metal wire changed with the frequency changing. The distance between the proper location and the antenna element was found to be approximately $0.5\lambda_0$, corresponding to the frequency. In addition, the improvement on the channel capacity by a metal wire was also affected by the frequency. The channel capacity improvement in the frequency from 5GHz to 25GHz was clearly considerable. However, the improvement was negligible when the frequency was larger than 30GHz.

Confidently, the research of the effect of the element HPBW and the objects between Tx and Rx introduced in this study can be beneficially applied in actual network preparation of future near-field MIMO wireless communications in which the improvement in the channel capacity are required.

Acknowledgments

The research for this doctoral dissertation has been carried out in the Graduate School of Engineering, Department of System Design Engineering, University of Fukui, Fukui, Japan, during the years 2009-2012. The financial support for this study was provided by the Ministry of Education, Culture, Sports, Science and Technology (MEXT), the Japanese Government, through the monthly Monbukagakusho scholarship.

First of all, I wish to express my deep gratitude to my supervisor, Prof. Dr. Toshikazu Hori, not only for his excellent academic advice, continuous encouragement, and kind support during the course of this work, but also for introducing me to the area of MIMO wireless communications. It has been an honor to work with such deeply dedicated teacher as well as outstanding researcher.

I am very glad to express my sincere appreciation to my co-supervisor, Asst. Prof. Dr. Mitoshi Fujimoto, for his kind advices and fruitful guidance about the MIMO systems, and his critical suggestions and comments on all of our co-authored technical papers. I have learned so much from him.

I wish to show my special thanks to Prof. Kiyoshi Nakashima, the Deputy Director of the International Student Center, as well as Ms. Mariko Hayashi, and all staffs of the International Student Office, for providing me a kind cooperation to begin my study here. Without their trust and help, I would not have had an opportunity to pursue my doctoral course in Japan.

I would like to thank all current and former members of the Hori Laboratory as well as all friends at this university for the wonderful friendships and all the joys we had together, especially Ms. Yuki Kawakami and Mr. Sirichai Hemrungrote, for giving me their kind hands to begin my life as well as my research in Japan.

Last but not least, I wish to express my warmest gratitude to my parents and all my relatives for their permanent care and encouragement, as well as to all my dear friends for their warm companies. Foremost, I would like to thank my wife Qi Gui, who is by my side days after days, giving me constant understanding and love throughout the ups and downs in my study.

I am so lucky to have them all in my life.

Dalin Zhang
University of Fukui
September 2013

References

[1] E.W.T. Ngai and A. Gunasekaran, "A Review For Mobile Commerce Research and Applications", Decision Support Systems, 43 (1), pp. 3-15, 2007.

[2] E. Strömmer, J. Kaartinen, J. Pärkkä, A. Ylisaukko-oja and I. Korhonen, "Application of near field communication for health monitoring in daily life," Proc. 28th IEEE EMBS Annual International Conference, New York City, 2006, pp. 3246-3249.

[3] NFC-Forum, "Technical Specification of Type 4 Tag Operation,"

[4] E. Siira and V. Törmänen, "The impact of NFC on multimodal social media application", in Proceedings of Second International Workshop on Near Field Communication, 2010, pp. 51-56.

[5] M. Csapodi and A. Nagy, "New applications for NFC devices", Proc. 16th IST Mobile and Wireless Communications, Budapest, HUNGARY, IEEE, 2007, pp. 245-249.

[6] B. Benyo, A. Vilmos, K. Kovacs and L. Kutor, "NFC Applications and Business Model of the Ecosystem," in Proc. 16th IST Mobile and Wireless Communications Summit, pp. 15, July 2007.

[7] T.W.C. Brown and T. Diakos, "On the design of NFC antennas for contactless payment applications," Antennas and Propagation (EUCAP), Proceedings of the 5th European Conference, pp. 44- 47, April 2011.

[8] M. Roland and J. Langer "Digital signature records for the NFC data exchange format", *Proc. 2nd Int. Workshop Near Field Commun.*, pp.71 -76, 2010.

[9] Mohinder Jankiraman, "Space-Time Codes and MIMO Systems," book, Cambridge university press.

[10] S.Hemrungrote, T.Hori, M.Fujimoto and K.Nishimori,"Channel capacity characteristics of multi-user MIMO systems in urban area," IEEE Antennas and Prop. Soc. Int. Symposium, pp. 1-4, 11-17, 2010.

[11] J. Lv, Y. Lu, Y. Wang, H. Zhao, and C. Y. Han, "Antenna spacing effect on indoor MIMO channel capacity," in Proceedings of Asia-Pacific Microwave Conference, pp.1-3 Dec. 2005.

[12] A.J. Paularj, D.A. Gore, R.U. Babar and B. Helmut, "An overview of MIMO Communications-A Key to Gigabit Wireless," Proceeding of the IEEE, Vol. 92, No. 2, pp.198-218, 2004.

[13] Z. Daud, M. Z. A. Abd Aziz, M. K. Suaidi, M. F. Abdul Kadir and M.K.A Rahim, "Wireless MIMO Channel Capacity Analysis Based on Multiple Spatial Diversity for Indoor Propagation," in roc. IEEE EUCAP 2011, pp. 1659-1661.

[14] S.Nanba, N.Miyazaki, Y.Hirota, and Y.Kishi, "MIMO Capacity Estimation Based on Single and Dual-Polarization MIMO Channel Measurements," in Proc. APCC 2010, pp. 359-364, Oct. 2010.

[15] Y. Karasawa, “MIMO propagation channel modeling,” IEICE Trans. Commun., vol. E88-B, no. 5, pp. 1829-1842, May 2005.

[16] A. Goldsmith, S.A. Jafar, N. Jindal, and S. Vishwanath, “Capacity limits of MIMO channels,” IEEE J. on Selected Areas in Commun., vol. 21, no. 5, pp. 684-702, Jun. 2003.

[17] G. Fettweis, E. Zimmermann, V. Jungnickel and E. A. Jorswieck, “Challenges in future short range wireless systems,” IEEE Vehicular Technology Magazine, vol. 2, no. 1, pp. 24-31, June 2006.

[18] C. Jansen, R. Piesiewicz, D. Mittleman, T. Kürner, and M. Koch, “The impact of reflections from stratified building materials on the wave propagation in future indoor terahertz communication systems,” IEEE Trans. Antennas Propag. vol. 56, no. 5, pp. 1413-1418, May 2008.

[19] E. Biglieri, R. Calderbank, A. Constantinides, A. Goldsmith, A. Paulraj and H. V. Poor, MIMO Wireless Communications, Cambridge University Press, New York, 2007.

[20] Y. Karasawa, “Innovative antenna and propagation studies for MIMO systems,” IEICE Trans. Commun., vol. E90-B, no. 9, pp. 2194-2202, Sept. 2007.

[21] N. Honma, K. Nishimori, T. Seki, and M. Mizoguchi, “Short range MIMO communication,” Proc. of EuCAP2009, Berlin, Germany, pp. 1763-1767, Mar. 2009.

[22] K. Nishimori, N. Honma, T. Seki, and K. Hiraga, “On the transmission method for short-range MIMO communication,” IEEE Trans. Veh. Technol., vol. 60, no. 3, March 2011.

[23] J. Jiang and M. A. Ingram, “Spherical-wave model for short-range MIMO,” IEEE Trans. Commun., vol. 53, no. 9, pp. 1534-1541, Sept. 2005.

[24] F. Bohagen, P. Orten, and G. Oien, “Optimal design of uniform rectangular antenna arrays for strong line-of-sight MIMO channels,” EURASIP J. Wirel. Commun. Netw., vol. 2007, no. 2, pp. 12-12, 2007.

[25] C. Waldschmidt, T. Fugen, and W. Wiesbeck, “Spiral and dipole antennas for indoor MIMO-systems,” IEEE Antennas Wireless Propag. Lett., vol. 1, no. 9, pp. 176–178, 2002.

[26] G. International Telecommunication Union (ITU), “Itu internet reports 2005: The internet of things, executive summary,” november 2005, last visited on January 19th 2012. [Online]. Available:

http://www.itu.int/osg/spu/publications/internetofthings/InternetofThings_summary.pdf

[27] Harri Niemelä, "The study of business opportunities and value add of NFC applications in security access control solutions," Master´s thesis, TORNIO 2011.

[28] Michail Matthaiou, "Characterisation and Modelling of Indoor and Short-Range MIMO Communications," Doctor's thesis, The University of Edinburgh, November 2008.

[29] Near Field Communication, White paper, ECMA international, December 2003.

[30] R. Want, "Near field communication," Pervasive Computing, IEEE, vol. 10, no. 3, pp. 4 –7, march 2011.

[31] B. Sodor, G. Fordos, T. Doktor, and B. Benyo, "Building a contactless university examination system using nfc," in Intelligent Engineering Systems (INES), 2011 15th IEEE International Conference on, june 2011, pp. 57 –61.

[32] Renee Montes,"Examining the technology,security and application of NFC and Evaluateing the possible success of near field communication application in US Markets", Master thesis , Bowie State Univerity,May 2009

[33] Ernst Haselsteiner and KlemensBreitfu, "Security in Near Field Communication (NFC) - Strengths and Weaknesse", Philips Semiconductors, Mikronweg , Gratkorn, Austria, 2006.

[34] HUSSEIN AHMAD AL-OFEISHAT and MOHAMMAD A.A.AL RABABAH, "Near Field Communication (NFC)," IJCSNS International Journal of Computer Science and Network Security, VOL.12 No.2, pp. 93-99, February 2012.

[35] K. Finkenzeller, RFID Handbook: Radio-frequency Identification Fundamentals and Applications, 2nd ed.: Wiley, 2004.

[36] P. V. Nikitin, K. V. S. Rao and S. Lazar, "An overview of near field UHF RFID," IEEE International Conferenceon on RFID, Mar. 2007, pp. 167-174.

[37] S. Ortiz Jr. "Is near-field communication close to success?", Computer, vol. 39, pp.18-20, 2006.

[38] A. D. Yaghjian "An overview of near-field antenna measurements", *IEEE Trans. Antennas Propag.*, vol. 34, pp.30 1986.

[39] L. Nagy "Indoor propagation modeling for short range devices", *Proc. 2nd Eur. Conf. on Antennas and Propagation*, pp.1 2007.

[40] M. Burden, "Near Field Communications (NFC) in Public Transport," RFID and Electronic Vehicle Identification in Road Transport, pp. 21-38, Nov. 2006

[41] A. Goldsmith, Wireless Communications, Cambridge University Press, England, 2005.

[42] Y. Karasawa, "Innovative antennas and propagation studies for MIMO systems," IEICE Trans. Commun., vol. E90-B, no. 9, pp. 2194-2202, Sep. 2007.

[43] H. Kuwahara, T. Hori, M. Fujimoto, and K. Nishimori, "Change in characteristics in urban area environment," Proc. ISAP2004, Sendai, Japan, pp. 741-744, Aug. 2004.

[44] A. Paulraj, R. Nabar, and D. Gore, Introduction to Space-Time Wireless Communications, Cambridge University Press, England, 2003.

[45] L.H. Brandenburg, and A.D. Wyner, "Capacity of the Gaussian channel with memory: the multivariate case," Bell System Tech. J., vol. 53, no. 5, pp. 745-778, May-June 1974.

[46] J. Salz, and A.D. Wyner, "On data transmission over cross coupled multi-input, multi-output linear channels with applications to mobile radio," AT&T MEMO, 1990.

[47] N. Honma, K. Nishimori, R. Kudo, Y. Takatori, T. Hiraguri and M. Mizoguchi, "A stochastic approach to design MIMO antenna with parasitic elements based on propagation characteristics," IEICE Trans. Commun., vol. E93-B, no. 10, pp. 2578-2585, Oct. 2010.

[48] H. Hirayama, G. Matsui, N. Kikuma and K. Sakakibara, "Channel capacity improvement in short-range MIMO using side and back reflectors," IEICE Trans. Commun., vol. E94-B, no. 5, pp. 1280-1283, May 2011.

[49] G. J. Foschini and M. J. Gans, "On limits of wireless communications in a fading environment when using multiple antennas," Wireless Personal Communications, vol. 6, no. 3, pp. 311-335, Mar. 1998.

[50] E. Biglieri, R. Calderbank, A. Constantinides, A. Goldsmith, A. Paulraj, H.V. Poor, MIMO Wireless Communications, Cambridge University Press, England, 2010.

[51] A. Abdi and M. Kaveh, "A space-time correlation model for multielement antenna systems in mobile fading channels", IEEE J. Select. Areas Commun., vol. 20, pp.550 -561 2002.

[52] B. Friedlander and S. Scherzer, "Spatial diversity vs. array gain in cellular communication systems," Signals, Systems and Computers, 2002. Conference Record of the Thirty-Sixth Asilomar Conference, vol.1, pp: 584-588, Nov. 2002.

[53] H. Bolcskei, D. Gesbert, and A. J. Paulraj, "On the capacity of OFDM-based spatial multiplexing systems," IEEE Trans. Commun., vol. 50, no. 2, pp. 225-234, Feb. 2002.

[54] G.J. Foschini, "Layered space-time architecture for wireless communication in a fading environment when using multi-element antennas," Bell Labs. Tech. J., vol. 1, no. 2, pp. 41-59, Aug. 1996.

[55] I.E. Teletar, "Capacity of multi-antenna Gaussian channels," Euro. Trans. Telecommun., vol. 10, no. 6, pp. 585-595, Jun. 1999.

[56] G. Wetzker, “Definition of spatial multiplexing gain,” Electronics Letters, Issue: 11, vol. 41, pp. 656-657, May 2005.

[57] H. M. Karkhanechi and B. C. Levy "Spatial multiplexing and diversity gain in OFDM-based MIMO systems", *Proc. IEEE Wireless Commun. Technol.*, pp.299 2003.

[58] C. Shannon, “A mathematical theory of communication,” Bell Sys. Tech. J., pp. 379-423, 623-656, 1948.

[59] C. Shannon, “Communications in the presence of noise,” Proc. IRE1949, pp. 10-21, 1949.

[60] C. Shannon and W. Weaver, The Mathematical Theory of Communication, University of Illinois Press, USA, 1949.

[61] G. Caire, G. Taricco, and E. Biglieri, “Optimum power control over fading channels,” IEEE Trans. Inform. Theory, vol. 45, no. 5, pp. 1468-1489, Jul. 1999.

[62] S. Hanly and D. Tse, “Multi-access fading channels - part II: delay-limited capacities,” IEEE Trans. Inform. Theory, vol. 44, no. 7, pp. 2816-2831, Nov. 1998.

[63] L. Li, N. Jindal, and A. Goldsmith, “Outage capacities and optimal power allocation for fading multiple-access channels,” IEEE Trans. Inform. Theory, vol. 51, no. 4, pp. 1326-1347, Apr. 2005.

[64] H. Shin, and J.H. Lee, “Capacity of multiple-antenna fading channels: spatial fading correlation, double scattering, and keyhole,” IEEE Trans. Inform. Theory, vol. 49, no. 10, pp. 2636-2647, Oct. 2003.

[65] E.M. Mohamed, O. Muta and H. Furukawa, “Static and dynamic channel estimation techniques for MIMO Constant Envelope Modulation,” *GLOBECOM Workshops (GC Wkshps)*, pp. 549– 54, 2011 IEEE.

[66] Z. Shen , R. W. Heath Jr., J. G. Andrews and B. L. Evans "Comparison of space-time water-filling and spatial water-filling for MIMO fading channels", Proc. IEEE Global Telecommun. Conf., vol. 1, pp.431 2004.

[67] Runhua Chen, Zukang Shen, Andrews, J.G., Heath, R.W., "Multimode Transmission for Multiuser MIMO Systems With Block Diagonalization", *Signal Processing, IEEE Transactions on,* On page(s): 3294 - 3302 Volume: 56, Issue: 7, July 2008

[68] V. L. Girko, "A refinement of the central limit theorem for random determinants," Theory Probab. Applic., vol. 42, no. 1, pp. 121-129, 1998.

[69] A.L. Moustakas, S.H. Simon, and A.M. Sengupta, "MIMO capacity through correlated channels in the presence of correlated interferers and noise: a (not so) large N analysis," IEEE Trans. Inform. Theory, vol. 48, pp. 2545-2561, Oct. 2003.

[70] Q. Spencer , A. Swindlehurst and M. Haardt "Zero-forcing methods for downlink spatial multiplexing in multiuser MIMO channels", IEEE Trans. Signal Process., vol. 52, no. 2, pp.461 -471 2004.

[71] W. Li and M. Latva-aho "An efficient channel block diagonalization method for generalized zero forcing assisted MIMO broadcasting systems", IEEE Trans. Wireless Commun., vol. 10, no. 3, pp.739 -744 2011

[72] J.G. Proakis, Digital Communications, McGraw-Hill, USA, 1995.

[73] H. Harashima, and H. Miyakawa, "Matched-transmission techniques for channels with intersymbol interference," IEEE Trans. Commun., vol. 20, pp. 774-780, Aug. 1972.

[74] J. S. Jiang and M. A. Ingram, "Distributed source model for short-range MIMO, " Proc. IEEE VTC 2003, pp. 357-362, Oct. 2003.

[75] L. L. Liu and W. Hong, et al. "Characterization of line-of-sight MIMO channel for fixed wireless communications, " IEEE Antennas Wireless Propag. Lett., vol.6, pp.36-39, 2007.

[76] A. A. Hutter, F. Platbrood, and J. Ayadi, "Analysis of MIMO capacity gains for indoor propagation channels with LOS component, " Proc. IEEE PIMRC 2002, pp. 1337-1347, Sept. 2002.

[77] Yu-Wei Fan, Hui-Huang Zhong, Zhi-Qiang Li, Heng Zhou, Wei-Hong Zhou, Jun Zhu and Ling Luo, "A short dipole antenna," High Power Particle Beams (BEAMS), 2008 17th International Conference, pp. 1-4, July 2008.

[78] M.C. Liang, "Frequency Tunable Patch Antenna Device," US-Patent US6462712B1.issued Oct. 8, 2002, filed Jul. 24. 2001.

[79] M.C. Liang, S.T. Lin, S.A. Yang, "The ground effect on bended C-patch Antenna strip" 2004 IEEE Antennas and Propagation Society International Symposium and USNC/URSI National Radio Science Meeting, Vol. 4, pp. 3537-3540, June 2004.

[80] K. Akaki, A. Mase, Y. Kogi, K. Uchino, Y. Nagayama, K. Kawahata, S. Yamaguchi, S. Inagaki and Kang Wook Kim," Study of dual-dipole antenna array for millimeter wave imaging," Infrared, Millimeter, and Terahertz Waves, 2009. IRMMW-THz 2009. 34th International Conference. pp. 1-2, Sept. 2009.

[81] C. A. Balanis, Antenna Theory, Analysis and Design, 2nd edition, New York: John Wiley & Sons, 1997, pp. 586-598.

[82] K. Nishimori, Y. Makise, M. Ida, R. Kudo, and K. Tsunekawa, "Channel capacity measurement of 8×2 MIMO transmission by an-tenna configurations in an actual cellular environment," IEEE Trans. Antennas and Propagation, vol. 54, no. 6, pp. 3285-3291, Jun. 2006.

[83] X. Q. Gao, B. Jiang, X. Li, A. B. Gershman, and M. R. McKay, "Statistical eigenmode transmission over jointly correlated MIMO channel,"IEEE Trans. Inform. Theory, vol. 55, no. 8, pp. 3735-3750, Aug. 2009.

[84] I. E. Telatar, "Capacity of multi-antenna Gaussian channels," Europ. Trans. Telecommun., vol. 10, no. 6, pp. 586-595, Nov./Dec. 1999.

[85] M. K. Ozdemir and E. Arvas "Dynamics of spatial correlation and implications on MIMO systems", IEEE Commun. Mag., vol. 42, no. 6, pp.S14 -S19 2004.

[86] A. Derneryd and G. Kristensson "Signal correlation including antenna coupling", *Electron. Lett.*, vol. 40, no. 3, pp.157 -159, 2004.

[87] R. Narasimhan, "Spatial multiplexing with transmit antenna and constellation selection for correlated MIMO fading channels," IEEE Trans. Signal Processing, vol. 51, no. 11, pp. 2829-2838, Nov. 2003.

[88] D. Gesbert, M. Shafi, D. Shiu, P. J. Smith and A. Naguib "From theory to practice: an overview of MIMO space-time coded wireless systems " IEEE J. Selected Areas in Comm., Vol. 21, No. 3, pp. 281-302, April 2003.

[89] S. Ting, K. Sakaguchi and K. Araki, “Performance analysis of MIMO Eigenmode transmission system under realistic channel and system conditions,” IEICE Trans. Commun., vol. E87-B, no. 8, pp. 2222-2232, Aug. 2004.

[90] F. Boccardi, and H. Huang, “A near-optimum technique using linear precoding for the MIMO broadcast channel,” Proc. IEEE ICASSP2007, Honolulu, Hawaii, USA, Apr. 2007.

[91] R.W. Heath, Jr., S. Sandhu, and A. Paulraj, “Antenna selection for spatial multiplexing systems with linear receivers,” IEEE Commun. Lett., vol. 5, no. 4, pp. 142-144, Apr. 2001.

[92] M. Sellathurai, and S. Haykin, Space-Time Layered Information Processing for Wireless Communications, Wiley-IEEE Press, USA, 2009.

[93] M. Kassouf, H. Leib, “Shannon capacity and eigen-beamforming for space dispersive multipath MIMO channels,” Wireless Communications and Networking, 2003, vol.1, pp. 156-161, March 2003.

[94] T. Svantesson and A. L. Swindlehurst, "A Performance Bound for Prediction of a Multipath MIMO Channel", *Proc. 37th Asilomar Conf. Sig., Sys., and Comp., Session: Array Processing for Wireless Commun.*, 2003.

[95] Sarris, I., Nix, A.R., "A Line-of-Sight Optimised MIMO Architecture for Outdoor Environments", Vehicular Technology Conference, 2006. VTC-2006 Fall. 2006 IEEE 64th, On page(s): 1 - 5

[96] Ken Hiraga, Tomohiro Seki, Kentaro Nishimori and Kazuhiro Uehara, “Effectiveness of Short-Range MIMO Using Dual-Polarized Antenna,” IEICE Transactions on Communications, Volume E95.B, Issue 1, pp. 87-96, 2012.

[97] K. Wang and D.M. Mittleman, "Metal wires for terahertz wave guiding", Letters to Nature, Vol. 432, 2004, pp. 376-379.

[98] M. J. King, and J. C. Wiltse, "Surface-wave propagation on coated or uncoated metal wire at millimeter wavelengths", IRE Trans. Antennas Propag. 10, 246-254 (1962).

[99] X. Zhuge and A. Yarovoy "Near-field ultra-wideband imaging with two-dimensional sparse MIMO array", *Proc. 4th EuCAP*, pp.1 -4 2010.

[100] H. Hirayama , G. Matsui , N. Kikuma and K. Sakakibara "Improvement of channel capacity of near-field MIMO", *Proc. 4th Eur. Conf. Antennas Propag.*, pp.1 -4 2010.

[101] J. W. Wallace, and M. A. Jensen, "MIMO capacity variation with SNR and multipath richness from full-wave indoor FDTD simulations," Proc. of APS 2003, vol. 2, pp. 523-526, Jun. 2003.

[102] K. Nishimori, T. Seki, K. Hiraga and N. Honma, “Experimental evaluation in short range MIMO communication with simple transmission scheme,” Antennas and Propagation Society International Symposium (APSURSI) 2010, pp. 1-4, July 2010.

[103] K. Nishimori et al. "16×16 MIMO testbed for MU-MIMO downlink transmission, " IEICE Trans. Commun. Vol.E93-B no.2, 2010.

Appendix: MATLAB Source Code

I. Setting parameters and launching EEM-MOM

```
clear all;

global num_calc num_calc_total
global TxRx_Tx TxRx_Rx Delta_d
global ObjectShape_horizontal ObjectShape_vertical ObjectShape_cross
ObjectShape_without ObjectShape_mesh ObjectShape_2cross
ObjectShape_crossNoConnection;% for main,ObjectShape
global ArrangeType_horizontal ArrangeType_vertical ArrangeType_square
ArrangeType_crossHorizontal ArrangeType_crossVertical
ArrangeType_crossSquare ArrangeType_crossCross
ArrangeType_crossCross_big ArrangeType_xSquare
global DipoleType_horizontal DipoleType_vertical
DipoleType_dualVertical DipoleType_leftBias DipoleType_rightBias;
global filename fid_bat; % for Make_batFile.m
global lambda_0 D d Nt Nr ob_offset_x ob_offset_y ob_offset_z L
TotalObjectNum ArrangeType ObjectShape ObjectRadius
DistanceOfMetalWire% for main program
global foldername_mom foldername_main foldername_sub foldername
filename_bat % for main program
global MeshGap MeshWireNum % for objectShape

DipoleType_horizontal=11;
DipoleType_vertical=12;
DipoleType_dualVertical=13;
DipoleType_leftBias=14;
DipoleType_rightBias=15;

ArrangeType_horizontal=21;
ArrangeType_vertical=22;
ArrangeType_square=23;
ArrangeType_crossHorizontal=24;
ArrangeType_crossVertical=25;
ArrangeType_crossSquare=26;
ArrangeType_crossCross=27;
ArrangeType_crossCross_big=28;
ArrangeType_xSquare=29;

ObjectShape_horizontal=31;
ObjectShape_vertical=32;
ObjectShape_cross=33;
ObjectShape_mesh=34;
ObjectShape_2cross=35;
ObjectShape_crossNoConnection=36;
ObjectShape_without=39;
```

```
TxRx_Tx=41;
TxRx_Rx=42;
%%%%%%%%%%%%%%%%%%%%%%%%%%%%%%%%%%%%%%%%%%%%%%%%%%%%%%%%%%%%%%%%%%%%%%
%%%%%%%%%%%%%%%%%%%%%%%%%%%%%%%%%%%%%%%%%%%%%%%%%%%%%
run_bat=1;     % Whether lauch the EEM-MOM or not. 1 is to launch, 0 is
not to launch.
foldername_mom='C:¥Users¥zhang¥Documents¥EEM-MOM¥'; % Access to save the
files of .bat to lauch the EEM-MOM
foldername_main='C:¥Work¥EEM-MOM5¥'; % Main Access to save the files of
models and results
foldername_sub='20120920_Object_cross_D'; % Sub access to save the files
of models and results
foldername=[foldername_main,foldername_sub,'¥'];
filename_bat=[foldername_mom,foldername_sub,'.bat'];
fid_bat=fopen(filename_bat,'w');

lambda_0=100e-3;    % wavelength
D=1*lambda_0:0.5*lambda_0:5*lambda_0;   % Range of antenna distance
d=[1*lambda_0:0.1*lambda_0:1*lambda_0]; % Range of element spacing
Delta_d=0*lambda_0:0.01*lambda_0:0*lambda_0;    % Range of internal
distance
Nt=8;   % Number of transmitting antennas
Nr=Nt;  % Number of receiving antennas
ArrangeType=[ArrangeType_crossSquare];  % Arrange types of arrays
ObjectShape=[ ObjectShape_cross];       % Shape of objects
ObjectRadius=0.1e-3;                  % Radius of metal wire
DistanceOfMetalWire=0e-3:2e-3:0e-3;     % Distance of two metal wires,
unit is meter
L=20*lambda_0;                          % Length of metal wire
TotalObjectNum=1;                        % Number of objects
MeshGap=2*lambda_0:0.5*lambda_0:2*lambda_0; % Interval in mesh
MeshWireNum=2*(floor((L-MeshGap)/2./MeshGap)+1);  % MidleHole
ob_offset_x=0*lambda_0:0.05*lambda_0:4*lambda_0;
ob_offset_y=0*lambda_0:0.05*lambda_0:0*lambda_0;
ob_offset_z=0*lambda_0:0.05*lambda_0:4*lambda_0;

if ObjectShape==ObjectShape_without
    TotalObjectNum=0;
end
if TotalObjectNum==0
    ob_offset_x=0;
    ob_offset_y=0;
    ob_offset_z=0;
    ObjectShape=ObjectShape_without;
end

num_calc=0;
num_calc_total=length(Nt)*length(ArrangeType)*length(D)*length(d)*len
gth(Delta_d)*length(ObjectShape)*length(ob_offset_x)*length(ob_offset
_y)*length(ob_offset_z)*length(MeshGap)*length(ObjectRadius)*length(D
istanceOfMetalWire); %*length(MeshWireNum);
save initial_parameters.mat
initial_mat=[foldername_sub, '_ini.mat'];
save (initial_mat);
```

```
creatModel; % Launch the fuction of creating models

if run_bat
winopen(filename_bat); % Lauch the EEM-MOM
end
```

II. Calculation of channel capacity

```
clear all;
load initial_parameters.mat;

global num_calc num_calc_total
global TxRx_Tx TxRx_Rx Delta_d
global ObjectShape_horizontal ObjectShape_vertical ObjectShape_cross
ObjectShape_without ObjectShape_mesh ObjectShape_2cross
ObjectShape_crossNoConnection;
global ArrangeType_horizontal ArrangeType_vertical ArrangeType_square
ArrangeType_crossHorizontal ArrangeType_crossVertical
ArrangeType_crossSquare ArrangeType_crossCross
ArrangeType_crossCross_big ArrangeType_xSquare
global DipoleType_horizontal DipoleType_vertical
DipoleType_dualVertical DipoleType_leftBias DipoleType_rightBias;
global filename fid_bat; % for Make_batFile.m
global lambda_0 D d Nt Nr ob_offset_x ob_offset_y ob_offset_z L
TotalObjectNum ArrangeType ObjectShape ObjectRadius
DistanceOfMetalWire% for main program
global foldername_mom foldername_main foldername_sub foldername
filename_bat % for main program
global MeshGap MeshWireNum % for objectShape

initialProgramParameter; % initial the parameters of program

initialModelParameter; % initial the parameters of models

for i_Nt=1:length(Nt)
    for i_Nr=i_Nt
        for i_ArrangeType=1:length(ArrangeType)
            for i_D=1:length(D)
                for i_d=1:length(d)
                    for i_Delta_d=1:length(Delta_d)
                        for i_ObjectShape=1:length(ObjectShape)
                            for i_ObjectRadius=1:length(ObjectRadius)
                                for i_MeshGap=1:length(MeshGap)
                                    for i_MeshWireNum=i_MeshGap
                                        for
i_DistanceOfMetalWire=1:length(DistanceOfMetalWire);
                                            for i_ox=1:length(ob_offset_x)
                                                for
i_oy=1:length(ob_offset_y)
                                                    for
i_oz=1:length(ob_offset_z)
```

```
                                                    for Num_MoM=1:Nt
                                                        load
ModelParameterDefault.mat;

                                                    switch
ArrangeType(i_ArrangeType)
                                                        case
ArrangeType_horizontal
filename_arrangeType='ArrangeType_horizontal_';
                                                        case
ArrangeType_vertical
filename_arrangeType='ArrangeType_vertical_';
                                                        case
ArrangeType_square
filename_arrangeType='ArrangeType_square_';
                                                        case
ArrangeType_crossHorizontal
filename_arrangeType='ArrangeType_crossHorizontal_';
                                                        case
ArrangeType_crossVertical
filename_arrangeType='ArrangeType_crossVertical_';
                                                        case
ArrangeType_crossSquare
filename_arrangeType='ArrangeType_crossSquare_';
                                                        case
ArrangeType_crossCross
filename_arrangeType='ArrangeType_crossCross_';
                                                        case
ArrangeType_crossCross_big
filename_arrangeType='ArrangeType_crossCross_big_';
                                                        case
ArrangeType_xSquare
filename_arrangeType='ArrangeType_xSquare_';

                                                    end

                                                    switch
ObjectShape(i_ObjectShape)
                                                        case
ObjectShape_horizontal
filename_objectShape='ObjectShape_horizontal_';
                                                        case
ObjectShape_vertical
filename_objectShape='ObjectShape_vertical_';
                                                        case
ObjectShape_cross
```

```
filename_objectShape='ObjectShape_cross_';
                                                        case
ObjectShape_without

filename_objectShape='';
                                                        case
ObjectShape_mesh

filename_objectShape='ObjectShape_mesh_';
                                                        case
ObjectShape_2cross

filename_objectShape='ObjectShape_2cross_';
                                                        case
ObjectShape_crossNoConnection

filename_objectShape='ObjectShape_crossNoConnection_';
                                                    end


filename_sub=sprintf('%d_of_%d_D%2.1f_d%2.1f_dd%2.3f_obx%2.3f_oby%2.3
f_obz%2.3f_obr%2.1fmm',...

Num_MoM,Nt(i_Nt),D(i_D)/lambda_0,d(i_d)/lambda_0,Delta_d(i_Delta_d)/l
ambda_0,ob_offset_x(i_ox)/lambda_0,ob_offset_y(i_oy)/lambda_0,ob_offs
et_z(i_oz)/lambda_0,ObjectRadius(i_ObjectRadius)/1e-3);
                                                    if
ObjectShape(i_ObjectShape)==ObjectShape_mesh|
ObjectShape(i_ObjectShape)==ObjectShape_2cross

filename_sub=sprintf('%d_of_%d_D%2.1f_d%2.1f_dd%2.3f_gap%2.3f_meshwir
enum%d_obx%2.3f_oby%2.3f_obz%2.3f_obr%2.1fmm',...

Num_MoM,Nt(i_Nt),D(i_D)/lambda_0,d(i_d)/lambda_0,Delta_d(i_Delta_d)/l
ambda_0,MeshGap(i_MeshGap)/lambda_0,MeshWireNum(i_MeshWireNum),ob_off
set_x(i_ox)/lambda_0,ob_offset_y(i_oy)/lambda_0,ob_offset_z(i_oz)/lam
bda_0,ObjectRadius(i_ObjectRadius)/1e-3);
                                                    end
                                                    if
ObjectShape(i_ObjectShape)==ObjectShape_crossNoConnection

filename_sub=sprintf('%d_of_%d_D%2.1f_d%2.1f_dd%2.3f_gap%2.3f_meshwir
enum%d_obx%2.3f_oby%2.3f_obz%2.3f_obr%2.1fmm_dmw%2.1fmm',...

Num_MoM,Nt(i_Nt),D(i_D)/lambda_0,d(i_d)/lambda_0,Delta_d(i_Delta_d)/l
ambda_0,MeshGap(i_MeshGap)/lambda_0,MeshWireNum(i_MeshWireNum),ob_off
set_x(i_ox)/lambda_0,ob_offset_y(i_oy)/lambda_0,ob_offset_z(i_oz)/lam
bda_0,ObjectRadius(i_ObjectRadius)/1e-3,DistanceOfMetalWire(i_Distanc
eOfMetalWire)/1e-3);
                                                    end


filename=[foldername,filename_arrangeType,filename_objectShape,filena
me_sub];
%%%%%%%%%%%%%%%%%%%%%%%%%%%%%%%%%%%%%%%%%%%%%%%%%%%%%%%%%%%%%%%%%%%%%%%
%%%%%%%%%%%%%%%%%%%%%%%%%%%%%%%%%%%%%%%%%%%%%%%%%%%%%%%%%%%%%%%%%%%%%%%
```

```
filename_current=[filename,'_current.log'];
                                                    clear fid_current;

fid_current=fopen(filename_current);

num_element=13*(2*Nt(i_Nt)+Nr(i_Nr));

FormatString=[repmat(' %f',1,6)];
                                                    current.data=
cell2mat(textscan(fid_current,FormatString,num_element,'HeaderLines',
1));

fclose(fid_current);


current.amp=current.data(:,2);

current.pha=current.data(:,3);

current.r=current.data(:,4);

current.i=current.data(:,5);

current.type=current.data(:,6);


index.feedpoint=find(current.type==1);

index.loadpoint=find(current.type==2,Nr(i_Nr),'last');

                                                    for
n=1:length(index.loadpoint)

current.loadpoint(n,1)=current.r(index.loadpoint(n))+sqrt(-1)*current
.i(index.loadpoint(n));
                                                    end

                                                    for
n=1:length(index.feedpoint)

current.feedpoint(n,1)=current.r(index.feedpoint(n))+sqrt(-1)*current
.i(index.feedpoint(n));
                                                    end


v_loadpoint=(current.loadpoint*70.987/1000);

h_v(:,Num_MoM)=v_loadpoint;

                                                end


h_ave_0=mean(mean(abs(h_v)))
```

```
h_ave_1=0.04012558048405; %imp=70.987
                                                    h=h_v
                                                    h_1=h_v/h_ave_1
%%% calculating SNR %%%

signal_power=sum(sum(abs(h_1).^2));

signal_power_eigen=sum((abs(h_1).^2)')' % Total receiving power


noise_power=0.297077976949821;

snr=signal_power/noise_power;

snr_eigen=signal_power_eigen./noise_power; % SNR in each branch
                                                    gamma = snr;    %
average received signal-to-noise ratio (Watts)

H(:,:,i_ox,i_oz,i_D)=h_1; % normalized response matrix

Eigenvalue_sqrt(:,i_ox,i_oz,i_D)=svd(h_1)'; % normalized sqare root of
eigenvalue

Eigenvalue(:,i_ox,i_oz,i_D)=Eigenvalue_sqrt(:,i_ox,i_oz,i_D).^2;  %
normalized eigenvalue

H_origin(:,:,i_ox,i_oz,i_D)=h_v; % original response matrix

Eigenvalue_sqrt_origin(:,i_ox,i_oz,i_D)=svd(h_v)'; % original sqare
root of eigenvalue

Eigenvalue_origin(:,i_ox,i_oz,i_D)=Eigenvalue_sqrt_origin(:,i_ox,i_oz
,i_D).^2;  % original eigenvalue

Eigenvalue_origin_db(:,i_ox,i_oz,i_D)=20*log10(Eigenvalue_origin(:,i_
ox,i_oz,i_D));

cc_1=abs(log2(det(eye(Nr(i_Nr))+gamma/Nt(i_Nt)*h_1*h_1')));
                                                    cc_2=0;
                                                    for i=1:Nt(i_Nt)

cc_2=cc_2+log2(1+Eigenvalue(i,i_D)*snr_eigen(i)); % Channel capacity
calulated by eigen value
                                                    end


cc_data(i_ox,i_oz,i_D)=cc_1;

cc_data_eigen(i_ox,i_oz,i_D)=cc_2;
                                                    clear current index
v_loadpoint
                                                    clear h_v;
                                                    clear cc_1 cc_2;
                                                end
                                            end
                                        end
                                    end
                                end
```

```
                        end
                    end
                end
            end
        end
    end
end

cc_data_format='i_ox,i_oz,i_D';
matname=[foldername_sub, '_result.mat'];
save (matname);
```

III. Creating near-field MIMO Models

```
function creatModel

tic
global num_calc num_calc_total
global TxRx_Tx TxRx_Rx Delta_d
global ObjectShape_horizontal ObjectShape_vertical ObjectShape_cross
ObjectShape_without ObjectShape_mesh ObjectShape_2cross
ObjectShape_crossNoConnection;
global ArrangeType_horizontal ArrangeType_vertical ArrangeType_square
ArrangeType_crossHorizontal ArrangeType_crossVertical
ArrangeType_crossSquare ArrangeType_crossCross
ArrangeType_crossCross_big ArrangeType_xSquare
global DipoleType_horizontal DipoleType_vertical
DipoleType_dualVertical DipoleType_leftBias DipoleType_rightBias;
global filename fid_bat; % for Make_batFile.m
global lambda_0 D d Nt Nr ob_offset_x ob_offset_y ob_offset_z L
TotalObjectNum ArrangeType ObjectShape ObjectRadius
DistanceOfMetalWire% for main program
global foldername_mom foldername_main foldername_sub foldername
filename_bat % for main program
global MeshGap MeshWireNum % for objectShape

initialModelParameter;

for i_Nt=1:length(Nt)
    for i_Nr=i_Nt
        for i_ArrangeType=1:length(ArrangeType)
            for i_D=1:length(D)
                for i_d=1:length(d)
                    for i_Delta_d=1:length(Delta_d)
                        for i_ObjectShape=1:length(ObjectShape)
                            for i_ObjectRadius=1:length(ObjectRadius)
                                for i_MeshGap=1:length(MeshGap)
                                    for i_MeshWireNum=i_MeshGap
                                        for
i_DistanceOfMetalWire=1:length(DistanceOfMetalWire);
                                            for i_ox=1:length(ob_offset_x)
                                                for
```

```
i_oy=1:length(ob_offset_y)
                                                    for i_oz=1:i_ox
%%%%%%%%%%%%%%%%%%%%%%%%%%%%%%
                                                        for Num_MoM=1:Nt

                                                            load
ModelParameterDefault.mat;

                                                            switch
ArrangeType(i_ArrangeType)
                                                                case
ArrangeType_horizontal

filename_arrangeType='ArrangeType_horizontal_';
                                                                case
ArrangeType_vertical

filename_arrangeType='ArrangeType_vertical_';
                                                                case
ArrangeType_square

filename_arrangeType='ArrangeType_square_';
                                                                case
ArrangeType_crossHorizontal

filename_arrangeType='ArrangeType_crossHorizontal_';
                                                                case
ArrangeType_crossVertical

filename_arrangeType='ArrangeType_crossVertical_';
                                                                case
ArrangeType_crossSquare

filename_arrangeType='ArrangeType_crossSquare_';
                                                                case
ArrangeType_crossCross

filename_arrangeType='ArrangeType_crossCross_';
                                                                case
ArrangeType_crossCross_big

filename_arrangeType='ArrangeType_crossCross_big_';
                                                                case
ArrangeType_xSquare

filename_arrangeType='ArrangeType_xSquare_';

                                                            end

                                                            switch
ObjectShape(i_ObjectShape)
                                                                case
ObjectShape_horizontal

filename_objectShape='ObjectShape_horizontal_';
                                                                case
```

```
ObjectShape_vertical

filename_objectShape='ObjectShape_vertical_';
                                                        case
ObjectShape_cross

filename_objectShape='ObjectShape_cross_';
                                                        case
ObjectShape_without

filename_objectShape='';
                                                        case
ObjectShape_mesh

filename_objectShape='ObjectShape_mesh_';
                                                        case
ObjectShape_2cross

filename_objectShape='ObjectShape_2cross_';
                                                        case
ObjectShape_crossNoConnection

filename_objectShape='ObjectShape_crossNoConnection_';
                                                    end


filename_sub=sprintf('%d_of_%d_D%2.1f_d%2.1f_dd%2.3f_obx%2.3f_oby%2.3
f_obz%2.3f_obr%2.1fmm',...

Num_MoM,Nt(i_Nt),D(i_D)/lambda_0,d(i_d)/lambda_0,Delta_d(i_Delta_d)/l
ambda_0,ob_offset_x(i_ox)/lambda_0,ob_offset_y(i_oy)/lambda_0,ob_offs
et_z(i_oz)/lambda_0,ObjectRadius(i_ObjectRadius)/1e-3);
                                                    if
ObjectShape(i_ObjectShape)==ObjectShape_mesh|
ObjectShape(i_ObjectShape)==ObjectShape_2cross

filename_sub=sprintf('%d_of_%d_D%2.1f_d%2.1f_dd%2.3f_gap%2.3f_meshwir
enum%d_obx%2.3f_oby%2.3f_obz%2.3f_obr%2.1fmm',...

Num_MoM,Nt(i_Nt),D(i_D)/lambda_0,d(i_d)/lambda_0,Delta_d(i_Delta_d)/l
ambda_0,MeshGap(i_MeshGap)/lambda_0,MeshWireNum(i_MeshWireNum),ob_off
set_x(i_ox)/lambda_0,ob_offset_y(i_oy)/lambda_0,ob_offset_z(i_oz)/lam
bda_0,ObjectRadius(i_ObjectRadius)/1e-3);
                                                    end
                                                    if
ObjectShape(i_ObjectShape)==ObjectShape_crossNoConnection

filename_sub=sprintf('%d_of_%d_D%2.1f_d%2.1f_dd%2.3f_gap%2.3f_meshwir
enum%d_obx%2.3f_oby%2.3f_obz%2.3f_obr%2.1fmm_dmw%2.1fmm',...

Num_MoM,Nt(i_Nt),D(i_D)/lambda_0,d(i_d)/lambda_0,Delta_d(i_Delta_d)/l
ambda_0,MeshGap(i_MeshGap)/lambda_0,MeshWireNum(i_MeshWireNum),ob_off
set_x(i_ox)/lambda_0,ob_offset_y(i_oy)/lambda_0,ob_offset_z(i_oz)/lam
bda_0,ObjectRadius(i_ObjectRadius)/1e-3,DistanceOfMetalWire(i_Distanc
eOfMetalWire)/1e-3);
                                                    end
```

```
filename=[foldername,filename_arrangeType,filename_objectShape,filena
me_sub];

                                                    %%%%%%%%%%%%%%%%%%%
                                                    %%% Make .bat File %%
                                                    %%%%%%%%%%%%%%%%%%%

                                                    Make_batFile;

                                                    %%%%%%%%%%%%%%%%%%%
                                                    %%% PRINT DATA %%
                                                    %%%%%%%%%%%%%%%%%%%


filename_model=[filename,'_model.mom'];    % the name of the .mom file

print_data(filename_model,model_title,Freq,ground,div_wavelength,r_wi
re,Incidence,Solver);

                                                    %%%%%%%%%%%%%%%%%%%
                                                    %%% PRINT MODEL %%
                                                    %%%%%%%%%%%%%%%%%%%

%%% Print Tx %%%%%%%%%%

[TxShapeAxes]=dipoleType(DipoleType_vertical,Delta_d);

[Dipole_num_in_element, Dipole_Axes]=size(TxShapeAxes);

                                                    for
ElementNum=1:Nt(i_Nt)
                                                        for
i_dipole_num_in_element=1:Dipole_num_in_element

Vertex(1,:)=TxShapeAxes(i_dipole_num_in_element,1:3);

Vertex(2,:)=TxShapeAxes(i_dipole_num_in_element,4:6);

elementArrangement(ArrangeType(i_ArrangeType),D(i_D),d(i_d),Delta_d(i
_Delta_d),Nt(i_Nt),ElementNum,TxRx_Tx,Num_MoM);

print_model(filename_model,type_shape,type_coord,type_comment,Vertex,
Feed_point,Load_point,Division,Wire_radius,Offset);
                                                        end
                                                    end

%%% Print Rx %%%%%%%%%%

[RxShapeAxes]=dipoleType(DipoleType_vertical,Delta_d);

[Dipole_num_in_element, Dipole_Axes]=size(RxShapeAxes);
```

```
                                                    for
ElementNum=1:Nr(i_Nr)
                                                        for
i_dipole_num_in_element=1:Dipole_num_in_element

Vertex(1,:)=RxShapeAxes(i_dipole_num_in_element,1:3);

Vertex(2,:)=RxShapeAxes(i_dipole_num_in_element,4:6);

elementArrangement(ArrangeType(i_ArrangeType),D(i_D),d(i_d),Delta_d(i
_Delta_d),Nr(i_Nr),ElementNum,TxRx_Rx,Num_MoM);

print_model(filename_model,type_shape,type_coord,type_comment,Vertex,
Feed_point,Load_point,Division,Wire_radius,Offset);
                                                        end
                                                    end

%%% Print Object %%%%%%%%%%


[ObjectAxes]=objectShape(ObjectShape(i_ObjectShape),L,MeshGap(i_MeshG
ap),MeshWireNum(i_MeshWireNum),DistanceOfMetalWire(i_DistanceOfMetalW
ire));

[Metal_wire_num_in_object, Metal_wire_Axes]=size(ObjectAxes);

                                                    for
ObjectNum=1:TotalObjectNum
                                                        for
i_Metal_wire_num_in_object=1:Metal_wire_num_in_object

Vertex(1,:)=ObjectAxes(i_Metal_wire_num_in_object,1:3);

Vertex(2,:)=ObjectAxes(i_Metal_wire_num_in_object,4:6);

objectPosition(-1*(-1)^ObjectNum*ob_offset_x(i_ox),ob_offset_y(i_oy),
-1*(-1)^ObjectNum*ob_offset_z(i_oz));

Division(1:2)=[1,round(40*L/lambda_0)];

Wire_radius=[1,ObjectRadius(i_ObjectRadius)];

print_model(filename_model,type_shape,type_coord,type_comment,Vertex,
Feed_point,Load_point,Division,Wire_radius,Offset);
                                                        end
                                                    end
                                                end
 %%%% Evaluate the Remain Time %%%%%%%%%%%%%%%%%%

                                                num_calc=num_calc+1;
                                                sprintf('Now creating
the %dth out of %d models', num_calc,num_calc_total)


percent_finish=num_calc/num_calc_total*100;
```

```
percent_finish_text=sprintf('Completed %f', percent_finish);
                                                    time_used=toc;

time_remain=time_used/(percent_finish/100)-time_used;

time_used_text=sprintf('%f Seconds Passed', time_used);

time_remain_text=sprintf('%f Seconds Remain', time_remain);
                                                    fprintf
(percent_finish_text);fprintf('%%');
                                                    fprintf('->');

fprintf(time_used_text);
                                                    fprintf('->');

fprintf(time_remain_text);
                                                    fprintf('¥n');
                                                end
                                            end
                                        end
                                    end
                                end
                            end
                        end
                    end
                end
            end
        end
    end
end

fclose(fid_bat);
fclose('all');
```

IV. Making .bat files for EEM-MOM

```
function Make_batFile

    global filename fid_bat;
    filename_model=[filename,'_model.mom'];    % the name of the .mom file
    filename_current=[filename,'_current.log'];
    fprintf(fid_bat,'type ');
    fprintf(fid_bat,'%s',filename_model);
    fprintf(fid_bat,' > inp.dat¥r¥n');
    fprintf(fid_bat,'mom2.exe -n 32¥r¥n');
    fprintf(fid_bat,'copy current.log ');
    fprintf(fid_bat,'%s',filename_current);
    fprintf(fid_bat,'¥r¥n');
    fprintf(fid_bat,'¥r¥n');
```

V. *Initialization of parameters of models*

```
%%%%%%%%%%%%%%%%%%%%%%%%%%%%%%%%%%%%%%%%%%%%%%%%%%%%%%%%%%%%%%%%%%%%%%%%
%%%                    MODEL PARAMETER                              %%%
%%% Initial parameters of models for print_model  %%%
%%%%%%%%%%%%%%%%%%%%%%%%%%%%%%%%%%%%%%%%%%%%%%%%%%%%%%%%%%%%%%%%%%%%%%%%

function initialModelParameter

global Vertex Feed_point Load_point Division Wire_radius Offset Freq
Incidence Solver;

%%====TYPE&COMMENT====%%
type_shape=0;                       % Shape 0=Wire; 1=Quadangle; 2=Box
type_coord=0;                       % Coordinate 0=XYZ; 1=Cylinder; 2=Polar
type_comment='';                    % Comment

%%====VERTEX====%%
Vertex_1(1)=0;                      % Vertex_1 if Coordinate=XYZ then X[m];
if Cylinder then R[m]; if Polar then R[m]
Vertex_1(2)=0;                      % Vertex_1 if Coordinate=XYZ then Y[m];
if Cylinder then phi[deg]; if Polar then theta[deg]
Vertex_1(3)=-25e-3;                 % Vertex_1 if Coordinate=XYZ then
Z[m]; if Cylinder then Z[m]; if Polar then phi[deg]

Vertex_2(1)=0;                      % Vertex_2 if Coordinate=XYZ then X[m];
if Cylinder then R[m]; if Polar then R[m]
Vertex_2(2)=0;                      % Vertex_2 if Coordinate=XYZ then Y[m];
if Cylinder then phi[deg]; if Polar then theta[deg]
Vertex_2(3)=25e-3;                  % Vertex_2 if Coordinate=XYZ then Z[m];
if Cylinder then Z[m]; if Polar then phi[deg]

Vertex_3(1)=0;                      % Vertex_3 if Coordinate=XYZ then X[m];
if Cylinder then R[m]; if Polar then R[m]
Vertex_3(2)=0.0040;                 % Vertex_3 if Coordinate=XYZ then
Y[m]; if Cylinder then phi[deg]; if Polar then theta[deg]
Vertex_3(3)=-0.0025;                % Vertex_3 if Coordinate=XYZ then
Z[m]; if Cylinder then Z[m]; if Polar then phi[deg]

Vertex_4(1)=0;                      % Vertex_4 if Coordinate=XYZ then X[m];
if Cylinder then R[m]; if Polar then R[m]
Vertex_4(2)=0.0040;                 % Vertex_4 if Coordinate=XYZ then
Y[m]; if Cylinder then phi[deg]; if Polar then theta[deg]
Vertex_4(3)=-0.0025;                % Vertex_4 if Coordinate=XYZ then
Z[m]; if Cylinder then Z[m]; if Polar then phi[deg]

%%====FEED POINT====%%
feed_sel=0;                        % Feed select: 1=selected; 0=not
seclected
feed_volt=1;                       % Feed Voltage value [V]
feed_phase=0;                      % Feed Phase value [deg]

%%====LOAD POINT====%%
load_sel=0;                        % Load select: 1=selected; 0=not
seclected
```

```
load_r=50;                          % Load R value [Ohm]
load_l=0;                           % Load L value [Henry]
load_c=0;                           % Load C value [Farad]

%%====DIVISION====%%
div_sel=1;                          % Divisions select: 1=selected;
0=default
div_1=13;                           %
div_2=0;                            %
div_3=0;                            %

%%====WIRE RADIUS====%%
w_radius_sel=0;                      % Wire Radius select: 1=selected;
0=default
w_radius_val=0;                      % Wire Radius value [m]

%%====OFFSET====%%
offset_sel=1;                        % Offset select: 1=selected; 0=not
seclected
offset_x=0;                         % Offset on X axis value [m]
offset_y=0;                         % Offset on Y axis value [m]
offset_z=0;                         % Offset on X axis value [m]


%%%%%%%%%%%%%%%%%%%%%%
%%% DATA PARAMETER %%
%%%%%%%%%%%%%%%%%%%%%%

model_title='';                      % the name of the model, default as ''

%%====FREQ====%%
freq_start=3e09;
freq_stop=3e09;
freq_div=00;                        % division number between freq_start and
freq_stop, when freq_start=freq_stop the freq_div should be set as 0

%%====GROUND====%%
ground=0;                           % 0 means the ground doesn't exist, 1
means the ground exists, default as 0

%%====DIVISION====%%
div_wavelength=25;                   % division of wavelength

%%====RADIUS====%%
r_wire=0.1e-3;                      % wire radius with the unit as (m), and
the nagative value means the radius/length

%%====INCIDENCE====%%
inc_plane_wave=0;                    % Plane Wave Incidence, 0 means not
exist, 1 means exist
inc_theta=0;                        % the input plane wave angle theta with
the unit (degree)
inc_phi=0;                          % the input plane wave angle phi with the
unit (degree)
inc_polar=0;                        % the Polarization of the plane wave 0
```

```
= Vertical, 1 = Horizontal, 2 = RHCP, 3 = LHCP

%%====SOLVER====%%
sol_sel=0;                        % to select the solver: 0=Cholesky,
1=Conjugate Gradient; default as 0
sol_max_ite=3000;                  % when sol_sel=1, Max iterations
sol_conv=1.0e-5;                   % when sol_sel=1, Convergence
sol_out_int=100;                   % when sol_sel=1, Output interval

%%%%%%%%%%%%%%%%%%%%%%%%%%%%%%%%%%
%%% ADJUST PARAMERTER FORMAT %%
%%%%%%%%%%%%%%%%%%%%%%%%%%%%%%%%%%
%adjust the paramerter format for the subfunctions%

Vertex=[Vertex_1;Vertex_2;Vertex_3;Vertex_4];
Feed_point=[feed_sel,feed_volt,feed_phase];
Load_point=[load_sel,load_r,load_l,load_c];
Division=[div_sel,div_1,div_2,div_3];
Wire_radius=[w_radius_sel,w_radius_val];
Offset=[offset_sel,offset_x,offset_y,offset_z];

Freq=[freq_start,freq_stop,freq_div];
Incidence=[inc_plane_wave,inc_theta,inc_phi,inc_polar];
Solver=[sol_sel,sol_max_ite,sol_conv,sol_out_int];

save ModelParameterDefault.mat;
```

VI. Printing parameter data for EEM-MOM model files

```
function
print_data(filename,model_title,Freq,ground,div_wavelength,r_wire,Inc
idence,Solver)

freq_start=Freq(1);
freq_stop=Freq(2);
freq_div=Freq(3);

inc_plane_wave=Incidence(1);
inc_theta=Incidence(2);
inc_phi=Incidence(3);
inc_polar=Incidence(4);

sol_sel=Solver(1);
sol_max_ite=Solver(2);
sol_conv=Solver(3);
sol_out_int=Solver(4);

%%%%%%%%%%%%%%%%%%%%%%%%
%%  PRINT PARAMETER   %%
%%%%%%%%%%%%%%%%%%%%%%%%

fid=fopen(filename,'w');
fprintf(fid,'EEM-MOM¥r¥n');
```

```
fprintf(fid,'2,0¥r¥n');
fprintf(fid,'%s¥r¥n',model_title);
fprintf(fid,'====FREQ====¥r¥n');
fprintf(fid,'%d,%d,%d¥r¥n',freq_start,freq_stop,freq_div);
fprintf(fid,'====GROUND====¥r¥n');
fprintf(fid,'%d¥r¥n',ground);
fprintf(fid,'====DIVISION====¥r¥n');
fprintf(fid,'%d¥r¥n',div_wavelength);
fprintf(fid,'====RADIUS====¥r¥n');
fprintf(fid,'%f¥r¥n',r_wire);
fprintf(fid,'====INCIDENCE====¥r¥n');
if inc_plane_wave==1

fprintf(fid,'%d,%d,%d,%d¥r¥n',inc_plane_wave,inc_theta,inc_phi,inc_po
lar);
elseif inc_plane_wave==0
    fprintf(fid,'%d¥r¥n',inc_plane_wave);
end
fprintf(fid,'====SOLVER====¥r¥n');
if sol_sel==1

fprintf(fid,'%d,%d,%d,%d¥r¥n',sol_sel,sol_max_ite,sol_conv,sol_out_in
t);
elseif sol_sel==0
    fprintf(fid,'%d¥r¥n',sol_sel);
end
fprintf(fid,'====DATA====¥r¥n');
fclose(fid);
```

VII. Printing the model data for EEM-MOM model files

```
function
print_model(filename,type_shape,type_coord,type_comment,Vertex,Feed_p
oint,Load_point,Division,Wire_radius,Offset)


Vertex_1=Vertex(1,:);
Vertex_2=Vertex(2,:);
Vertex_3=Vertex(3,:);
Vertex_4=Vertex(4,:);

feed_sel=Feed_point(1);
feed_volt=Feed_point(2);
feed_phase=Feed_point(3);

load_sel=Load_point(1);
load_r=Load_point(2);
load_l=Load_point(3);
load_c=Load_point(4);

div_sel=Division(1);
div_1=Division(2);
div_2=Division(3);
div_3=Division(4);
```

```
w_radius_sel=Wire_radius(1);
w_radius_val=Wire_radius(2);

offset_sel=Offset(1);
offset_x=Offset(2);
offset_y=Offset(3);
offset_z=Offset(4);

%%%%%%%%%%%%%%%%%%%%%%%%%%%%%%
%%    ADJUST FOMAT OF DATA   %%
%%%%%%%%%%%%%%%%%%%%%%%%%%%%%%

if type_shape==0
    division=[div_sel,div_1];
elseif type_shape==1
    division=[div_sel,div_1,div_2];
    %feed_sel=0;
    %load_sel=0;
elseif type_shape==2
    division=[div_sel,div_1,div_2,div_3];
    %feed_sel=0;
    %load_sel=0;
end

if feed_sel==0
    feed_point=[feed_sel];
elseif feed_sel==1
    feed_point=[feed_sel,feed_volt,feed_phase];
end

if load_sel==0
    load_point=[load_sel];
elseif load_sel==1
    load_point=[load_sel,load_r,load_l,load_c];
end

if div_sel==0
    division=[div_sel];
end

if w_radius_sel==0
    w_radius=[w_radius_sel];
elseif w_radius_sel==1
    w_radius=[w_radius_sel,w_radius_val];
end

%if offset_sel==0
%    offset=[offset_sel];
%elseif offset_sel==1
%    offset=[offset_sel,44,offset_x,44,offset_y,44,offset_z];
%end

%%%%%%%%%%%%%%%%%%%%%%%%%
%% PRINT MODEL DATA %%
```

```
%%%%%%%%%%%%%%%%%%%%%%%%

fid=fopen(filename,'a');
%fprintf(fid,'====DATA====¥n');
fprintf(fid,'%d,%d,%s¥r¥n',type_shape,type_coord,type_comment);

if (type_shape==0)||(type_shape==2)
    fprintf(fid,'%d,%d,%d,%d,%d,%d¥r¥n',Vertex_1,Vertex_2);
elseif type_shape==1

fprintf(fid,'%d,%d,%d,%d,%d,%d,%d,%d,%d,%d,%d,%d¥r¥n',Vertex_1,Vertex
_2,Vertex_3,Vertex_4);
end

if type_shape==0
    fprintf(fid,'%d,',feed_point);
    fprintf(fid,'%d,',load_point);
end

fprintf(fid,'%1.0f,',division);
fprintf(fid,'%d,',w_radius);

if offset_sel==0
    fprintf(fid,'%d¥r¥n',offset_sel);
elseif offset_sel==1

fprintf(fid,'%d,%d,%d,%d¥r¥n',offset_sel,offset_x,offset_y,offset_z);
     % (%s 44)=','
end


fclose(fid);
```

VIII. Setting type of dipoles in elements

```
%%% Type and orietation of dipole %%%%
function [DipoleAxes]=dipoleType(DipoleType,Delta_d)

global Vertex Feed_point Load_point Division Wire_radius Offset Freq
Incidence Solver;
global DipoleType_horizontal DipoleType_vertical
DipoleType_dualVertical DipoleType_leftBias DipoleType_rightBias;

StartPoint=[0,0,0]; % Start point [x,y,z]
StopPoint=[0,0,0]; % Stop point [x,y,z]

switch DipoleType
    case DipoleType_horizontal
        StartPoint=[-25e-3,0,0];
        StopPoint=[25e-3,0,0];
        Vertex(1,:)=StartPoint;
        Vertex(2,:)=StopPoint;
        clear DipoleAxes;
```

```
        DipoleAxes(1,:)=[StartPoint,StopPoint];
    case DipoleType_vertical
        StartPoint=[0,0,-25e-3];
        StopPoint=[0,0,25e-3];
        Vertex(1,:)=StartPoint;
        Vertex(2,:)=StopPoint;
        clear DipoleAxes;
        DipoleAxes(1,:)=[StartPoint,StopPoint];
    case DipoleType_dualVertical
        clear DipoleAxes;
        StartPoint=[-Delta_d/2,0,-25e-3];
        StopPoint=[-Delta_d/2,0,25e-3];
        DipoleAxes(1,:)=[StartPoint,StopPoint];
        StartPoint=[Delta_d/2,0,-25e-3];
        StopPoint=[Delta_d/2,0,25e-3];
        DipoleAxes(2,:)=[StartPoint,StopPoint];
    case DipoleType_leftBias
        StartPoint=[25e-3/sqrt(2),0,-25e-3/sqrt(2)];
        StopPoint=[-25e-3/sqrt(2),0,25e-3/sqrt(2)];
        Vertex(1,:)=StartPoint;
        Vertex(2,:)=StopPoint;
        clear DipoleAxes;
        DipoleAxes(1,:)=[StartPoint,StopPoint];
    case DipoleType_rightBias
        StartPoint=[-25e-3/sqrt(2),0,-25e-3/sqrt(2)];
        StopPoint=[25e-3/sqrt(2),0,25e-3/sqrt(2)];
        Vertex(1,:)=StartPoint;
        Vertex(2,:)=StopPoint;
        clear DipoleAxes;
        DipoleAxes(1,:)=[StartPoint,StopPoint];

end
```

IX. Setting arrangement of elements in arrays

```
%%% element arrangement %%%%

function
elementArrangement(ArrangeType,D,d,Delta_d,TotalElementNum,ElementNum
,TxRx,Num_MoM)


global Vertex Feed_point Load_point Division Wire_radius Offset Freq
Incidence Solver;
global TxRx_Tx TxRx_Rx
global ArrangeType_horizontal ArrangeType_vertical ArrangeType_square
ArrangeType_crossHorizontal ArrangeType_crossVertical
ArrangeType_crossSquare ArrangeType_crossCross
ArrangeType_crossCross_big ArrangeType_xSquare
global DipoleType_horizontal DipoleType_vertical
DipoleType_dualVertical DipoleType_leftBias DipoleType_rightBias;

%% Decision of elements' positons %%
ElementOffset=[0,0,0]; % ElementOffset=[offset_x,offset_y,offset_z];
```

```
switch ArrangeType

    case ArrangeType_horizontal
        offset_x=(TotalElementNum-1)/2*(-d)+(ElementNum-1)*d;
        switch TxRx
            case TxRx_Tx
                offset_y=-D/2;
            case TxRx_Rx
                offset_y=D/2;
        end % Checking it is Tx or Rx
        offset_z=0;
        ElementOffset=[offset_x,offset_y,offset_z];
        Offset(1)=1;
        Offset(2:4)=ElementOffset;

    case ArrangeType_vertical
        offset_x=0;
        switch TxRx
            case TxRx_Tx
                offset_y=-D/2;
            case TxRx_Rx
                offset_y=D/2;
        end % % Checking it is Tx or Rx
        offset_z=(TotalElementNum-1)/2*(-d)+(ElementNum-1)*d;
        ElementOffset=[offset_x,offset_y,offset_z];
        Offset(1)=1;
        Offset(2:4)=ElementOffset;

    case ArrangeType_square
        %fprintf ('The tx array is square.');
        Num_in_edge=sqrt(TotalElementNum);
        Index_in_x=mod(ElementNum,Num_in_edge);
        Index_in_z=ceil(ElementNum./Num_in_edge);
        if Index_in_x==0;
            Index_in_x=Num_in_edge;
        end
        offset_x=((Num_in_edge-1)/2-(Index_in_x-1))*d;
        switch TxRx
            case TxRx_Tx
                offset_y=-D/2;
            case TxRx_Rx
                offset_y=D/2;
        end % % Checking it is Tx or Rx
        offset_z=((Num_in_edge-1)/2-(Index_in_z-1))*d;
        ElementOffset=[offset_x,offset_y,offset_z];
        Offset(1)=1;
        Offset(2:4)=ElementOffset;

    case ArrangeType_crossHorizontal
        if mod(TotalElementNum,2)~=0
            fprintf('The number of Nt should be even number!!');
        else
            if ElementNum<=TotalElementNum/2
                dipoleType(DipoleType_horizontal,0);
                offset_x=(TotalElementNum/2-1)/2*(-d)+(ElementNum-1)*d;
```

```
                switch TxRx
                    case TxRx_Tx
                        offset_y=-D/2-Delta_d/2;
                    case TxRx_Rx
                        offset_y=D/2-Delta_d/2;
                end % % Checking it is Tx or Rx
                offset_z=0;
                ElementOffset=[offset_x,offset_y,offset_z];
                Offset(1)=1;
                Offset(2:4)=ElementOffset;
            else
                dipoleType(DipoleType_vertical,0);

offset_x=(TotalElementNum/2-1)/2*(-d)+(ElementNum-1-TotalElementNum/2
)*d;
                switch TxRx
                    case TxRx_Tx
                        offset_y=-D/2+Delta_d/2;
                    case TxRx_Rx
                        offset_y=D/2+Delta_d/2;
                end % % Checking it is Tx or Rx
                offset_z=0;
                ElementOffset=[offset_x,offset_y,offset_z];
                Offset(1)=1;
                Offset(2:4)=ElementOffset;
            end
        end

    case ArrangeType_crossVertical
        if mod(TotalElementNum,2)~=0
            fprintf('The number of Nt should be even number!!');
        else
            if ElementNum<=TotalElementNum/2
                dipoleType(DipoleType_horizontal,0);
                offset_x=0;
                switch TxRx
                    case TxRx_Tx
                        offset_y=-D/2-Delta_d/2;
                    case TxRx_Rx
                        offset_y=D/2-Delta_d/2;
                end % % Checking it is Tx or Rx
                offset_z=(TotalElementNum/2-1)/2*(-d)+(ElementNum-1)*d;
                ElementOffset=[offset_x,offset_y,offset_z];
                Offset(1)=1;
                Offset(2:4)=ElementOffset;
            else
                dipoleType(DipoleType_vertical,0);
                offset_x=0;
                switch TxRx
                    case TxRx_Tx
                        offset_y=-D/2+Delta_d/2;
                    case TxRx_Rx
                        offset_y=D/2+Delta_d/2;
                end % % Checking it is Tx or Rx

offset_z=(TotalElementNum/2-1)/2*(-d)+(ElementNum-1-TotalElementNum/2
)*d;
```

```
            ElementOffset=[offset_x,offset_y,offset_z];
            Offset(1)=1;
            Offset(2:4)=ElementOffset;
        end
    end

    case ArrangeType_crossSquare
        if ElementNum<=TotalElementNum/2
            dipoleType(DipoleType_horizontal,0);

elementArrangement(ArrangeType_square ,D,d,Delta_d,TotalElementNum/2,
ElementNum,TxRx,Num_MoM);
            Offset(3)=Offset(3)-Delta_d/2;
        else
            dipoleType(DipoleType_vertical,0);

elementArrangement(ArrangeType_square,D,d,Delta_d,TotalElementNum/2,E
lementNum-TotalElementNum/2,TxRx,Num_MoM);
            Offset(3)=Offset(3)+Delta_d/2;


        end

    case ArrangeType_crossCross
        if ElementNum<=TotalElementNum/2

elementArrangement(ArrangeType_crossHorizontal ,D,d,Delta_d,TotalElem
entNum/2,ElementNum,TxRx,Num_MoM);
        else

elementArrangement(ArrangeType_crossVertical,D,d,Delta_d,TotalElement
Num/2,ElementNum-TotalElementNum/2,TxRx,Num_MoM);
        end


    case ArrangeType_crossCross_big
        if ElementNum<=TotalElementNum/2

elementArrangement(ArrangeType_crossHorizontal ,D,d*sqrt(2),Delta_d,T
otalElementNum/2,ElementNum,TxRx,Num_MoM);
        else

elementArrangement(ArrangeType_crossVertical,D,d*sqrt(2),Delta_d,Tota
lElementNum/2,ElementNum-TotalElementNum/2,TxRx,Num_MoM);
        end


        case ArrangeType_xSquare
        if ElementNum<=TotalElementNum/2
            dipoleType(DipoleType_leftBias,0);

elementArrangement(ArrangeType_square ,D,d,Delta_d,TotalElementNum/2,
ElementNum,TxRx,Num_MoM);
            Offset(3)=Offset(3)-Delta_d/2;
        else
            dipoleType(DipoleType_rightBias,0);

elementArrangement(ArrangeType_square,D,d,Delta_d,TotalElementNum/2,E
lementNum-TotalElementNum/2,TxRx,Num_MoM);
```

```
            Offset(3)=Offset(3)+Delta_d/2;

        end
end
%% Decision of Feed point or Load point %%%

switch TxRx
    case TxRx_Tx
        if ElementNum==Num_MoM
            Feed_point=[1,1,0];
            Load_point=[0,0,0,0];
        else
            Feed_point=[0,0,0];
            Load_point=[1,70.987,0,0];
        end
    case TxRx_Rx
        Feed_point=[0,0,0];
        Load_point=[1,70.987,0,0];
end
```

X. Setting shape of objects

```
%%% Setting the shape of objects %%%

function
[ObjectAxes]=objectShape(ObjectType,ObjectLength,MeshGap,MeshWireNum,
DistanceOfMetalWires)

global Vertex Feed_point Load_point Division Wire_radius Offset Freq
Incidence Solver;
global ObjectShape_horizontal ObjectShape_vertical ObjectShape_cross
ObjectShape_without TotalObjectNum ObjectShape_mesh ObjectShape_2cross
ObjectShape_crossNoConnection ;
% global MeshGap MeshWireNum

ObjectStartPoint=[0,0,0]; % Start point [x,y,z]
ObjectStopPoint=[0,0,0]; % Stop point [x,y,z]

switch ObjectType
    case ObjectShape_horizontal
        ObjectStartPoint=[-ObjectLength/2,0,0];
        ObjectStopPoint=[ObjectLength/2,0,0];
        Vertex(1,:)=ObjectStartPoint;
        Vertex(2,:)=ObjectStopPoint;
        ObjectAxes=[ObjectStartPoint,ObjectStopPoint];

    case ObjectShape_vertical
        ObjectStartPoint=[0,0,-ObjectLength/2];
        ObjectStopPoint=[0,0,ObjectLength/2];
        Vertex(1,:)=ObjectStartPoint;
        Vertex(2,:)=ObjectStopPoint;
        ObjectAxes=[ObjectStartPoint,ObjectStopPoint];
```

```
    case ObjectShape_cross
        ObjectStartPoint=[-ObjectLength/2,0,0];
        ObjectStopPoint=[ObjectLength/2,0,0];
        ObjectAxes(1,:)=[ObjectStartPoint,ObjectStopPoint]; % parallel
metal wire
        ObjectStartPoint=[0,0,-ObjectLength/2];
        ObjectStopPoint=[0,0,ObjectLength/2];
        ObjectAxes(2,:)=[ObjectStartPoint,ObjectStopPoint]; %
perpendicular metal wire
    case ObjectShape_without
        TotalObjectNum=0;
        ObjectAxes=[ObjectStartPoint,ObjectStopPoint];
    case ObjectShape_mesh
        for i_MeshWireNum=1:MeshWireNum

ObjectStartPoint=[-ObjectLength/2,0,-(MeshWireNum-1)/2*MeshGap+(i_Mes
hWireNum-1)*MeshGap];

ObjectStopPoint=[ObjectLength/2,0,-(MeshWireNum-1)/2*MeshGap+(i_MeshW
ireNum-1)*MeshGap];

ObjectAxes(i_MeshWireNum,:)=[ObjectStartPoint,ObjectStopPoint]; %
parallel metal wire
        end
        for i_MeshWireNum=MeshWireNum+1:2*MeshWireNum

ObjectStartPoint=[-(MeshWireNum-1)/2*MeshGap+(i_MeshWireNum-MeshWireN
um-1)*MeshGap,0,-ObjectLength/2];

ObjectStopPoint=[-(MeshWireNum-1)/2*MeshGap+(i_MeshWireNum-MeshWireNu
m-1)*MeshGap,0,ObjectLength/2];

ObjectAxes(i_MeshWireNum,:)=[ObjectStartPoint,ObjectStopPoint]; %
perpendicular metal wire
        end
    case ObjectShape_2cross
        for i_MeshWireNum=1:2

ObjectStartPoint=[-ObjectLength/2,0,-(MeshWireNum-1)/2*MeshGap+(i_Mes
hWireNum-1)*MeshGap];

ObjectStopPoint=[ObjectLength/2,0,-(MeshWireNum-1)/2*MeshGap+(i_MeshW
ireNum-1)*MeshGap];

ObjectAxes(i_MeshWireNum,:)=[ObjectStartPoint,ObjectStopPoint]; %
parallel metal wire
        end
        for i_MeshWireNum=3

ObjectStartPoint=[-(MeshWireNum-1)/2*MeshGap+(i_MeshWireNum-MeshWireN
um-1)*MeshGap,0,-ObjectLength/2];

ObjectStopPoint=[-(MeshWireNum-1)/2*MeshGap+(i_MeshWireNum-MeshWireNu
m-1)*MeshGap,0,ObjectLength/2];

ObjectAxes(i_MeshWireNum,:)=[ObjectStartPoint,ObjectStopPoint]; %
perpendicular metal wire
```

```
        end
    case ObjectShape_crossNoConnection

        ObjectStartPoint=[-ObjectLength/2,-DistanceOfMetalWires/2,0];
        ObjectStopPoint=[ObjectLength/2,-DistanceOfMetalWires/2,0];
        ObjectAxes(1,:)=[ObjectStartPoint,ObjectStopPoint]; % parallel
metal wire
        ObjectStartPoint=[0,DistanceOfMetalWires/2,-ObjectLength/2];
        ObjectStopPoint=[0,DistanceOfMetalWires/2,ObjectLength/2];
        ObjectAxes(2,:)=[ObjectStartPoint,ObjectStopPoint];%
perpendicular metal wire
end
```

XI. Setting position of objects

```
%%%%% Setting the position of objects %%%%

function objectPosition(offset_x,offset_y,offset_z)
global Vertex Feed_point Load_point Division Wire_radius Offset Freq
Incidence Solver;

ObjectOffset=[0,0,0]; % ElementOffset=[offset_x,offset_y,offset_z];

ObjectOffset=[offset_x,offset_y,offset_z];
Offset(1)=1;
Offset(2:4)=ObjectOffset;
Feed_point=[0,0,0];
Load_point=[0,0,0,0];
```